Characterization of the TMBIM protein family and the role of TMBIM6 (Bax Inhibitor-1) in vivo

Inaugural Dissertation

zur Erlangung des Doktorgrades der Mathematisch-Naturwissenschaftlichen Fakultät der Heinrich-Heine-Universität Düsseldorf

vorgelegt von

Dmitrij Lisak

aus Düsseldorf

Düsseldorf, 12. März 2015

Aus der Klinik für Neurologie

des Universitätsklinikums Düsseldorf und

dem Institut für funktionelle Zellmorphologie

der Heinrich-Heine-Universität Düsseldorf

Gedruckt mit der Genehmigung der Mathematisch-Naturwissenschaftlichen Fakultät der Heinrich-Heine-Universität Düsseldorf

Referent: Prof. Dr. Axel Methner

Koreferent: Prof. Dr. Hermann Aberle

Tag der mündlichen Prüfung: 24.06.2015

Summary

The endoplasmic reticulum (ER) is an intracellular organelle that serves a multitude of functions like protein folding and modification but is also the largest cellular Ca^{2+} store and thereby controls myriads of downstream processes through Ca^{2+} release. Misfolded proteins cause ER stress, which is sensed through the three proteins IRE1α, PERK and ATF6, which try to reestablish ER homeostasis through a process called the unfolded protein response (UPR).

Bax Inhibitor-1 (BI-1) is an evolutionary extremely conserved ER membrane protein containing six transmembrane domains with a C-terminal di-aspartyl pH sensor. By being a pH-dependent Ca^{2+}-leak channel on the one hand and by directly interacting with IRE1α on the other hand, it bridges the two important functions of Ca^{2+} homeostasis and ER stress resolution.

BI-1 is also the founding member of the transmembrane BAX inhibitor motif containing (TMBIM) protein family. In this work, I first studied the relationship between the six TMBIM family members, their structure and their impact on the intracellular Ca^{2+} homeostasis. We found the di-aspartyl pH sensor to be conserved in all TMBIM proteins as well as in their bacterial homologue BsYetJ. They also share a similar structure, computed by bioinformatical tools and are mainly located in intracellular Ca^{2+} stores like the ER and Golgi apparatus, which is reflected by a decrease of the intracellular Ca^{2+} levels caused by their overexpression.

In my second study, I investigated the effects of a BI-1 knockout in vivo. I, together with my collaborators, observed increased numbers of splenic marginal zone B cells in BI-1-deficient mice, which was accompanied by constitutive nuclear translocation of NF-κB proteins. This correlated with increased ER Ca^{2+} content but not with ER stress. T and B cells show increased apoptosis in culture due to an exhausted mitochondrial Ca^{2+} buffer capacity. In vivo, T cell-dependent experimental autoimmune encephalomyelitis and B cell-dependent antibody production are attenuated in BI-1 KO mice, suggesting that BI-1 plays a major role in the functioning of the adaptive immune system by regulating intracellular Ca^{2+} homeostasis in lymphocytes.

Zusammenfassung

Das Endoplasmatische Retikulum (ER) ist der größte intrazelluläre Ca^{2+}-Speicher und beeinflusst eine Vielzahl nachfolgender Prozesse durch Ca^{2+}-Ausschüttung. Es ist weiterhin an der Faltung und Modifikation einer Vielzahl von Proteinen beteiligt. Fehlgefaltete Proteine verursachen ER Stress, der durch die Proteine IRE1α, PERK und ATF6 wahrgenommen wird und die versuchen die ER Homöestase durch einen Prozess namens "unfolded protein response" (UPR) wiederherzustellen.

Bax Inhibitor-1 (BI-1) ist ein evolutionär konserviertes Protein, das über sechs Transmembran-Domänen verfügt, in der ER Membran lokalisiert ist und einen C-terminalen di-Aspartat pH-Sensor hat. BI-1 ist ein Ca^{2+}-Kanal und interagiert mit IRE1α; es stellt daher eine Brücke zwischen dem intrazellularen Ca^{2+}-Haushalt und der UPR dar.

BI-1 ist auch der Begründer der transmembrane BAX inhibitor motif containing (TMBIM) Proteinfamilie und in unserer ersten Publikation haben wir die Verwandschaftsverhältnisse zwischen den sechs TMBIM Proteinen, ihrer Struktur und ihre mögliche Funktion als kalziumregulierende Proteine untersucht. Wir entdeckten, dass der di-Aspartat pH-Sensor bei allen TMBIM Proteinen sowie in deren bakteriellen Homolog BsYetJ konserviert ist. Zudem haben sie eine ähnliche sekundäre Struktur und sind hauptsächlich in den Membranen von intrazellulären Ca^{2+}-Speichern zu finden. Korrelierend mit ihrer Lokalisierung führte ihre Überexpression zur Verringerung der Ca^{2+} Menge in den intrazellulären Speichern.

In der zweiten Studie untersuchte ich den Effekt eines BI-1 Knockout in vivo. Wir beobachteten eine erhöhte Anzahl von Marginalzonen B-Zellen in BI-1 KO Mäusen, was mit einer konstitutiven Translokation von NF-κB in den Nukleus einherging. Dies korrelierte mit einer erhöhten ER Ca^{2+}-Konzentration, aber nicht mit ER-Stress. T- und B-Zellen in Kultur leiden unter erhöhtem Zelltod welcher von einer Ca^{2+}-Überfüllung der Mitochondrien herrührt. In vivo ist sowohl die T-Zell abhängige Experimentelle autoimmune Enzephalomyelitis als auch die B-Zell abhängige Antikörper Produktion beeinträchtigt, was darauf hindeutet dass BI-1 eine wichtige Funktion während der adaptiven Immunantwort spielt indem es den intrazellulären Kalziumhaushalt in Lymphozyten reguliert.

Table of contents

Introduction

The endoplasmic reticulum

The endoplasmic reticulum (ER) is a major intracellular organelle consisting of a large membranous network which is responsible for lipid biosynthesis (1), protein folding (2), posttranslational protein modification and trafficking (3) and calcium (Ca^{2+}) handling (4). The ER can be subdivided into two phenotypes: the rough endoplasmic reticulum (RER) and the smooth endoplasmic reticulum (SER). The RER is characterized by the integration of ribosomes and is mainly responsible for protein synthesis while the SER lacks ribosomes and is mostly involved in phospholipid synthesis and Ca^{2+} homeostasis (5). Which of the two phenotypes is prevalent in the cell is dependent on the cell function and the cell's needs. Highly secretory cells like B cells and pancreatic cells will have mostly RER while liver cells which are mainly involved in drug detoxification will be largely comprised of SER (6). However, the ER is not a fixed structure but can reorganize itself appropriately if needed through processes called 'tubule sliding', 'tubule branching' and 'ring closure' (7) which for example can be observed after oocyte fertilization (8,9), during mitosis (10) and after sustained Ca^{2+} signaling (11).

Endoplasmic reticulum stress

A large portion of human diseases are linked to misfolded proteins (12) and about one third of the human proteome is folded and assembled into native structures by chaperones in the ER (13). It is therefore crucial for the cell to have a protective response against ER stressors like reactive oxygen species (ROS) which alter protein conformation by oxidizing sulfur residues and thereby promote the accumulation of misfolded proteins in the ER (14). On the other hand, the lack of sufficient oxygen during hypoxia causes the accumulation of unfolded proteins since chaperones require an electron acceptor in order to properly fold proteins (15). Viral infections can cause ER stress as well by hijacking the cellular translation machinery to produce large amounts of viral proteins (16). Disturbances of the Ca^{2+} homeostasis also result in ER stress by directly activating the ER-resident caspase 12 due to the overfilling of the ER with Ca^{2+} (17). The resulting accumulation of misfolded proteins is countered by the unfolded protein response (UPR). Three different transmembrane ER proteins are responsible for sensing ER stress and initiating the UPR in order to restore the protein folding capacity of the ER: inositol-requiring kinase 1 (IRE1α), activating transcription factor 6 (ATF6), and double-stranded RNA-activated protein kinase

(PKR)-like endoplasmic reticulum kinase (PERK). During normal conditions these three activators are inhibited by the ER chaperone binding immunoglobulin protein (BIP), which is also known as 78 kDa glucose-regulated protein (Grp78). Accumulated malfolded proteins lead to the dissociation of BIP from IRE1α, ATF6 and PERK since it acts as a chaperone which is attracted by the exposed hydrophobic regions of misfolded proteins (18). The three freed UPR sensors are then able to activate their respective pathways.

IRE1α

Dissociation of BIP from IRE1α starts a chain of events which begins with the oligomerization of IRE1α, thereby opening the Serine/Threonine (Ser/Thr) kinase domain on the cytosolic C-terminal and allowing trans-autophosphorylation (19). This leads to the activation of the IRE1α-endoribonuclease domain, which splices the X-box protein 1 (XBP1) mRNA to spliced XBP1 (sXBP1) by cleaving a 26 nucleotide intron, resulting in its translation to the basic Leucine Zipper Domain (bZIP)-family transcription factor XBP1. Upon its translocation to the nucleus, XBP1 can either dimerize or act together with other transcription factors to regulate genes which are involved with endoplasmic reticulum-associated degradation (ERAD) by binding to the endoplasmic reticulum stress response element (ERSE) promoter (20). Activated IRE1α also interacts with adapter proteins like tumor necrosis factor receptor-associated factor 2 (TRAF2) in order to modulate the cellular stress response. TRAF2 is able to recruit the apoptosis signal-relating kinase (ASK1) (21) which has been shown to activate c-Jun N-terminal kinase (JNK), leading to proapoptotic and neurodegenerative signaling (22). Other IRE1α-activated proteins which modulate the cellular stress response include extracellular signal-regulated kinases (ERKs) (23) and nuclear factor kappa-light-chain-enhancer of activated B cells (NF-κB) (24,25).

PERK

Upon activation, PERK dimerizes and undergoes autophosphorylation in analogy to IRE1α (26) and begins to phosphorylate its main target: the eukaryotic translation initiation factor (eIF2α). As the name suggests, eIF2α initiates translation in cells and is inhibited by being phosphorylated at serine residue 51. Inhibition by PERK thus reduces the protein load in the ER during UPR by inhibiting the translation of proteins and additionally causes cell cycle arrest (27). Interestingly, some proteins may escape translational arrest by phosphorylated eIF2α (P-eIF2α) due to their internal ribosome entry site (IRES) outside of the actual eIF2α translational block (28). One of these proteins is the activating transcription factor 4 (ATF4), a cAMP response element binding (CREB) family member which itself induces expression of genes which are responsible for cell survival (29-31). The activation of NF-κB is an additional consequence of the phosphorylation of eIF2α by PERK

which shows that the PERK and IRE1α pathways partly result in the same outcome (32). PERK also causes the nuclear erythroid 2 p45-related factor 2 (Nrf2) to translocate to the nucleus by phosphorylating its inhibitor kelch-like ECH-associated protein 1 (Keap1). Nrf2 normally resides in the cytoplasm, sequestered by Keap1, which releases Nrf2 upon its phosphorylation and allows it to enter the nucleus where it causes the transcription of genes responsible to relieve cell stress caused by ROS (33).

ATF6

ATF6 is an unusual transcription factor as, upon its release by BIP, a Golgi localization signal becomes unmasked (34). In the Golgi ATF6 is subject to proteolytic cleavage, a process called regulated intermembrane proteolysis (RIP) (35). The cleaved transcription factor (ATF6 p50) then translocates to the nucleus, where it can either homodimerize or heterodimerize with other transcription factors such as the aforementioned XBP1 (36). Specific genes which are regulated by ATF6 remain to be identified, it is however known that homodimers of ATF6 bind to regions which are associated with chaperone genes such as BIP and $p58^{IPK}$ while heterodimers with XBP1 bind to regions which code for ERAD components (37).

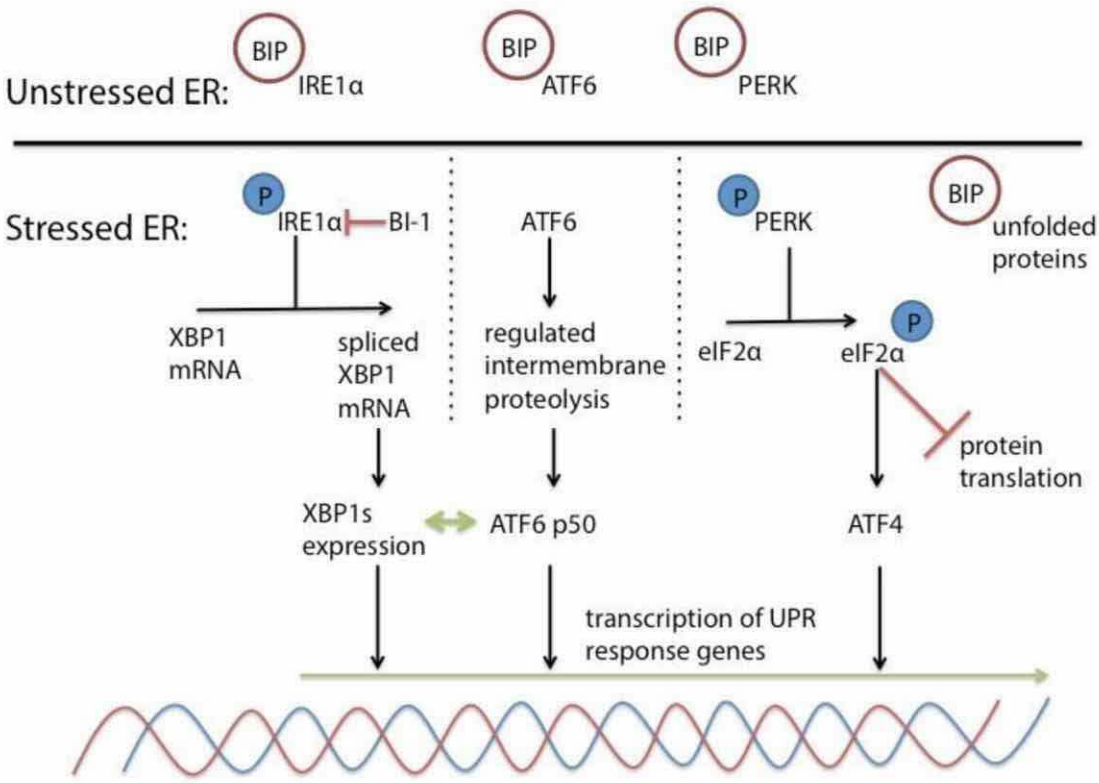

Figure 1: Overview of the ER Stress response. Under normal conditions, the three ER stress sensors IRE1α, ATF6 and PERK are bound to the chaperone protein BIP in the ER membrane and are nonfunctional. During ER stress, BIP binds to the accumulated unfolded proteins since their exposed hydrophobic regions attract it. The freed IRE1α undergoes autophosphorylation, which activates its endoribonuclease domain leading to the splicing of XBP1 mRNA, which results in the expression of the transcription factor XBP1s. XBP1s is responsible for the transcription of UPR response genes and genes associated with ER associated degradation (ERAD). Upon its dissociation from BIP, ATF6 translocates to the Golgi apparatus where it is cleaved to ATF6 p50 during a process called regulated intermembrane proteolysis (RIP). ATF6 p50 is a transcription factor which translocates to the nucleus where it can homodimerize or heterodimerize with XBP1s and facilitate the transcription of ER-stress response elements (ERSE). PERK undergoes similar autophosphorylation to IRE1α, which leads to the phosphorylation of the transcription factor eIF2α, resulting in translational arrest by phosphorylated eIF2α. The transcription factor ATF4 is able to escape translational arrest due to its internal ribosome entry site (IRES) and is also responsible for the transcription of UPR target genes.

Endoplasmic reticulum stress and apoptosis

Unresolved ER stress leads to apoptosis, although the mechanisms which lead to programmed cell death after prolonged ER stress are not fully understood (38). Two distinct pathways exist for apoptosis: the extrinsic and the intrinsic pathway. The extrinsic pathway is characterized by extensive CD95/Fas receptor signaling which results in sustained Ca^{2+} release from the ER, thereby activating the apoptotic pathway (39). The intrinsic pathway is generally activated by DNA damage, oxidative stress, energy deficiency through the lack of ATP or ER stress leading to cytochrome c release from the mitochondria (40).

One possibility how persisting ER stress causes apoptosis is the continuous activation of IRE1α. As previously described, IRE1α can lead to the activation of JNK which orchestrates apoptosis in two different ways, either by acting on gene transcription in the nucleus or directly by acting on the mitochondria. In the nucleus, JNK is responsible for the phosphorylation of a variety of transcription factors, including JunD, ATF2, ATF3, Elk-1, Elk-3, p53, RXRα, RARα, AR, NFAT4, HSF-1, and c-Myc (41). Of special note is the phosphorylation of c-JUN by JNK since this leads to the formation of c-Jun homodimers and c-Jun heterodimers with c-Fos, which are both the building blocks of the transcription factor AP-1 (42). AP-1 is responsible for the increased expression of an array of proapoptotic proteins like TNFα, Fas-L, and Bak (43). A second way of JNK to act proapoptotic is the phosphorylation of the p53 family members p53 (44) and p73 (45). Phosphorylation of both proteins inhibits their ubiquitin-mediated degradation, thereby increasing their overall levels and enabling them to promote the transcription of proapoptotic genes like p53 upregulated promoter of apoptosis (PUMA) (46) and BCL2-associated X protein (Bax) (45).

The way JNK acts proapoptotic in the mitochondria is less clear. It has been shown that JNK readily translocates to the mitochondria upon activation (47) where it is critically required for the release of cytochrome c (48) which is achieved by phosphorylating, and thereby activating, proapoptotic proteins like Bim and Bmf (49) or by inducing the cleavage (and activation) of the proapoptotic protein Bid (50).

However, IRE1α activation is not the only way in which ER stress can lead to apoptosis. The aforementioned transcription factor ATF4, which is activated by one of the main ER stress sensors PERK, is not solely responsible for the expression of survival genes, but can also cause the transcription of C/EBP-homologous protein (CHOP) (38). CHOP on the one hand causes the upregulation of the proapoptotic protein Bim and on the other hand the downregulation of the antiapoptotic BCL-2 (51).

In summary, ER stress activates the UPR, a complex cell protective mechanism, which is controlled and modulated by the three ER stress sensors IRE1α, PERK and ATF6. Activation of these sensors leads to translational arrest to relieve some burden of the ER, the expression of genes responsible for cell survival and the upregulation of chaperones and other antiapoptotic proteins. The integration of all the signals during the UPR is complex

and, dependent on the duration and the nature of the ER stress, the UPR might be insufficient to reestablish cell homeostasis, which leads to apoptosis. Interestingly, apoptosis is caused and regulated by the same three ER stress sensors, which are initially responsible to rescue the cell.

Calcium

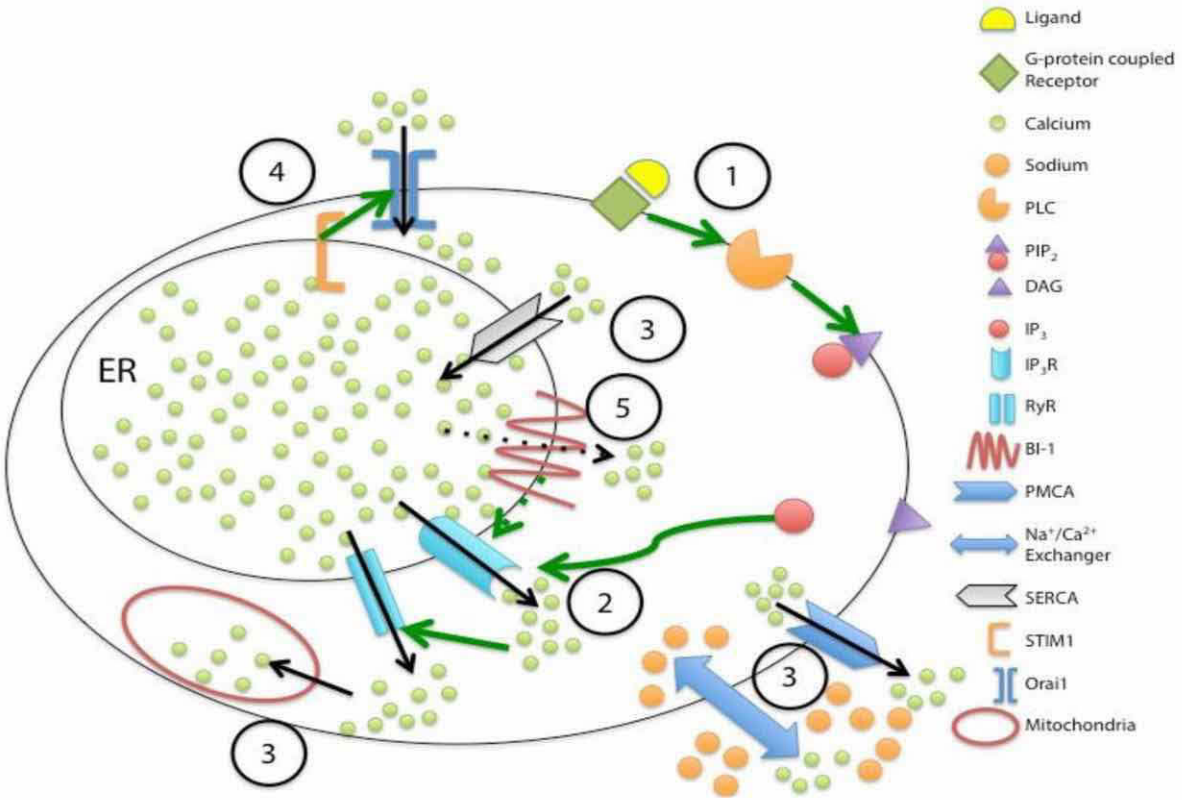

Figure 2: Overview of the cellular Ca^{2+} machinery. **(1)** When a ligand binds to a G-protein coupled receptor, its Gq subunit activates phospholipase C, which in turn cuts PIP2 into DAG and IP_3. **(2)** While DAG stays in the plasma membrane, IP_3 diffuses through the cytoplasm and activates IP_3 receptors (IP_3Rs). The resulting Ca^{2+} release from the ER causes Ca^{2+} induced Ca^{2+} release (CICR), for example by activating Ryanodine receptors (RyRs) which results in further Ca^{2+} release from the ER and sustains the initial Ca^{2+} signal. **(3)** The excess cytosolic Ca^{2+} is cleared by plasma membrane Ca^{2+} ATPases (PMCAs), the Na^+/Ca^{2+} exchanger in the plasma membrane, by SERCA pumps, which actively refill the ER and by mitochondria which also buffer some of the Ca^{2+}. **(4)** The emptied state of the ER is sensed by STIM1 molecules, which interact with Orai1 in he plasma membrane and allow the influx of extracellular Ca^{2+} in order to refill the intracellular Ca^{2+} stores. **(5)** BI-1 resides in the ER membrane and is a pH dependent Ca^{2+} leak channel but is also able to sensitize IP_3Rs through direct interaction and thereby lower their EC_{50}, which results in increased Ca^{2+} releases upon IP_3R activation.

Calcium (Ca^{2+}) is one of the most important and universal second messengers. It relays signals in a spatiotemporal manner and is responsible for a wide array of cellular processes from short term events like exocytosis at the synaptic cleft to the hour long regulation of gene expression (52). Most of the intracellular calcium is stored in the ER with lesser amounts in the Golgi apparatus and mitochondria. For Ca^{2+} being able to regulate that many intracellular processes and even being able to target specific subcellular locations, the cytosolic Ca^{2+} concentration has to be kept in the nanomolar range, while the concentrations in the extracellular space and the ER are orders of magnitude higher. Cells invest a considerable amount of energy into adenosine triphosphate (ATP)-driven Ca^{2+} pumps to keep the delicate intracellular Ca^{2+} homeostasis in check (53). Disturbances in this homeostasis are associated with a wide array of diseases, including Alzheimer's disease,

Parkinson's disease, epilepsy and amyotrophic lateral sclerosis (54). Ca^{2+} is of special importance in immune cells, where, upon activation of the cell, it is responsible for maturation, cytokine release, antigen presentation and activation of intracellular transcription factors which are crucial for immune cell function (55).

Ca^{2+} signaling

Calcium can enter a cell by different means, depending on the cell type and the available Ca^{2+} channels. Neurons for example allow Ca^{2+} influx mainly through either voltage-dependent Ca^{2+} channels (VDCC) or ligand-gated Ca^{2+}-channels (LGCC). While VDCCs mainly trigger pre-synaptic neurotransmitter release during an action potential (6), LGCCs are found on the post-synaptic membrane and open upon binding of their ligands. For example, N-Methyl-D-aspartate (NMDA) and 2-amino3-(3-hydroxy-5-methyl-isoaxol-4-yl)propanoic acid (AMPA) receptors open when glutamate binds (56,57).
Alternatively, when a ligands bind to a G_q-coupled receptor (e.g. metabotropic glutamate receptors) or a tyrosine-kinase-coupled receptor like B- and T cell receptors, the plasma membrane-bound phospholipase C (PLC) is activated and proceeds to cut phosphatidylinositol 4,5-bisphosphate (PIP2) to inositol 1,4,5-triphosphate (IP_3) and diacylglycerol (DAG). While both products readily diffuse through the cytosol, only IP3 is directly responsible for Ca^{2+} release from the ER by binding to IP_3 receptors 1-3 (IP_3R1-3) which are located in the ER membrane (58). The sharp rise of the cytosolic Ca^{2+} concentration leads to calcium-induced calcium release (CICR), for example by opening the calcium-sensitive ryanodine receptors (RyR) which leads to an amplification of the initial Ca^{2+} signal (59). The cell removes the excess cytosolic calcium either through energy dependent plasma membrane calcium ATPases (PMCAs), through the sodium-calcium exchanger (Na^+/Ca^{2+} exchanger) or by refilling the ER through the action of sarco/endoplasmic reticulum Ca^{2+}-ATPases (SERCA).

Store-operated Ca^{2+} entry

The rise of the intracellular Ca^{2+} concentration following the depletion of the calcium stores activates plasma membrane channels named Ca^{2+}-release activated Ca^{2+} (CRAC) channels in order to refill the Ca^{2+} depots, a process called store-operated Ca^{2+} entry (SOCE) (60,61). The mechanism of how CRAC channels are activated was an intensively debated topic until stromal interaction molecule 1 (STIM1) was identified in an RNA interference (RNAi) screen as the main ER-Ca^{2+} content sensor which activates Ca^{2+} influx into the cell after store depletion (62,63). STIM1 is single-transmembrane protein that is mainly located in the ER membrane and to a lesser extent in the plasma membrane (64) and which can sense the ER-Ca^{2+} content through a luminal EF hand domain (63). Upon store depletion, STIM1 clusters

into so-called punctae at spots where the ER is close to the plasma membrane (65) and activates ORAI1, a CRAC channel, through direct interaction via its CRAC activation domain (66). ORAI1 activation results in an increased intracellular Ca^{2+} concentration which is required to refill the Ca^{2+} stores, since the Ca^{2+} which was initially released from the stores can only partially be recycled and is mostly secreted via PMCAs (66). The Ca^{2+} from the SOCE is quickly transported into the ER by SERCAs which also form punctae on the ER membrane to allow rapid Ca^{2+} transport (67,68).

Further studies have proven the role of STIM1 and ORAI1 by showing that only by co-overexpressing STIM1 and ORAI1 the SOCE could be significantly increased, while overexpressing ORAI1 alone decreases SOCE and overexpression of STIM1 alone only increases it slightly (69). It has been further shown that the ratio of ORAI1 to STIM1 should be close to 1:1 for optimal SOCE conditions and that increasing this ratio to 4:1 or higher increases the SOCE progressively less (67).

Ca^{2+} and cell death

Cell death is an important process which is required during embryonic development, immune responses and tissue renewal (70) and Ca^{2+} plays an important role in controlling these events (71). A distinction is made between two forms of cell death: cellular insult and trauma lead to necrosis while programmed and controlled cell death is called apoptosis (72). Apoptosis is characterized by apoptotic bodies which are a result of caspase-mediated cell fragmentation and DNA condensation (73). Apoptotic bodies are phagocytized by macrophages in order to prevent an inflammatory response form the surrounding tissue (74).

Apoptosis can be triggered by a wide variety of stimuli and the intrinsic pathway is distinguished from the extrinsic pathway while both are responsible for the initiation of apoptosis (75). The extrinsic pathway is initiated through cytokines, TNFα and Fas-L binding to plasma membrane located CD95/FAS-receptors, resulting in sustained elevated intracellular Ca^{2+} levels through ER Ca^{2+} release which acts as initiator of apoptosis (39). The intrinsic pathway is dependent on the mitochondria and is associated with irreparable DNA-damage, oxidative stress or insufficient ATP-synthesis. It is characterized by overfilling of mitochondria with Ca^{2+} as a consequence of the sustained elevated cytosolic Ca^{2+} concentration which ultimately results in bursting of the mitochondrial outer wall (76) which releases apoptosis mediators like cytochrome c, apoptosis-inducing factor (AIF) and procaspase 9 into the cytosol (75,77). One substrate of cytochrome c are PMCAs and the Na^{+}/Ca^{2+} exchanger in the plasma membrane and their cleavage leads to reduced Ca^{2+} clearance from the cytosol, thereby maintaining the elevated Ca^{2+} levels which are required for apoptosis (75,78,79). The intracellular Ca^{2+} additionally regulates apoptosis by activating

a family of Ca^{2+}-dependent cytosolic cysteine proteases called calpains, which consist of pro- and antiapoptotic family members (80,81).
Additionally, members of the BCL-2 family which are located in the mitochondrial and in the ER membrane and include pro- and antiapoptotic proteins have been shown to modulate the intracellular Ca^{2+} homeostasis (82). The antiapoptotic BCL-2 reduces the ER-Ca^{2+} load as well as the SOCE (83,84) and BCL-2 and BCL2-like 1 (BCL-XL) reduce the IP_3-induced Ca^{2+} release from the ER by directly interacting with the IP_3Rs (85).

Nuclear factor kappa-light-chain-enhancer of activated B cells

Nuclear factor kappa-light-chain-enhancer of activated B cells (NF-κB) proteins are a family of transcription factors consisting of five members, which are subdivided into class I and class II. Class I proteins are NF-κB1 (p105/p50) and NF-κB2 (p100/p52) which reside in the cytoplasm and translocate to the nucleus upon activation where they can form homodimers or heterodimers with the class II proteins RelA (p65), c-Rel and RelB (86). These homo- and heterodimers control the transcription of a wide variety of genes, which are responsible for apoptosis and proliferation, cell adhesion, the innate- and adaptive immune response, inflammation, the cellular stress response and tissue remodeling (87).

All five NF-κB proteins share an N-terminal DNA binding domain, which is both required for DNA binding as well as dimerization (88). Class I proteins are synthesized as the longer precursor proteins p105 and p100 and are processed at the C-terminus by proteolytic degradation after stimulation by various agents such as TNFα, interleukin-1 (IL-1), activation of the T- and B Cell receptors and lipopolysaccharide (LPS) (89). Only the processed forms p50 and p52 are able to form dimers with other NF-κB family members and regulate transcription. Both p50 and p52 contain several C-terminal anykrin-repeats and are thought to repress protein translation if they form homodimers. Class II proteins have a transactivation domain instead of the anykrin-repeats which is responsible for transcriptional activation (90). RelA, RelB and c-Rel are sequestered in the cytoplasm by inhibitory IκBα proteins. Upon stimulation IκBα is phosphorylated by the IκB Kinase (IKK) complex, which results in ubiquitin mediated degradation of phosphorylated IκBα, the release of the sequestered NF-κB proteins and their translocation to the nucleus (91). This process is known as the canonical pathway. A second way of NF-κB activation is the non-canonical pathway, which is relevant during B- and T cell organ development. It is characterized by the very selective activation by distinct ligands such as Lymphotoxin B (LTβ), B-cell activating factor (BAFF) and CD40. Their binding leads to the activation of the NF-κB inducing kinase (NIK), which phosphorylates an IKKα homodimer, resulting in the liberation of a p52/RelB complex previously sequestered in the cytoplasm (92). The general consensus is that several more activating pathways are likely to exist but they are difficult to recognize and distinguish from each other due to a high interconnection of NF-κB signaling.

For example, it has been shown that ER stress and the UPR can result in NF-κB activation. One study demonstrated that one of the proteins affected by the translational arrest following eIF2α phosphorylation by PERK is IκBα, meaning that less IκBα is available to hold NF-κB in the cytoplasm and therefore more NF-κB is able to translocate to the nucleus and regulate transcription (32). Since only the overall levels of IκBα were affected but not the levels of phosphorylated IκBα, whose phosphorylation is dependent on the IKK complex, it was suggested that NF-κB activation by the UPR is independent of IKK activity or regulation (93). However, a later study showed that another ER stress sensor, IRE1α,

directly interacts with the IKK complex after activation, leading to increased IκBα phosphorylation and therefore ubiquitination of p-IκBα and NF-κB liberation (25). A recent study linked both observations, arguing that IRE1α maintains a constant activation of the IKK complex through the adaptor molecule TRAF2 and in the context of ER stress, translational arrest of IκBα by PERK and the phosphorylation of the remaining IκBα through IRE1α and IKK work in tandem to achieve sustained NF-κB activation (94). NF-κB activation through the UPR pathway is mainly results in the expression of stress response genes.

Another way of NF-κB activation similar to the UPR but independent from it is the ER overload response (EOR). The EOR is caused by the retention of membrane or viral proteins in the ER and is distinguished from the UPR by the lack of BIP/Grp78 activation (95). Additionally, the EOR has been directly linked to NF-κB activation, which appears to be dependent on Ca^{2+} signaling. While EOR-induced NF-κB activation could be suppressed by the Ca^{2+} chelator TMB-8, the TNFα-induced NF-κB activation was completely unaffected by TMB-8 (96). The same study demonstrated that EOR-induced NF-κB activation could be further increased by elevating the cytosolic Ca^{2+} concentrations through the application of the selective SERCA inhibitors thapsigargin and cyclopiazonic acid (96). The Ca^{2+}-dependence of NF-κB activation has been confirmed by a follow up study, which used additional Ca^{2+} chelators like BAPTA-AM and which also showed that the Ca^{2+} efflux during EOR increased the reactive oxygen species (ROS) within the cell, which is also crucial for the activation of NF-κB in response to the EOR (97). The important role of Ca^{2+} in the activation of NF-κB in B cells has been further highlighted by showing that only short and large Ca^{2+} transients are able to evoke NF-κB activation in these cells whereas lower and sustained Ca^{2+} elevations lead to NFAT activation (98). This fits the previous studies since the increased cytosolic Ca^{2+} concentrations caused by thapsigargin and cyclopiazonic acid cause short lived and very high Ca^{2+} transients.

In summary, NF-κB is a very important transcription factor, which is very important for multiple cellular functions, including cytokine- and antibody production in immune cells. Its activity can be evoked by a multitude of ways, including classical pathways through cell surface receptor activation like T- and B cell receptors, as well as by intracellular stimuli like ER stress. Ca^{2+} appears to plays a prominent role in the context of intracellular stressors as has been demonstrated by the NF-κB activation being dependent on Ca^{2+} during the EOR.

BAX inhibitor-1

BAX-inhibitor-1 (BI-1) is an extremely evolutionary conserved protein that has been first identified in a screen for human proteins capable of inhibiting BAX-mediated cell death in yeast (99). It was initially known as testis enhanced gene transcript (TEGT) due to its high expression in rat and mouse testis. It was then discovered that TEGT is expressed in spleen, brain, liver, kidney, thymus, lung, ovary and heart and its homologues were found in cattle, frogs and humans (100,101).

BI-1 is a highly hydrophobic, six transmembrane protein with a C-terminal reentry loop which resides in the ER membrane (102) where it interacts with BCL-2 and BCL-XL (99) and where it is able to form a pore which is responsible for a passive Ca^{2+} leak from the ER (103). The leak properties of BI-1 are pH dependent and the Ca^{2+} flux decreases when the pH is increased or decreased from its physiological state (102). A recent study, which conducted a structural analysis of the bacterial BI-1 homologue BsYetJ confirmed its seven transmembrane structure and its properties as a pH-sensitive Ca^{2+}-pore by showing that the open and closed conformation of the pore can be altered by the pH (104). By measuring the Ca^{2+} flux in BsYetJ-containing proteoliposomes, the study showed that the leak channel was open around a physiological pH of 7 and closed above a pH of 7.4 or below a pH of 6. The authors suggested that a di-aspartyl pH sensor at the residues 171 and 195 in BsYetJ is responsible for the bell-shaped pH dependent Ca^{2+}-flux (104). We could previously show that mammalian BI-1 also possesses similar bell-shaped pH dependent Ca^{2+}-flux properties (102) and that human BI-1 has an aspartyl residue at position 213, which corresponds to residue 195 in BsYetJ and is critical for the Ca^{2+} leak across the ER membrane (103). At a pH around 7, thus under physiological conditions, the di-aspartyl sensor is sufficiently deprotonated to allow Ca^{2+}-flux. At a mildly basic pH above 7.4, a hydrogen bond between D209 and H78 in human BI-1 can form that blocks the Ca^{2+} efflux. At an acidic pH of 6 and lower, D188 and D213 in human BI-1 become protonated, additionally to a hydrogen bond between D188 and D209 which again greatly reduces the Ca^{2+}-flux through the pore (105).

Most studies describe BI-1 as a Ca^{2+}-homeostasis modulating protein and link this to its antiapoptotic function. Chae et al. first showed that neurons and hepatocytes from BI-1 KO mice had an increased ER Ca^{2+} content by applying thapsigargin, a non-competitive SERCA inhibitor, which facilitates the passive Ca^{2+} leak from the ER. This thapsigargin-releasable Ca^{2+} pool is generally regarded to reflect the ER Ca^{2+} content (106). Conversely, HT1080 cells, which were overexpressing BI-1, had a decreased thapsigargin releasable pool. These data were corroborated when Westphalen et al. measured agonist induced Ca^{2+} release in BI-1 transfected CHO cells. ATP was employed as an agonist, which results in IP_3-mediated Ca^{2+} release from the ER, and BI-1 overexpressing cells indeed showed a dramatically reduced agonist-inducible Ca^{2+} release (107). In addition to its role as a Ca^{2+} regulating protein, both studies showed that BI-1 protected from cell death, be it from ER stress mediated cell death by thapsigargin treatment (106) or from cell death resulting from glucose deprivation

through doxycycline application (107). The Ca^{2+}-releasing properties of BI-1 are dependent on its C-terminal domain, which resembles the pH-sensing domain of other channels (108). Kim et al. were able to demonstrate that BI-1 lacking its C terminus is unable to moderate the thapsigargin or agonist induced Ca^{2+} release and in addition showed that Ca^{2+}-flux from BI-1 transfected microsomes increases up to an acidic pH of 5.5 (108). The heightened Ca^{2+} leak was accompanied by the translocation of BAX to the mitochondria and subsequent cytochrome c release, which lead to the proposition that BI-1 transforms from an antiapoptotic to a proapoptotic protein under acidic conditions. While it was indeed corroborated that the Ca^{2+}-leak property of BI-1 is pH dependent, it was revealed that the Ca^{2+} flux peaks at a physiological pH of 6.8 and actually decreases when the pH became increasingly acidic (102). Our group previously demonstrated that BI-1 forms a Ca^{2+} pore in the ER membrane which is responsible for the decreased ER Ca^{2+} levels observed in BI-1 overexpressing cells and that the pore formation is dependent on the pH sensing C terminus of BI-1 (103). It was therefore concluded that that the increased Ca^{2+} flux during very acidic conditions is independent of BI-1 since Ca^{2+} flux could even be evoked in BI-1 KO mouse embryonic fibroblasts (MEFs) during cytosolic acidosis (102).

Since it was previously established that BI-1 directly interacts with BCL-XL (99) and BCL-XL is also known to decrease the ER Ca^{2+} pool as part of its antiapoptotic function (109), Xu et al. investigated whether the effect of BCL-XL is downstream of BI-1. While BCL-XL overexpression decreased the ER-Ca^{2+} content as predicted, this effect was abolished by knocking down BI-1 (110). In BI-1 KO MEFs, BCL-XL overexpression even resulted in increased ER Ca^{2+} concentrations. Co-expression of SERCA restored the decreased ER Ca^{2+} phenotype which lead to the conclusion that BI-1 acts downstream of BCL-XL and functions by either being a channel itself or by modulating Ca^{2+}-releasing proteins (110). Recent studies actually suggested that the BI-1 C terminus is not only critical for the channel formation of BI-1 and its pH sensing properties, but is also able to interact with IP_3Rs and it was demonstrated that BI-1 co-immunoprecipitates with IP_3R1 and IP_3R3 (111). By measuring the flux of radioactive $^{45}Ca^{2+}$ in saponin-permeabilized BI-1 KO MEFs, the authors demonstrated that BI-1 is able to sensitize the IP_3Rs and thereby significantly lower the EC_{50} of IP_3 induced Ca^{2+} release (111).

In addition to its proposed roles as a Ca^{2+} channel and an IP_3R sensitizing protein, BI-1 was also suggested to be a Ca^{2+}/H^+ antiporter (112). Proteolisosomes were loaded with a pH-sensitive fluorescent probe and radioactive $^{45}Ca^{2+}$ and upon exposing the proteolisosomes to an acidic environment, an influx of H^+-ions was observed which matched the efflux of Ca^{2+} (112). However, a recent study conducted a structural analysis of the bacterial BI-1 homologue BsYetJ and confirmed that BsYetJ indeed possesses a channel structure with a di-aspartyl pH sensor motif which is conserved across the whole TMBIM protein family and is able to reversibly change from a closed to an open conformation and vice versa

dependent on the pH (104). It is therefore likely that BI-1 is pH sensitive Ca^{2+} leak channel with secondary IP_3R sensitizing properties and not a Ca^{2+}/H^+ exchanger (105).

Although Ca^{2+} and cell death are the most studied paradigms in regard to BI-1, a few other potential functions have been proposed in different studies. After it was discovered that XBP-1 splicing, a marker for ER stress, is increased in BI-1 KO mice (113), follow-up studies showed that BI-1 is a negative regulator of the ER stress sensor IRE1α (114). While IRE1α induced XBP-1 splicing was attenuated over time in WT cells, it stayed constantly active in KO cells as long as a stress stimulus like thapsigargin was applied. It was also shown that BI-1 reduces the expression level of cytochrome P450 2E1, a member of the microsomal monooxygenase system which is responsible for the generation of reactive oxygen species (ROS), resulting in cellular stress (115). However, there is no proof that BI-1 directly interacts with cytochrome P450 2E1. BI-1 appears to rather interact with NADPH-P450 reductase, another member of the microsomal monooxygenase system. BI-1 is supposed to cause dissociation of NADPH-P450 reductase from cytochrome P450 2E1 and thereby ROS reduction by attenuating the electron transfer between these proteins (115).

Another study suggested that BI-1 increases cell adhesion through actin polymerization (116). Lee et al. were able to show that the C terminus of BI-1 is responsible for direct interaction with G-actin. But is has also to be kept in mind that actin polymerization is a highly Ca^{2+} dependent process and it remains unclear what role the Ca^{2+} modulating effects of BI-1 play on the observed phenotype. Lee et al. also later demonstrated that BI-1 is able to enhance cancer metastasis by shifting the cell's metabolism towards glycolysis and activating the Na^+/H^+-exchanger (117), although it remains unclear whether this is merely another secondary effect of the altered Ca^{2+} flux in BI-1 overexpressing cells.

BI-1 expression has also been shown to be upregulated in different tumors like gliomas (118), anaplastic large cell lymphomas (119), prostate (120) and breast cancer (121), pulmonary adenocarcinomas (122), nasopharyngeal carcinomas (123) and acute myeloid leukemia (124). Regarding its proposed role as an antiapoptotic protein it is not surprising to find BI-1 highly expressed in variety of cancers.

BI-1 family

Its high evolutionary conservation makes BI-1 an exciting studying object. Not only are homologues of BI-1 found in bacteria and plants, but orthologues from plants are able to substitute for mammalian BI-1 in regard to its antiapoptotic function (125). Additionally, BI-1 is the founding member of a protein family, which consists of five more members. All six proteins are predicted to have seven transmembrane domains and they all share a signature pattern which spans form the beginning of the third transmembrane domain and ends in the middle of the fourth (Prosite PDOC00957). These proteins have been identified independently by different groups and have been given various different names. The nomenclature accepted by the HUGO gene nomenclature committee for this gene family is TMBIM (transmembrane BAX inhibitor motif containing) 1-6 with BI-1 being TMBIM6.

TMBIM1

TMBIM1, also known as RECS1, PP1201, LFG3, MST100 and MSTP100, is a 35 kDa protein. Northern blotting analysis showed that it is expressed in brain, heart, lung, liver, kidney, stomach, intestine, ovary, uterus, skeletal muscle, skin and adipose tissue but not in the spleen, thymus or testis and that it subcellular localization is mainly in lysosomes and endosomes (126). Little is known about its function but it seems to play a protective role during vascular remodeling (126) and it also protects from Fas-mediated apoptosis by reducing Fas expression (127). Upon aging, mice lacking TMBIM1 are susceptible to cystic medial degeneration, which is characterized by the breakdown of collagen and smooth muscle in the arterial walls (126).

TMBIM2

TMBIM2 is a 35 kDa protein also known as NMP35, LFG, FAIM2, LFG2, NGP35 and KIAA0950. It is located in the ER and in the Golgi apparatus (128) as well as in lipid rafts microdomains (129) and is predominantly expressed in the central nervous system (130), especially at the postsynaptic membrane (131). TMBIM2 is able to protect from Fas-L, but not from TNFα mediated apoptosis (128,129). Conversely, TMBIM2 downregulation by small interference RNA (siRNA) results in increased sensitivity of neurons to Fas-L induced cell death (129) and TMBIM2 knockout (KO) leads to increased caspase-associated cell death and stroke volume after cerebral ischemia in vivo (132).

TMBIM3

TMBIM3, which is also known as LFG1, NRGW, NMDARA1, MGC99687, GRINA and GBP, is a 41 kDa protein which was identified by screening a rat hippocampal cDNA expression library based on immunoreactivity against an antibody against the glutamate binding

protein (133). Unfortunately, little more is known about this protein except that it belongs to a group of 28 genes which are preferentially expressed beneath the marginal zone in the developing cerebral cortex in the mouse (134).

TMBIM4

TMBIM4 has been also named GAAP, S1R, LFG4, ZPRO and CGI-119 and is a 27 kDa protein which is ubiquitously expressed throughout all tissues in the body (135). Its subcellular localization is similar to TMBIM2, thus mainly found in the ER and in the Golgi. Overexpression of human TMBIM4 protects from various apoptotic stimuli like Bax expression, staurosporine, cisplatin, doxorubicin and C_2-ceramide (135) and it reduces histamine-induced Ca^{2+} release by decreasing the ER-Ca^{2+} concentration and by desensitizing IP_3Rs (136).

TMBIM5

TMBIM5 is also known as GHITM, MICS1, DERP2, Myo21, PTD010, HSPC282, FLJ26584 and DKFZp566C0746. It is a 37 kDa protein which is also ubiquitously expressed in all tissues, albeit to a lesser extent in the intestine and in the thymus (137). It possesses a N-terminal signal sequence which might be cleaved in order to regulate the protein's function in vivo (137). On the subcellular level, TMBIM5 resides in the inner mitochondrial membrane where it appears to be crucial for mitochondrial health since its downregulation leads to failure of the mitochondrial network, disorganization of the cristae and release of proapoptotic proteins from the mitochondria (138). In contrast, overexpression of TMBIM5 stabilizes cytochrome c at the inner membrane regardless of the permeabilization of the outer mitochondrial membrane during apoptosis (138).

BI-1 knockout phenotype

In order to study the functions of BI-1, a BI-1 KO mice was created by inserting a proviral sequence in reverse orientation between exon 7 and exon 8 of BI-1 (125). This leads to a truncation of BI-1 after exon seven which means that a small C-terminally truncated part of BI-1 is still detectable in BI-1 KO mice (125). Although all previous publications as well as our second study in this thesis treats BI-1 KO mice as if they had a full knockout of BI-1 and Westphalen et al. showed that C-terminally truncated BI-1 loses its function (107), it is important to keep in mind that a small N-terminal rest of BI-1 remains in these animals, which is still detectable by northern blotting and RT-PCR and might still affect intracellular functions.

BI-1 KO mice have been employed in order to elucidate the function of BI-1 in vivo and no detrimental phenotype or histopathological abnormalities, which would have been expected from the lack of such a conserved protein which is involved in Ca^{2+} regulation and ER stress resistance, have been observed. It has been reported however that BI-1 KO mice injected with tunicamycin, an inhibitor of N-glycosylation in the ER and activator of the UPR, have increased tubular degeneration in their kidneys as well as increased neuronal cell death in the hippocampus (106). The same study also showed that BI-1 KO mice have an increased infarct volume after middle cerebral artery occlusion, a mouse stroke model, which was also linked to increased susceptibility to ER stress (106). On the other hand, BI-1 KO proved to be beneficial to liver regeneration after a partial hepatectomy (139). The authors hypothesized that BI-1 KO hepatocytes are able to enter their cell cycle faster, resulting in faster tissue regeneration, due to the increased ER Ca^{2+} load which was reflected in the increased nuclear translocation of nuclear factor of activated T cells (NFAT), a substrate of the Ca^{2+} sensitive phosphatase calcineurin (139).

Aims of the thesis

In this study, I, and other members of the Methner lab and scientific collaborators, characterized the TMBIM protein family by comparing their primary and secondary structure, their intracellular localization and their effects on the intracellular Ca^{2+} homeostasis. I also characterized the phenotype of BI-1-deficient mice in full detail by comparing its effect on ER stress and Ca^{2+} handling in immune cells.

Publications

The transmembrane BAX inhibitor motif (TMBIM) containing protein family: Tissue expression, intracellular localization and effects on the ER Ca^{2+}-filling state

Dmitrij A. Lisak[1], Teresa Schacht[1], Vitalij Enders[1], Jörn Habicht[1], Santeri Kiviluoto[2], Julia Schneider[1], Nadine Henke[1], Geert Bultynck[2], and Axel Methner[1#]

[1]Focus Program Translational Neuroscience (FTN), Rhine Main Neuroscience Network (rmn²), Johannes Gutenberg University Medical Center Mainz, Department of Neurology, Langenbeckstr. 1, D-55131 Mainz, Germany; [2]KU Leuven, Laboratory of Molecular and Cellular Signaling, Department of Cellular and Molecular Medicine, Campus Gasthuisberg O/N-I bus 802, Herestraat 49, BE-3000 Leuven, Belgium.

The publication is printed as published in BBA Molecular Cell Research:
The transmembrane Bax inhibitor motif (TMBIM) containing protein family: Tissue expression, intracellular localization and effects on the ER CA^{2+}-filling state. Biochim Biophys Acta. 2015 Sep;1853(9):2104–14.
Lisak DA, Schacht T, Enders V, Habicht J, Kiviluoto S, Schneider J, et al.

Author contributions:

Dmitrij Lisak participated in all experiments, the data analysis and creation of the following figures: 1, 2, 3, 4, 5, and 7 and was also responsible for co-authoring the whole manuscript.

Teresa Schacht participated in all experiments and the data analysis of the following figures: 5 and 6.

Vitalij Enders participated in all experiments and the data analysis of figure 7.

Jörn Habicht participated in all experiments, the data analysis and creation of the following figures: 1, 3 and 4.

Santeri Kiviluoto participated in the data analysis and creation of figure 2.

Julia Schneider participated in all experiments and the data analysis of the following figures: 5 and 6.

Nadine Henke participated in all experiments of figure 5 and was consulted for all experiments, which lead to figures 1, 3, 4 and 7.

Geert Bultynck provided scientific advice for experiments, which lead to the figures 1, 2, 3, 4 and 7.

Axel Methner provided scientific advice during all experiments, co-developed the methodology, reviewed the analysis and co-authored the whole manuscript.

Biochimica et Biophysica Acta 1853 (2015) 2104–2114

Contents lists available at ScienceDirect

Biochimica et Biophysica Acta

journal homepage: www.elsevier.com/locate/bbamcr

The transmembrane Bax inhibitor motif (TMBIM) containing protein family: Tissue expression, intracellular localization and effects on the ER CA^{2+}-filling state☆

Dmitrij A. Lisak [a], Teresa Schacht [a], Vitalij Enders [a], Jörn Habicht [a], Santeri Kiviluoto [b], Julia Schneider [a], Nadine Henke [a], Geert Bultynck [b], Axel Methner [a,*]

[a] Focus Program Translational Neuroscience (FTN), Rhine Main Neuroscience Network (rmn²), Department of Neurology, Johannes Gutenberg University Medical Center Mainz, Langenbeckstr. 1, Mainz D-55131, Germany

[b] Laboratory of Molecular and Cellular Signaling, Department of Cellular and Molecular Medicine, KU Leuven, Campus Gasthuisberg O/N-I bus 802, Herestraat 49, Leuven BE-3000, Belgium

ARTICLE INFO

Article history:
Received 18 September 2014
Received in revised form 19 January 2015
Accepted 1 March 2015
Available online 9 March 2015

Keywords:
RECS1
FAIM2
GRINA
GAAP
GHITM
MICS1

ABSTRACT

Bax inhibitor-1 (BI-1) is an evolutionarily conserved pH-dependent Ca^{2+} leak channel in the endoplasmic reticulum and the founding member of a family of six highly hydrophobic mammalian proteins named transmembrane BAX inhibitor motif containing (TMBIM) 1-6 with BI-1 being TMBIM6. Here we compared the structure, subcellular localization, tissue expression and the effect on the cellular Ca^{2+} homeostasis of all family members side by side. We found that all TMBIM proteins possess the di-aspartyl pH sensor responsible for pH sensing identified in TMBIM6 and its bacterial homologue BsYetJ. TMBIM1-3 and TMBIM4-6 represent two phylogenetically distinct groups that are localized in the Golgi apparatus (TMBIM1-3), endoplasmic reticulum (TMBIM4-6) or mitochondria (TMBIM5) but share a common structure of at least seven transmembrane domains with the last domain being semi-hydrophobic. TMBIM1 is mainly expressed in muscle, TMBIM2 and 3 in the nervous system, TMBIM4 and 5 are ubiquitously expressed and TMBIM6 in skeletal muscle, kidney, liver and spleen. All TMBIM proteins reduce the Ca^{2+} content of the endoplasmic reticulum, and all but TMBIM5 also reduce the cytosolic resting Ca^{2+} concentration. These results suggest that the TMBIM family has comparable functions in the maintenance of intracellular Ca^{2+} homeostasis in a wide variety of tissues. This article is part of a Special Issue entitled: 13th European Symposium on Calcium. Guest Editors: Jacques Haiech, Claus Heizmann and Joachim Krebs.

1. Introduction

BAX inhibitor-1 (BI-1) is an anti-apoptotic protein of seven transmembrane domains first identified in a screen for human proteins capable of inhibiting BAX-mediated cell death in yeast [1]. In mammals, its cytoprotective properties are most evident in paradigms of endoplasmic reticulum (ER) stress and ischemia/reperfusion injury. Mammalian cells stably overexpressing BI-1 are protected against ER stress [2,3], and BI-1-deficient mice have increased infarct volumes after occlusion of the middle cerebral artery, a mouse stroke model, and increased sensitivity to tunicamycin-induced kidney toxicity [2]. The inhibitory effect of BI-1 on ER stress appears to be mediated via a direct interaction with inositol-requiring enzyme 1α (IRE1α), an ER resident serine/threonine protein kinase and endoribonuclease, which induces the expression of genes implicated in the unfolded protein response [4]. Lack of BI-1 therefore leads to a defective unfolded protein response and increased susceptibility to ER stress.

BI-1 also plays an important role in maintaining intracellular Ca^{2+} homeostasis. TMBIM6 knockout hepatocytes have an increased ER Ca^{2+} content [2], whereas overexpression of BI-1 causes reduced agonist-induced Ca^{2+} responses due to a reduced ER Ca^{2+} content [5]. A peptide corresponding to the semi-hydrophobic seventh transmembrane domain of BI-1 is capable of causing Ca^{2+} release from biological and artificial membranes, and this is abolished by the mutation of a single aspartic acid residue within this potential pore domain [6]. Also, full-length BI-1 with this mutation loses its ability to lower the ER Ca^{2+} content [6], suggesting that BI-1 is a Ca^{2+} leak channel in the ER membrane. Interestingly, decreases or increases in the intracellular pH shut down Ca^{2+} flux through the BI-1 channel but not in the pore-dead D213A mutant [7]). These observations are supported by a recent study characterizing the three-dimensional structure and pH-sensitive Ca^{2+}-flux properties of a bacterial homologue of BI-1, BsYetJ [8]. BsYetJ possesses a di-aspartyl pH sensor in its C-terminal pore domain (Asp171–

☆ This article is part of a Special Issue entitled: 13th European Symposium on Calcium. Guest Editors: Jacques Haiech, Claus Heizmann and Joachim Krebs.

* Corresponding author at: Department of Neurology, Johannes Gutenberg University Medical Center Mainz, Langenbeckstr. 1, Mainz D-55131, Germany. Tel.: +49 6131 17 2695; fax: +49 6131 17 5967.
E-mail address: axel.methner@gmail.com (A. Methner).

http://dx.doi.org/10.1016/j.bbamcr.2015.03.002
0167-4889/

Asp195), which corresponds to two aspartate residues in the pore domain of Bl-1 (Asp188–Asp213). We therefore recently proposed a homology model of Bl-1 and BsYetJ where the pore can be open (neutral pH), open and sealed (acidic pH) or closed (basic pH) depending on the cytosolic pH, explaining the bell-shaped effects of pH on Ca^{2+} flux mediated by Bl-1 [9].

Bl-1 is the founding member of a family consisting of a total of six Bl-1-like proteins that have been described based on a signature pattern (Prosite PDOC00957) corresponding to a region that starts with the beginning of the third transmembrane domain and ends in the middle of the fourth: G – *x*(2) – [LIVM] – [GC] – P – *x* – [LI] – *x*(4) – [SAGDT] – *x*(4,6) – [LIVM](2) – *x*(2) – A – *x*(2) – [MG] – T – *x* – [LIVM] – *x* – F. These Bl-1 family proteins have been identified in several instances by different groups and were given a wide variety of descriptive names. The nomenclature accepted by the HUGO gene nomenclature committee for this gene family is *TMBIM* (transmembrane BAX inhibitor motif containing) *1*-6 with *Bl-1* being *TMBIM6*. This nomenclature will be used for the remainder of the manuscript.

TMBIM1 (also known as RECS1, PP1201, LFG3, MST100, MSTP100) is a 35 kDa protein predicted to contain seven transmembrane domains located in endosomal/lysosomal membranes and ubiquitously expressed in brain, heart, lung, liver, kidney, stomach, intestine, ovary, uterus, skeletal muscle, skin, adipose tissue, but not in the thymus, spleen or testis [10]. TMBIM1/RECS1 plays a protective role in vascular remodeling and its deficiency induces susceptibility to cystic medial degeneration in aged mice [10]. TMBIM1/PP1201 also protects against Fas-mediated apoptosis by reducing Fas expression on the cell surface [11].

TMBIM2 (also known as NMP35, LFG, FAIM2, LFG2, NGP35, KIAA0950) is a 35 kDa protein also predicted to contain seven transmembrane helices. Intracellularly, TMBIM2 is located in the ER and in the Golgi apparatus as well as in lipid raft microdomains of the plasma membrane [12,13]. TMBIM2/NMP35 is predominantly expressed in the nervous system [14], most prominently in dendritic processes and in a subset of synapses at the postsynaptic membrane and density [15]. TMBIM2/LFG protects from cell death induced by the FAS ligand, but not by TNFα [12,13], and downregulation of endogenous TMBIM2/LFG by small interfering RNA increases sensitivity of neuronal cells to Fas ligand-induced cell death [12]. The lack of TMBIM2/FAIM2 increases caspase-associated cell death and stroke volume after cerebral ischemia in vivo [16].

TMBIM3 (also known as LFG1, HNRGW, NMDARA1, MGC99687, GRINA, GBP) is a 41 kDa protein predicted to have seven transmembrane helices first identified by expression cloning of a rat brain library based on immunoreactivity to an antibody against the glutamate-binding protein, a part of an NMDA-receptor-associated complex [17]. It was also identified as one out of 28 genes preferentially expressed beneath the marginal zone of the developing cerebral cortex of mice [18]. TMBIM3/GRINA is upregulated during ER stress and protects against ER stress-mediated cell death via a mechanism that involves TMBIM6 and IP_3Rs [19].

TMBIM4 (also known as GAAP, S1R, LFG4, ZPRO, CGI-119) is a 27 kDa protein predicted to contain seven transmembrane domains. TMBIM4/GAAP is expressed in many human tissues such as the heart, brain, placenta, lung, liver, skeletal muscle, kidney, pancreas, spleen, thymus, prostate, testis, ovary, small intestine and colon. Intracellularly, it is localized in membranes of the ER and Golgi apparatus. It was first identified in humans as GAAP with a highly conserved counterpart found in the vaccinia virus. The function of GAAP most closely resembles that of TMBIM6; human GAAP overexpression inhibits apoptosis triggered by intrinsic and extrinsic stimuli [20] and reduces histamine-induced Ca^{2+} release from intracellular stores by lowering the Ca^{2+} content of these stores and decreasing the efficacy of IP_3 [21].

TMBIM5 (also known as GHITM, MICS1, DERP2, My021, PTD010, HSPC282, FLJ26584, DKFZp566C0746) is a 37 kDa protein predicted to contain eight transmembrane domains. TMBIM5/GHITM is expressed ubiquitously in most tissues but less in the intestine and thymus [22]. Cleavage of a proposed N-terminal signal peptide results in its mature form in vivo [22]. TMBIM5/MICS1 appears to reside in the inner

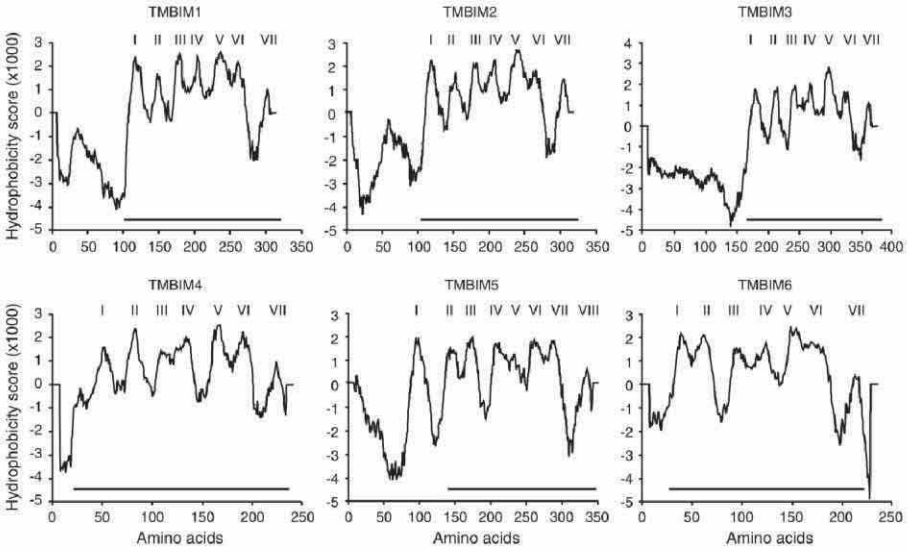

Fig. 1. The secondary protein structure of the TMBIM family. TMBIM1-6 all have at least 7 transmembrane domains, and the last domain is always much less hydrophobic than the others. Hydrophobicity plots of TMBIM1-6 were generated by TMpred. Putative transmembrane domains are indicated by roman numerals. The TMBIM6 homology domain is indicated by a horizontal line.

mitochondrial membrane and its downregulation results in the maintenance of the normal mitochondrial network and disorganization of cristae failing [23]. TMBIM5/MICS1 downregulation induces a rapid release of pro-apoptotic proteins from the mitochondria during apoptosis, whereas its overexpression induces a stabilization of cytochrome *c* at the inner membrane, irrespective of the permeabilization of the outer membrane during apoptosis [23].

In this work, we first studied the primary structure, phylogenetic relation and hydrophobicity of all mammalian TMBIM family proteins and BsYetJ. This revealed two groups of very similar structure and a complete conservation of the di-aspartyl sensor, suggesting comparable functions in the maintenance of intracellular Ca^{2+} homeostasis. We then compared tissue expression, intracellular localization and the effects on intracellular Ca^{2+} homeostasis of these proteins in parallel experiments.

2. Materials and methods

2.1. Cloning of TMBIM1-6 and generation of stable cell lines

TMBIM1-6 expressing HT22 cells were generated with the PiggyBac transposon system. cDNA sequences of TMBIM1-6 were generated by PCR and inserted into the pPB-CAG-EBNXN vector (obtained via the Sanger institute), N-terminally tagged with a hemagglutinin (HA) epitope and C-terminally followed by an internal ribosomal entry site (IRES) followed by the yellow fluorescent protein Venus. In TMBIM5-

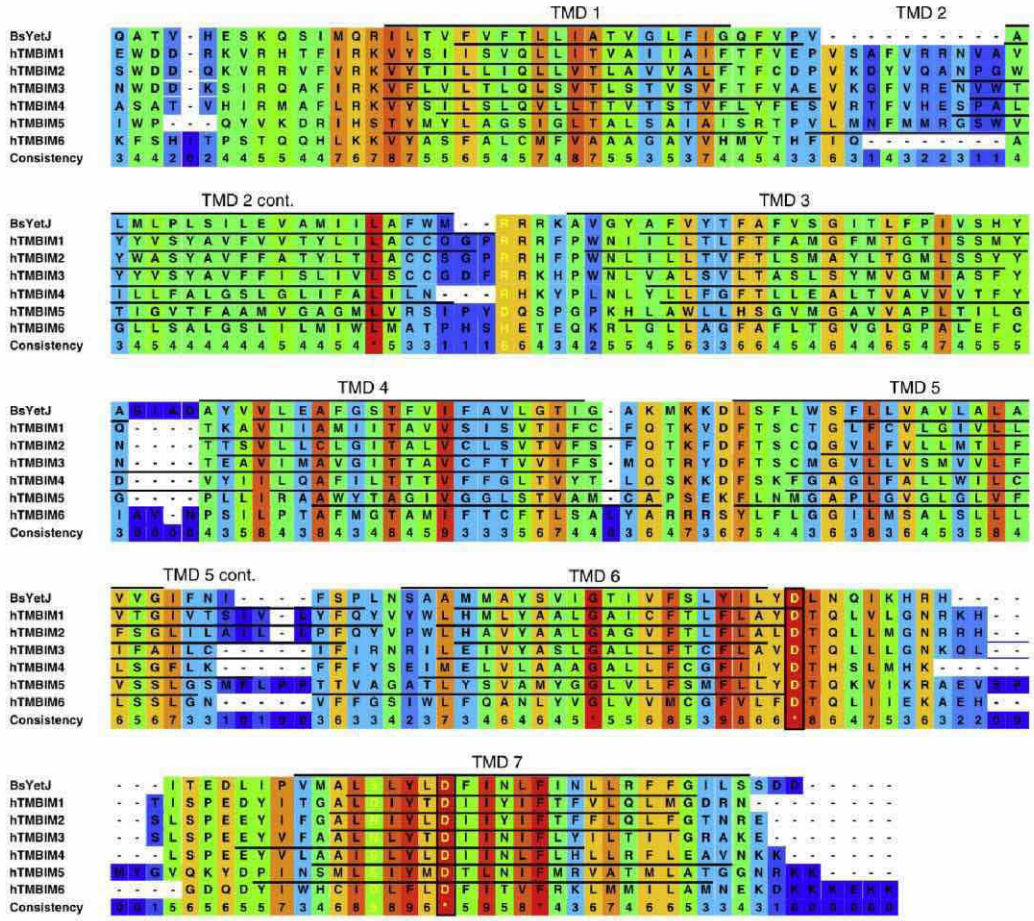

Fig. 2. Alignment of TMBIM proteins with the bacterial TMBIM6 ortholog BsYetJ. Multiple protein sequence alignment of the TMBIM protein family and the bacterial homologue BsYetJ was performed using PRALINE with the BLOSUM62 scoring matrix. The colors indicate the least conserved (blue) to the most conserved residues (red). Non-aligning N-termini of each protein were removed. Key residues previously shown to be important in gating pH-dependent Ca^{2+} leak by BsYetJ and putative corresponding residues in TMBIM6/BI-1 (H78, D188, D209 and D213) are shown in yellow. Note that only residues corresponding to D188 and D213 in TMBIM6 are strictly conserved across all proteins. Transmembrane domains (TMD) according to TMpred prediction are indicated by black lines.

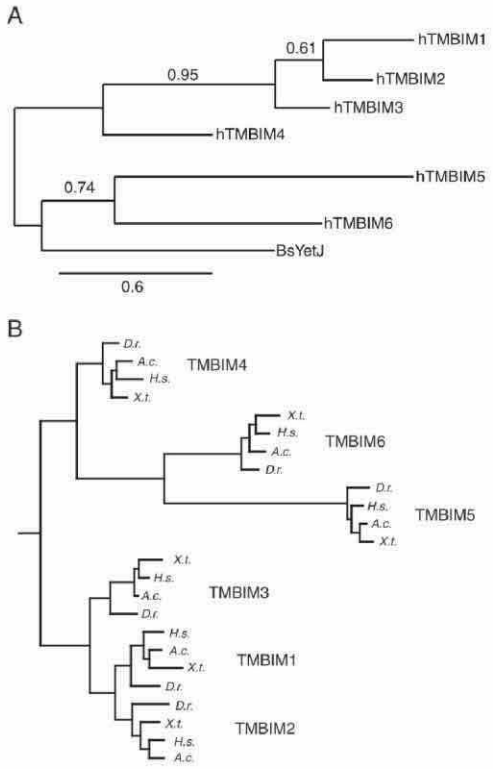

Fig. 3. TMBIM proteins share a common structure and fall into two separate groups. (A) Phylogenetic analysis of the sequence alignment of the TMBIM family and the bacterial homologue BsYetJ shows that BsYetJ is closest related to TMBIM5 and TMBIM6. The branch support values are indicated above the branches. (B) TMBIM6 clusters together with TMBIM5 and TMBIM4 and TMBIM1 clusters together with TMBIM2 and TMBIM3. TMBIM1 and TMBIM2 are the two most closely related proteins. TMBIM6 and TMBIM5 are more closely related to each other than to TMBIM4. Both phylogenetic trees were created using the Maximum Likelihood algorithm with the BLOSUM62 substitution matrix and 100 bootstrap trials.

mCherry, mCherry was cloned in frame C-terminally to TMBIM5. Each of these constructs was co-transfected in a ratio of 1:4 with a plasmid encoding a transposase into HT22 cells using Lipofectamine 2000 (Invitrogen) according to the manufacturer's protocol. The cDNA constructs, flanked by PiggyBac transposon sites, were stably inserted into the genome and 48 h after transfection Venus-positive cells were selected on a MoFlo XDP (Beckman-Coulter) cell sorter. After three to four repeated rounds of cell sorting, approximately 99% of cells were positive for Venus fluorescence and considered as stably transfected. Successful expression was confirmed by immunoblotting using an α-HA antibody (Sigma H6908, 1:2000).

2.2. Phylogenetic analysis and bioinformatic analysis

Multiple sequence alignment focusing on amino acid conservation was performed using the online tool PRALINE using the Blosum62 scoring matrix with default settings [24]. Alignments were preprocessed using PSI-BLAST with 3 iterations and an E-value cutoff of 0.01 [25]. The phylogenetic tree was constructed using the online tool phylogeny.fr [26]. In short, the tool aligns the sequences using MUSCLE (3.7) with default settings [27]. After alignment, ambiguous regions were removed by Gblocks (v0.91b) and reconstructed in a phylogenetic tree using the maximum likelihood method in PhyML (v3.0 aLRT). Graphics were created using TreeDyn (v198.3). The multiple sequence alignment of TMBIMs across species was created using MAFFT version 6 using the E-INS-i setting and the alignment trimmed with JalView 2.5 at a cutoff value of 85% gaps. For the analysis of the secondary structure of the TMBIM family, the amino acid sequence of each TMBIM protein family member was entered as plain text into the "Prediction of Transmembrane Regions and Orientation" (TMpred) application (ExPASy), and the prediction graphic of the preferred model with the highest score was chosen. The presence of signal peptides was evaluated with SignalP 4.0 [28] and of mitochondrial targeting sequences with MitoProt II [29].

2.3. Expression analysis

Wild-type C57/BL6 animals were sacrificed, and RNA was harvested from tissue samples with the ZN RNA Mini Prep Kit (ZYMO Research) according to the manufacturer's protocol. RNA was transcribed to

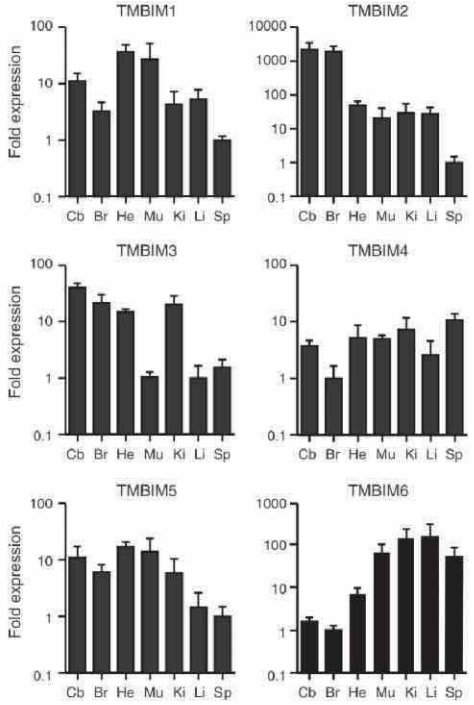

Fig. 4. Tissue expression of TMBIM family members. TMBIM1 is mainly expressed in the heart and in muscle and TMBIM2 and TMBIM3 are mostly found in the central nervous system where TMBIM6 is least expressed. TMBIM4 and TMBIM5 are relatively evenly distributed throughout the tissues. Expression of TMBIM 1-6 as assessed by quantitative PCR in various tissues shown as the mean fold ± SEM from 3 to 6 mice per protein measured in triplicate. The fold was calculated with the $2^{-[delta][delta]C1}$ method and was normalized to the tissue with the lowest expression.

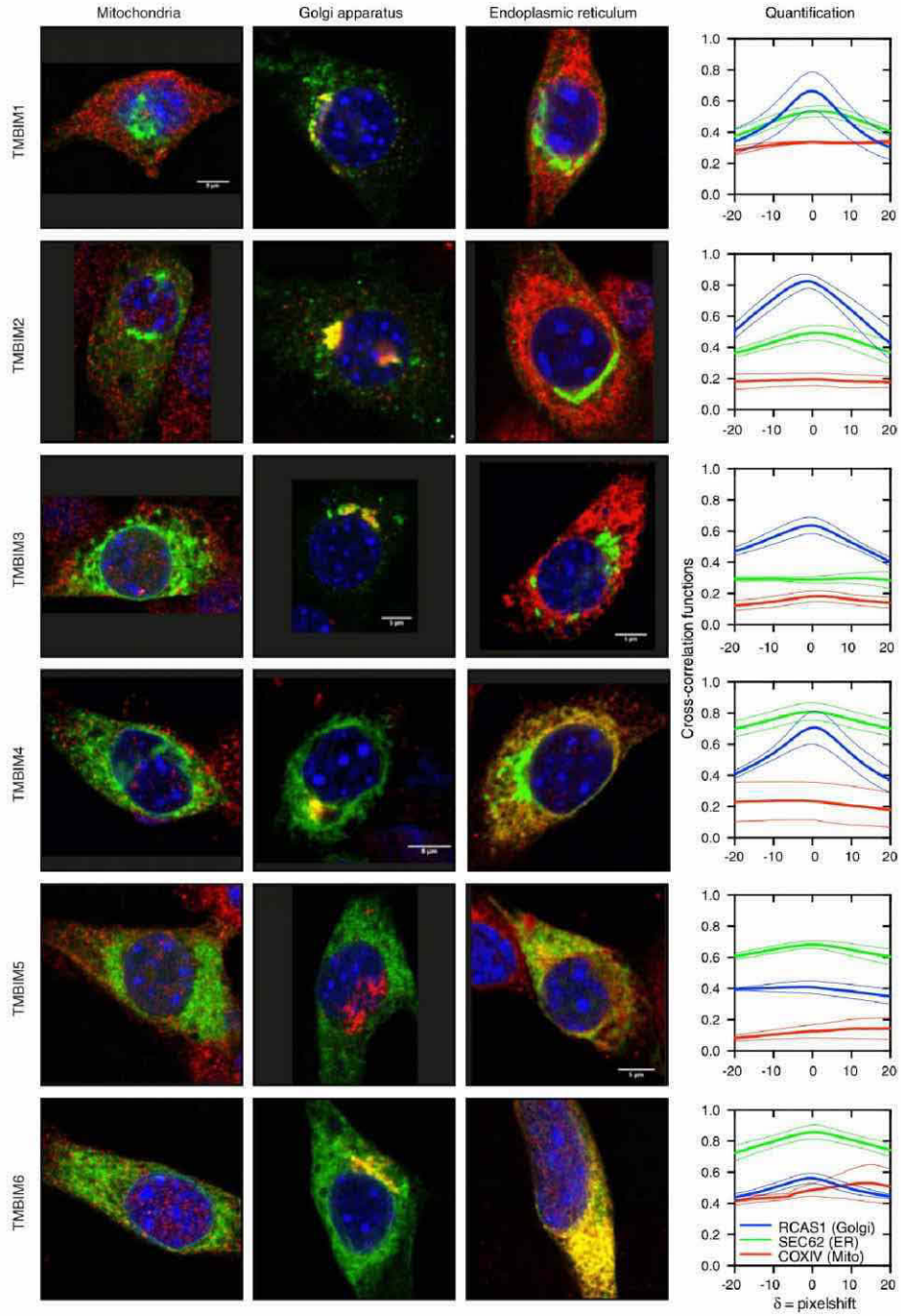
Mitochondria
Golgi apparatus
Endoplasmic reticulum
Quantification
TMBIM1
TMBIM2
TMBIM3
TMBIM4
TMBIM5
TMBIM6
Cross-correlation functions
RCAS1 (Golgi)
SEC62 (ER)
COXIV (Mito)
δ = pixelshift

cDNA with the High Capacity cDNA Reverse Transcription Kit (Applied Biosystems) using 2 μg of RNA. Quantitative PCR (qPCR) was employed to measure DNA levels in a 7500 Real Time System (Applied Biosystem), and the Universal Probe Library by Roche was used with the following primers: TMBIM1 forward: 5′-CAATGCCCATGAACTACGG-3′, TMBIM1 reverse: 5′-CCAGGACGAAAGCTGTCACT-3′, TMBIM2 forward: 5′-CCAC GCGGTCTATGCTGTA-3′, TMBIM2 reverse: 5′-CCATCAGCAACTGGGTAT CA-3′, TMBIM3 forward: 5′-CCGCATCCTGGAGATTGTAT-3′, TMBIM3 reverse: 5′-TGCTTGTTCCCCAGGAGTAG-3′, TMBIM4 forward: 5′-ACCTCT TCCTGCACCTGTTG-3′, TMBIM4 reverse: 5′-TCTCTGAACACTGCTCGGTT AC-3′, TMBIM5 forward: 5′-CTTGGAACCATCAATGGAAAA-3′, TMBIM5 reverse: 5′-AGAGCGCTCCAAGACCAAC-3′, TMBIM6 forward: 5′-GGGC CTATGTCCAGTGGT-3′, TMBIM6 reverse: 5′-CCATCAGCCAAATCATCA AG-3′. HPRT was used as an endogenous housekeeping gene. Fold expression was calculated with the $2^{-[delta][delta]Ct}$ method, and the expression of each protein was normalized to the tissue with the lowest fold.

2.4. Immunofluorescence

HT22 cells were plated in six-well tissue culture plates and grown for 24 h. Cells were then transiently transfected with the pPBCAG:HA-POI-IRES-Venus plasmids carrying the various TMBIM proteins using Attractene Transfection Reagent (Qiagen). After 24 h incubation, 75,000 cells were seeded on 12 mm coverslips and were grown for another 24 h. Cells were then washed with DPBS (Sigma-Aldrich) and fixed with 4 % paraformaldehyde for 20 min at 4 °C. Afterward, the cells were washed four times with DPBS (+0.1 M Glycin and 4 mM $MgCl_2$) for 5 min and then permeabilized and blocked with PSS (1x DPBS, 5% FCS, 0.1% Saponin) for 1 h at room temperature. Cells were incubated with the indicated primary antibodies (rabbit COXIV (1:750, Cell Signaling); rabbit RCAS1 (D2B6N, 1:100, Cell Signaling), mouse HA-Tag (6E2, Alexa Fluor 488 conjugate, 1:400, Cell Signaling), rabbit Sec62, (1:500, kind gift from Prof. Zimmermann, Universität des Saarlandes) in PSS overnight at 4 °C. After washing twice with PSS for 15 min, cells were incubated with the secondary antibody goat anti-rabbit Alexa568 (1:500, Milipore) for TMBIM 1-6 or goat anti-rabbit Alexa647 (1:1000, Invitrogen) for TMBIM5-mCherry in PSS for 1 h at 4 °C and washed three times with PSS for 5 min. The cell nuclei were stained with DAPI (Life Technologies) for 10 min and washed again twice with PSS. Coverslips were removed from the culture plate, washed with Aqua dest. and fixed on a microscope slide with mounting medium (Dako). Images were taken on a confocal microscope (SP5, Leica). Co-localization was quantified with the JACoP software (ImageJ) and the van Steensel approach [30].

2.5. Immunoblotting

HT22 cells were lysed in ice-cold RIPA buffer (Invitrogen) containing mini complete protease inhibitor cocktail (Roche) and centrifuged for 30 min at 16,000 g. Protein concentrations were determined using the bicinchoinic acid assay protein quantification kit (Interchim), samples were incubated for 10 min with 5x SDS loading dye with 8 M UREA. Fifty micrograms of each sample was loaded on polyacrylamide gels (Thermo Fisher Scientific), transferred onto nitrocellulose membranes with the iBlot System (Invitrogen) and blocked in 3% nonfat dry milk in PBS containing 0.5% Tween-20 (PBS-T). The membranes were incubated at 4 °C overnight with primary antibodies diluted 1:3000 for Anti-HA (ab9112, 1:3000, Abcam), Anti-Actin (MAB1501, clone C4, 1:4000, Millipore) or Anti-RFP (5 F8, 1:1000, Chromotek). Anti-mouse, anti-rabbit IgG (Fc) or Anti-rat infrared fluorescence conjugated secondary antibodies (Licor, 1:30.000) were added following washing with PBS-T and incubated for 1 h at RT. The membranes were scanned for infrared fluorescence at 680 and 800 nm using the Odyssey system (Licor).

2.6. Cytosolic Ca^{2+} measurements using Fura2

Fura2 Ca^{2+} imaging experiments were conducted on a BD Pathway 855 High Content Imaging System (BD Biosciences). HT22 cells were seeded in a density of 5000 cells/well on 96-well imaging plates (BD Bioscience) for 24 h and loaded with 5 μM Fura2-AM (Molecular Probes) in HBSS at 37 °C for 20 min prior to the experiment. Measurement was performed with excitation at 340 nm and 380 nm for radiometric analysis, and pictures were taken with a delay of 5 s. After baseline recording, ER Ca^{2+} stores were depleted in EGTA buffer (Ca^{2+}-free HBSS supplemented with 0.5 mM EGTA, 20 mM HEPES, 1 mM $MgCl_2$ and 1 g/l Glucose) with 2 μM thapsigargin for 8 min. Each cell type was measured at least three times and analyzed with Attovision 1.7.1.0 (BD Bioscience). Calibration was performed after each measurement, and Fura2 values were converted into absolute Ca^{2+} concentrations by the formula where the $k_d = 224$ nM, the min*Ratio* was measured in EGTA, max*Ratio* was measured in 20 mM Ca^{2+} and max380 and min380 represent the maximum and minimum values at 380 nm.

2.7. Statistical analysis

Data were analyzed as mean ± SEM and the statistical significance using two-tailed *t*-tests or analysis of variance (ANOVA) with Tukey's multiple comparison test as indicated.

3. Results

3.1. TMBIM proteins share a common structure and fall into two separate groups

We started by comparing the secondary protein structure of the human TMBIM family using TMpred, an algorithm that makes predictions about potential membrane-spanning regions and their orientation. This revealed a remarkably similar structure in all family members with at least seven domains with high hydrophobicity and an N-terminus of different lengths. Of note, in all TMBIM proteins, the last transmembrane domain is less or semi-hydrophobic as reported for TMBIM6 [6] and TMBIM4 [31]. These studies favored a six-transmembrane domain model with a putative reentrant loop at the C terminus and both termini located in the cytosol for these two proteins. Only TMBIM5, the only family member reported to have an N-terminal signal sequence that is cleaved in order to ensure proper protein expression and function [22], contains an additional transmembrane domain of significant hydrophobicity preceding the TMBIM6 homology region (Fig. 1). This domain, however, starts at amino acid 82 and likely does not serve as a signal peptide sequence, an aspect that is studied in more detail in this manuscript. We next aligned the sequences of all TMBIM proteins with the bacterial TMBIM6 ortholog BsYetJ using the online tool PRALINE. This

Fig. 5. Group-specific expression in the Golgi apparatus or the ER. TMBIM1-3 mainly co-localized with a Golgi apparatus marker and TMBIM4-6 with an ER marker. None of the N-terminally tagged TMBIM family member co-localized with mitochondria. HT22 cells were transiently transfected with HA-tagged TMBIM 1-6 and stained with primary antibodies against HA and either COXIV (mitochondria), RCAS1 (Golgi apparatus) or Sec62 (ER). FITC-labeled secondary antibodies against HA (green) and Cy3-labeled secondary antibodies against COX IV, RCAS1 and Sec62 (red) were used to assess intracellular localization of TMBIM1-6 with confocal microscopy. The scale bar corresponds to 5 μm. The JACoP software with the van Steensel approach was employed to quantify co-localization.

revealed a strong conservation of the first five amino acids preceding transmembrane domain (TMD) 1 and the TMD 6 and 7, respectively, 2 and 7/8 in TMBIM5. All proteins contain the completely conserved di-aspartyl pH sensor identified in BsYetJ [8]. Besides this, only two other residues were completely conserved in all proteins: a leucine in TMD 2 and a phenylalanine in TMD 7 (Fig. 2). We next generated a phylogenetic tree to clarify the relationship of the TMBIM family members to BsYetJ, which revealed that TMBIM6 is the closest relative to this ancestral protein (Fig. 3A). To more clearly delineate the relationship of the TMBIM family members to each other, we then constructed a phylogenetic tree using a completely unrelated TMD protein as an outlier and 100 bootstrap trials. We also chose orthologs of TMBIM1-6 from four evolutionarily separated vertebrates (*Homo sapiens*, *Anolis carolinensis*, *Xenopus tropicalis* and *Danio rerio*) to avoid species-specific changes or artifacts. The resulting phylogenetic tree clearly separated the six TMBIM family members and revealed two separate clades: group I (TMBIM1, TMBIM2 and TMBIM3) and group II (TMBIM4, TMBIM5 and TMBIM6). Within the groups, TMBIM1 and 2 and TMBIM5 and 6 clustered together (Fig. 3B). In summary, these results suggest a close homology of all TMBIM family members and reveal that the previously identified di-aspartyl pH sensor is conserved among all TMBIM proteins.

3.2. Tissue expression of TMBIM family members

The hydrophobic nature of the TMBIM family renders the generation of specific antibodies difficult. Despite considerable efforts, no functional antibodies that can distinguish between TMBIM6 deficient, and wild-type tissues are currently available (see supplementary data in [7]). We therefore used quantitative RT-PCR to quantitate the expression of the TMBIM family members in a comparable manner in the cerebellum, brain, heart, femoral muscle, kidney, liver and spleen. The housekeeping gene hypoxanthine-guanine phosphoribosyltransferase (*hprt*) served as an endogenous control, and the expression of each transcript was normalized to the tissue with the lowest expression. This revealed that TMBIM1 has its highest expression in the two muscle tissues, TMBIM2 and TMBIM3 in the two tissues from the central nervous system, TMBIM4 and TMBIM5 are rather ubiquitously expressed and TMBIM6 predominantly in skeletal muscle, the kidney, liver and spleen (Fig. 4).

3.3. Group-specific expression in the Golgi apparatus or the ER in HT22 cells

A number of different intracellular locations for each TMBIM family member were proposed mainly based on bioinformatic predictions. We decided to compare the intracellular localization of all family members in a comparable and quantitative manner and transiently transfected HT22 cells with N-terminally HA-tagged TMBIM1-6, which were then stained with an α-HA antibody and antibodies against the Golgi marker protein receptor binding cancer antigen expressed on SiSo cells (RCAS1) [32], the ER marker protein SEC62 [33] and the mitochondrial protein cytochrome *c* oxidase IV (COXIV) [34]. Co-localization was quantified by the van Steensel cross-correlation function and the Pearson coefficient [30]. This proved an interesting dichotomy in that group I (TMBIM1-3) showed a predominant localization in the Golgi apparatus and group II (TMBIM4-6) in the endoplasmic reticulum (Fig. 5). Because of the reported mitochondrial localization of TMBIM5 [23] and the fact that its secondary structure differs from the other family members by the presence of an additional transmembrane domain preceding the TMBIM6 homology domain (Fig. 1), we decided to study this protein in more detail. Yoshida et al. [22] reported the presence of an N-terminal signal sequence, which we could not verify using the SignalP 4.0 detection method [28] (Fig. 6A). We, however, noted an enrichment of arginine, leucine, serine and alanine residues (shown in blue in Fig. 6A), a net charge of +18 and a predominance of basic amino acids in the TMBIM5 N-terminus. These are all characteristics of a mitochondrial targeting sequence [29] and an analysis with MitoProt II indeed indicated the presence of a potential cleavage site at position 57 of TMBIM5 (Fig. 6A). In the experiments described above, we tagged TMBIM5 with the 11-amino acid HA tag at its N-terminal end and used an antibody against this tag to determine the subcellular localization. Because we observed a band of the predicted size by immunoblotting this means that at least a part of TMBIM5 remains uncleaved and that this uncleaved TMBIM5 resides in the ER whereas cleaved TMBIM5 could reside in mitochondria. To distinguish between these two possibilities, we now cloned the red fluorescent mCherry protein in frame with the C terminus of TMBIM5 and studied the subcellular localization by co-localizing mCherry fluorescence with the organelle markers. In comparison to the N-terminally tagged protein, this revealed a reduced localization in the ER, an absent localization in the Golgi apparatus and a significant co-localization with the mitochondrial marker protein cytochrome *c* oxygenase IV (Fig. 6B). Also, when we immunoblotted transiently transfected TMBIM5-mCherry and stained with an α-mCherry antiserum, we observed two distinct bands of equal density but only one band when stained with an α-HA antiserum (Fig. 6C). This means that TMBIM5 can indeed be cleaved after the predicted mitochondrial targeting signal and translocate to mitochondria.

3.4. Profound effects of TMBIM 1-6 on the intracellular Ca^{2+} homeostasis in HT22 cells

Ca^{2+} is an important signaling molecule in the cytosol of virtually all cell types and several members of the TMBIM protein family, especially TMBIM6, have been reported to play a role in the control of intracellular Ca^{2+} homeostasis. We investigated the effect of each family member on intracellular Ca^{2+} by stably overexpressing HA-tagged TMBIM1-6 in HT22 cells. The expression of each protein was confirmed by immunoblotting (Fig. 7A). Ca^{2+} kinetics were measured in a high-throughput microscope which allows simultaneous measurement of several hundred cells independently. The ER Ca^{2+} content was measured by applying thapsigargin, an irreversible inhibitor of the SERCA pumps in the ER membrane, causing immediate Ca^{2+} efflux from the ER. In the presence of the extracellular Ca^{2+} buffer, Ca^{2+} influx from the extracellular medium is prevented and the thapsigargin-releasable Ca^{2+} in the cytosol is solely originating from the ER Ca^{2+} stores. The TMBIM-expressing HT22 cells were compared to HT22 cells that only expressed the empty vector. Fig. 7B shows the combined Ca^{2+} traces of each cell line and Fig. 7C a quantitative analysis of the baseline cytosolic [Ca^{2+}] and the peak [Ca^{2+}] reached after addition of thapsigargin. In these experiments, we examined one cell line after another and always compared against the control cell line explaining the higher number of analyzed cells. This revealed that all TMBIM family members reduced the ER Ca^{2+} content and all but TMBIM5 also reduced the basal Ca^{2+} concentration in the cytosol.

4. Discussion

This is the first work systematically describing the relationship, secondary structure, tissue expression, intracellular localization and effects on cellular Ca^{2+} homeostasis of the TMBIM protein family sharing the evolutionary conserved motif UPF0005. All family members are characterized by at least six transmembrane domains and an additional C-terminal domain that may serve as a reentrant loop, as previously proposed for TMBIM6 [6] and TMBIM4 [31]. Our phylogenetic analysis demonstrated two groups consisting of TMBIM1-3 on one hand and TMBIM4-6 on the other, which differ mainly in regard to intracellular localization. We could confirm that TMBIM1 [11], TMBIM2 [12] and TMBIM3 [19,35] are mainly located in the Golgi apparatus and to a lesser extent in the ER. TMBIM4 and TMBIM5 are more closely related to TMBIM6 and these three have a predominant localization in the ER. Gubser et al. [20] also found TMBIM4 primarily located in the ER and

partly in the Golgi apparatus in line with our results. Regarding TMBIM5, a previous study suggested that it is exclusively located in the mitochondria [23]. We indeed identified the presence of a mitochondrial targeting sequence in this protein leading to cleavage after residue 57 and therefore repeated our co-localization experiments using C-terminally tagged TMBIM5. This still demonstrated a predominant ER localization but also a substantial mitochondrial localization not present in the co-localization experiments with the N-terminal tag. We therefore assume that TMBIM5 can be localized at different organelles depending on the efficiency of cleavage that could be altered by the presence of the small HA tag at its N-terminus as suggested earlier [22]. It should be noted, however, that a bioinformatic analysis using PSORT II also suggested a predominant ER localization. Interestingly, a splice isoform of TMBIM5 (GenBank accession EAW80370.1) with 243 amino acids adding a novel N-terminus starting 10 amino acids before the TMBIM6 homology domain can be found in databases. Such a protein would most probably not localize to mitochondria. Finally, TMBIM6 was undoubtedly expressed in the ER in line with previous data using EGFP- [1,5] and mCherry-tagged [7] TMBIM6.

In line with Zhao et al., we detected the lowest expression of TMBIM1 in the spleen where it was below the detection limit of northern blotting. We observed the highest expression of TMBIM1 in the heart and in the skeletal muscle, followed by the cerebellum, which is similar to the expression pattern previously obtained by northern blotting [10]. Our results are also in line with previous observations from northern blotting [13,14], RT-PCR [12] and immunohistochemistry [15] that TMBIM2 is mainly expressed in the central nervous system. TMBIM3 was also found to be mainly expressed in the central nervous system and to a lower extent in the kidney by northern blotting and RT-PCR [35], supporting our own results which show a comparable expression pattern. TMBIM4 has been reported by PCR analysis to be ubiquitously expressed throughout all tissues with its lowest expression being in the brain [20], which exactly matches our results. Northern blot analysis showed that TMBIM5 is highly expressed in the brain, heart, liver kidney and muscle with lower expression in the intestines and in the thymus [22]. Our data support this analysis since we observed a similar expression pattern, although we measured a lower expression in the liver compared to the brain, heart and skeletal muscle. TMBIM6, also known as BI-1, is the best-characterized member of the TMBIM family yet. We were able to confirm its ubiquitous expression throughout the body [36–38] with the exception of the nervous system.

In line with the conserved overall structure and the homology with TMBIM6, we observed that the overexpression of each protein resulted in a decreased thapsigargin-releasable Ca^{2+} pool from the ER. A lowering effect on the ER Ca^{2+} content has been previously reported for TMBIM3 [19], TMBIM4 [21] and TMBIM6 [5]. Yet the impact of TMBIM1, TMBIM2 and TMBIM5 on intracellular Ca^{2+} homeostasis has not been reported before, but our data are now the first to indicate that these proteins indeed influence the Ca^{2+} handling of the ER. Westphalen et al. [5] transfected CHO cells with TMBIM6-EGFP and measured Ca^{2+} traces after ATP stimulation with the ratiometric Ca^{2+} dye Fura2-AM and the ER Ca^{2+} content after treatment with thapsigargin using the ER cameleon D1ER. Rojas-Rivera et al. stably

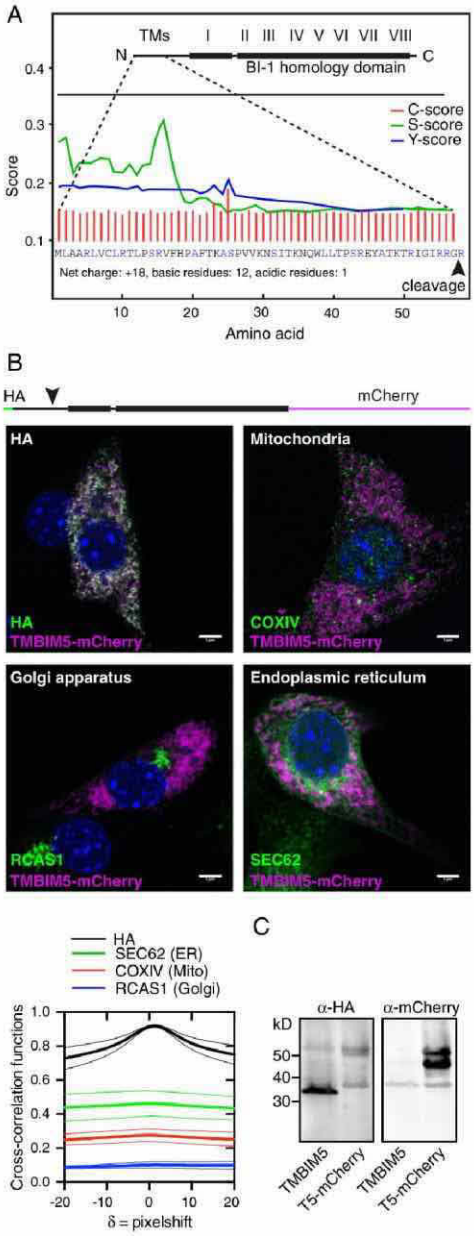

Fig. 6. Detailed analysis of the subcellular localization of TMBIM5. (A) TMBIM5 contains no signal peptide but a mitochondrial targeting sequence with a proposed cleavage after residue 57. The amino acid sequence was analyzed by SignalP 4.0 and MitoProt II. None of the scores reported by SignalP 4.0 (C, S, Y scores) reaches the threshold necessary for classification as signal peptide shown as horizontal line. However, the N-terminus possesses a net positive charge and 21 out of 57 residues typically found in mitochondrial targeting sequences (shown in blue). The predicted cleavage site is indicated by an arrow. (B) C-terminally mCherry-tagged TMBIM5 localizes to mitochondria and the ER. HT22 cells were transiently transfected with TMBIM5 tagged on both sides and stained with primary antibodies against HA and mCherry, or mCherry and either COXIV (mitochondria), RCAS1 (Golgi apparatus) or Sec62 (ER). FITC-labeled secondary antibodies against HA or the organelle markers (green) and Cy3-labeled secondary antibodies against mCherry (magenta) were used to assess intracellular localization with confocal microscopy. The scale bar corresponds to 5 μm. The JACoP software with the van Steensel approach was employed to quantify co-localization. (C) TMBIM5 is cleaved. HT22 cells were transiently transfected with HA-TMBIM5-mCherry and immunoblotted. The mCherry-stained blot reveals two bands corresponding to cleaved and uncleaved TMBIM5 whereas the HA-stained blots shows only a single band. Size is indicated.

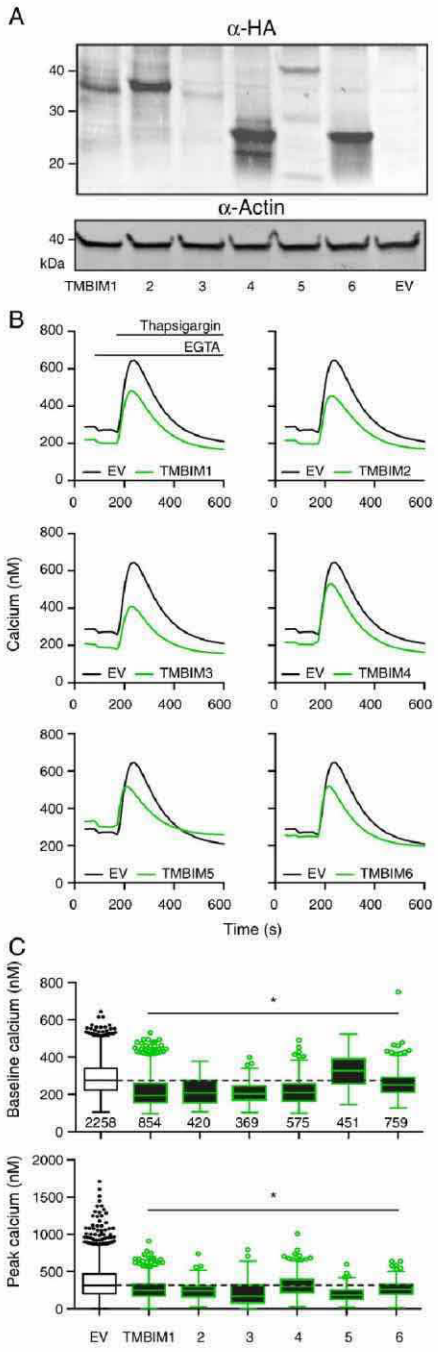

overexpressed TMBIM3-myc in mouse embryonic fibroblasts and measured Ca^{2+} release with Fluo4-AM after ATP stimulation [19]. HA-tagged TMBIM4 was stably overexpressed in U2OS cells, which were stimulated with histamine and Ca^{2+} was measured with Fura2-AM by de Mattia et al. [21]. In all cases, the overexpression of the TMBIM family members resulted in a decreased agonist-inducible Ca^{2+} pool, similarly to the reduced thapsigargin-releasable pool, which we observed after stably overexpressing TMBIM1-6 in HT22 cells. This property likely is not limited to mammalian TMBIM proteins since the overexpression of viral TMBIM4 has been shown to lower the ionomycin-releasable Ca^{2+} in cells [39]. However, it is important to note that the impact of TMBIM on agonist-induced Ca^{2+} release is not solely due to its impact on the filling state of the ER Ca^{2+} stores since several TMBIM family members (TMBIM3, TMBIM4 and TMBIM6) have been reported to interact with the IP3 receptor, an intracellular Ca^{2+}-release channel present at the ER Ca^{2+} stores. On one hand, TMBIM6 overexpression sensitizes IP3R to low [IP3] and thus promotes IP3-induced Ca^{2+} release in Ca^{2+}-flux assays performed in permeabilized cell systems [40]; on the other TMBIM3 [19] or TMBIM4 [21] overexpression suppressed IP3-induced Ca^{2+} release in these assays which could of course be also caused by the reduced ER Ca^{2+} content.

Whether the Ca^{2+} flux through all TMBIM family members is pH dependent remains to be investigated. The pH-dependent properties of TMBIM6 are due to a complex network of interactions with a prominent role for the di-aspartyl pH sensor (D188 and D213 of TMBIM6) conserved in all family members, but also on D209 and H78. At neutral pH, the D188, D209 and D213, which form the Ca^{2+}-permeable pore, are sufficiently negatively charged to allow Ca^{2+} flux. At more acidic pH (e.g. about pH 6), D188 and D213 become protonated (due to their relatively high p*K*a values) and prevent Ca^{2+} flux through the pore. At more basic pH, a hydrogen bond between H78 and D213 may be formed and thus alter the conformation, leading to closure of the Ca^{2+} pore (discussed in [9]). In contrast to D188 and D213 residues, which are conserved among all TMBIM family members, H78 and D209 are unique to TMBIM6. However, all other family members also contain a positively charged residue (namely R) at this position except TMBIM5, where it corresponds to a negatively charged residue (namely D). The importance of this residue for the function of the TMBIM family members awaits further investigation. It is interesting to note that all TMBIM family members except TMBIM5 caused a slight decrease in the basal cytosolic [Ca^{2+}], which matches an increased cytosolic Ca^{2+} content in TMBIM6 knockout splenocytes (own unpublished data). At this point, it is not clear what causes this and why TMBIM5 overexpression has the opposite effect. TMBIM5 differs from the other family members by the presence of a unique acidic (D) instead of a basic (H or R) residue near transmembrane domain 2, an additional transmembrane domain preceding the TMBIM6 homology domain and its unique localization in the mitochondrial membranes. This mitochondrial localization

Fig. 7. Profound effects of TMBIM 1-6 on the intracellular Ca^{2+} homeostasis. (A) Cells stably express HA-tagged TMBIM family members. HT22 cells were stably transfected with HA-tagged TMBIM1-6 or empty vector and expression was verified by immunoblotting. Actin was used as the loading control; size is indicated. (B) Each member of the TMBIM family, except for TMBIM5, lowered the baseline Ca^{2+} compared to cells transfected with the empty vector. Additionally, TMBIM1-6 lowered the thapsigargin-releasable pool. The traces show the calibrated absolute Ca^{2+} concentrations of each cell line compared to empty vector-transfected cells. Each cell line was measured at least three times and the total cell count is indicated in panel C. (C) Single-cell analysis of the Ca^{2+} traces shows that while TMBIM1-4 and TMBIM6 significantly but modestly lowered the basal cytosolic [Ca2+], TMBIM5 significantly increased it. Further, each TMBIM family member significantly decreased the ER Ca^{2+} pool when compared to empty vector-transfected cells. Fura2-AM-based Ca^{2+} traces were recorded with a high content imaging system. After baseline recording, extracellular Ca^{2+} was depleted by adding 2 mM EGTA. Then ER Ca^{2+} content was released through the addition of 2 μM thapsigargin. The box and whiskers plot represent the absolute Ca^{2+} values at baseline conditions as well as the maximum cytosolic Ca^{2+} concentrations as the mean ± SD. Data were analyzed with one-way ANOVA. *$P < 0.05$.

could alter the buffering capacity of the mitochondria and thereby alter the cytosolic Ca^{2+} levels.

The reduction of intracellular Ca^{2+} concentrations might impact the cell's susceptibility to apoptosis since Ca^{2+} is known to influence apoptosis pathways (reviewed in [41,42]). Ca^{2+} released from the ER can be taken up by the mitochondria, which is facilitated by the close proximity of these two organelles [43]. Although Ca^{2+} uptake by the mitochondria can activate oxidative metabolism and promote cell survival, dysregulated release of ER Ca^{2+} initiates programmed cell death by several mechanisms including mitochondrial Ca^{2+} overload, depolarization, ATP loss, generation of reactive oxygen species, and cytochrome *c* release (reviewed in [44]). The decreased ER and Golgi Ca^{2+} pool by the overexpressed members of the TMBIM family members might therefore correlate with their potential anti-apoptotic properties that has been recently reviewed elsewhere [45]. We were unfortunately not able to reliably measure cell death in our cell lines. This resulted primarily from very heterogeneous growth characteristics between the cell lines, also between empty vector-transfected cells and cells carrying the actual protein. It therefore remains to be investigated how the changes in the intracellular Ca^{2+} handling caused by the TMBIM family exactly relate to their anti-apoptotic properties.

Conflict of interest

The authors have no conflict of interest.

Traparency Document

The Transparency document associated with this article can be found, in the online version.

Acknowledgment

This work was supported by DFG ME1922/9-1 to Axel Methner. Support in the laboratory of Geert Bultynck was provided by the KU Leuven (OTSTRT1/10/044 and OT/14/101) and from the Research Foundation–Flanders (FWO; G.0571.12). We thank Darragh O'Neill for proofreading the manuscript. Confocal images were taken in the Core Facility Microscopy of the Institute of Molecular Biology (IMB) Mainz.

References

[1] Q. Xu, J.C. Reed, Bax inhibitor-1, a mammalian apoptosis suppressor identified by functional screening in yeast, Mol. Cell 1 (1998) 337–346.
[2] H.-J. Chae, H.-R. Kim, C. Xu, B. Bailly-Maitre, M. Krajewska, S. Krajewski, et al., BI-1 regulates an apoptosis pathway linked to endoplasmic reticulum stress, Mol. Cell 15 (2004) 355–366, http://dx.doi.org/10.1016/j.molcel.2004.06.038.
[3] B. Bailly-Maitre, C. Fondevila, F. Kaldas, N. Droin, F. Luciano, J.-E. Ricci, et al., Cytoprotective gene bi-1 is required for intrinsic protection from endoplasmic reticulum stress and ischemia-reperfusion injury, Proc. Natl. Acad. Sci. U. S. A. 103 (2006) 2809–2814, http://dx.doi.org/10.1073/pnas.0506854103.
[4] F. Lisbona, D. Rojas-Rivera, P. Thielen, S. Zamorano, D. Todd, F. Martinon, et al., BAX inhibitor-1 is a negative regulator of the ER stress sensor IRE1alpha, Mol. Cell 33 (2009) 679–691, http://dx.doi.org/10.1016/j.molcel.2009.02.017.
[5] B.C. Westphalen, J. Wessig, F. Leypoldt, S. Arnold, A. Methner, Bi-1 protects cells from oxygen glucose deprivation by reducing the calcium content of the endoplasmic reticulum, Cell Death Differ. 12 (2005) 304–306, http://dx.doi.org/10.1038/sj.cdd.4401547.
[6] G. Bultynck, S. Kiviluoto, N. Henke, H. Ivanova, L. Schneider, V. Rybalchenko, et al., The C terminus of Bax inhibitor-1 forms a Ca2 + -permeable channel pore, J. Biol. Chem. 287 (2012) 2544–2557, http://dx.doi.org/10.1074/jbc.M111.275354.
[7] S. Kiviluoto, T. Luyten, L. Schneider, D. Lisak, D. Rojas-Rivera, K. Welkenhuyzen, et al., Bax Inhibitor-1-mediated Ca(2 +) leak is decreased by cytosolic acidosis, Cell Calcium 54 (2013) 186–192, http://dx.doi.org/10.1016/j.ceca.2013.06.002.
[8] Y. Chang, R. Bruni, B. Kloss, Z. Assur, E. Kloppmann, B. Rost, et al., Structural basis for a pH-sensitive calcium leak across membranes, Science 344 (2014) 1131–1135, http://dx.doi.org/10.1126/science.1252043.
[9] G. Bultynck, S. Kiviluoto, A. Methner, Bax inhibitor-1 is likely a pH-sensitive calcium leak channel, not a H+/Ca2+ exchanger, Sci. Signal. 7 (2014) pe22, http://dx.doi.org/10.1126/scisignal.2005764.
[10] H. Zhao, A. Ito, S.H. Kimura, N. Yabuta, N. Sakai, M. Ikawa, et al., RECS1 deficiency in mice induces susceptibility to cystic medial degeneration, Genes Genet. Syst. 81 (2006) 41–50.
[11] A shear stress responsive gene product PP1201 protects against Fas-mediated apoptosis by reducing Fas expression on the cell surface, 162011. 162–173, http://dx.doi.org/10.1007/s10495-010-0556-y.
[12] M. Fernández, M.F. Segura, C. Solé, A. Colino, J.X. Comella, V. Ceña, Lifeguard/neuronal membrane protein 35 regulates Fas ligand-mediated apoptosis in neurons via microdomain recruitment, J. Neurochem. 103 (2007) 190–203, http://dx.doi.org/10.1111/j.1471-4159.2007.04767.x.
[13] N.V. Somia, M.J. Schmitt, D.E. Vetter, D. Van Antwerp, S.F. Heinemann, I.M. Verma, LFG: an anti-apoptotic gene that provides protection from Fas-mediated cell death, Proc. Natl. Acad. Sci. U. S. A. 96 (1999) 12667–12672.
[14] B. Schweitzer, V. Taylor, A.A. Welcher, M. McClelland, U. Suter, Neural membrane protein 35 (NMP35): a novel member of a gene family which is highly expressed in the adult nervous system, Mol. Cell. Neurosci. 11 (1998) 260–273, http://dx.doi.org/10.1006/mcne.1998.0697.
[15] B. Schweitzer, U. Suter, V. Taylor, Neural membrane protein 35/Lifeguard is localized at postsynaptic sites and in dendrites, Brain Res. Mol. Brain Res. 107 (2002) 47–56.
[16] Fas/CD95 Regulatory Protein Faim2 Is Neuroprotective after Transient Brain Ischemia, 312011. 225–233, http://dx.doi.org/10.1523/JNEUROSCI.2188-10.2011.
[17] K.N. Kumar, N. Tilakaratne, P.S. Johnson, A.E. Allen, E.K. Michaelis, Cloning of cDNA for the glutamate-binding subunit of an NMDA receptor complex, Nature 354 (1991) 70–73, http://dx.doi.org/10.1038/354070a0.
[18] Identification of molecules preferentially expressed beneath the marginal zone in the developing cerebral cortex, 602008. 135–146, http://dx.doi.org/10.1016/j.neures.2007.10.006.
[19] D. Rojas-Rivera, R. Armisén, A. Colombo, G. Martínez, A.L. Eguiguren, A. Díaz, et al., TMBIM3/GRINA is a novel unfolded protein response (UPR) target gene that controls apoptosis through the modulation of ER calcium homeostasis, Cell Death Differ. 19 (2012) 1013–1026, http://dx.doi.org/10.1038/cdd.2011.189.
[20] A New Inhibitor of Apoptosis from Vaccinia Virus and Eukaryote, 32007. e17, http://dx.doi.org/10.1371/journal.ppat.0030017.
[21] F. de Mattia, C. Gubser, M.M.T. van Dommelen, H.-J. Visch, F. Distelmaier, A. Postigo, et al., Human Golgi antiapoptotic protein modulates intracellular calcium fluxes, Mol. Biol. Cell 20 (2009) 3638–3645, http://dx.doi.org/10.1091/mbc.E09-05-0385.
[22] T. Yoshida, S. Nagata, H. Kataoka, Ghitm is an ortholog of the Bombyx mori prothoracic gland-derived receptor (Pgdr) that is ubiquitously expressed in mammalian cells and requires an N-terminal signal sequence for expression, Biochem. Biophys. Res. Commun. 341 (2006) 13–18, http://dx.doi.org/10.1016/j.bbrc.2005.12.141.
[23] T. Oka, T. Sayano, S. Tamai, S. Yokota, H. Kato, G. Fujii, et al., Identification of a novel protein MICS1 that is involved in maintenance of mitochondrial morphology and apoptotic release of cytochrome c, Mol. Biol. Cell 19 (2008) 2597–2608, http://dx.doi.org/10.1091/mbc.E07-12-1205.
[24] S. Henikoff, J.G. Henikoff, Amino acid substitution matrices from protein blocks, Proc. Natl. Acad. Sci. U. S. A. 89 (1992) 10915–10919.
[25] V.A. Simossis, J. Kleinjung, J. Heringa, Homology-extended sequence alignment, Nucleic Acids Res. 33 (2005) 816–824, http://dx.doi.org/10.1093/nar/gki233.
[26] A. Dereeper, V. Guignon, G. Blanc, S. Audic, S. Buffet, F. Chevenet, et al., Phylogeny.fr: robust phylogenetic analysis for the non-specialist, Nucleic Acids Res. 36 (2008) W465–W469, http://dx.doi.org/10.1093/nar/gkn180.
[27] R.C. Edgar, MUSCLE: multiple sequence alignment with high accuracy and high throughput, Nucleic Acids Res. 32 (2004) 1792–1797, http://dx.doi.org/10.1093/nar/gkh340.
[28] T.N. Petersen, S. Brunak, G. von Heijne, H. Nielsen, SignalP 4.0: discriminating signal peptides from transmembrane regions, Nat. Methods 8 (2011) 785–786, http://dx.doi.org/10.1038/nmeth.1701.
[29] M.G. Claros, P. Vincens, Computational method to predict mitochondrially imported proteins and their targeting sequences, Eur. J. Biochem. 241 (1996) 779–786.
[30] S. Bolte, F.P. Cordelières, A guided tour into subcellular colocalization analysis in light microscopy, J. Microsc. 224 (2006) 213–232, http://dx.doi.org/10.1111/j.1365-2818.2006.01706.x.
[31] G. Carrara, N. Saraiva, C. Gubser, B.F. Johnson, G.L. Smith, Six-transmembrane topology for Golgi anti-apoptotic protein (GAAP) and Bax inhibitor 1 (BI-1) provides model for the transmembrane Bax inhibitor-containing motif (TMBIM) family, J. Biol. Chem. 287 (2012) 15896–15905, http://dx.doi.org/10.1074/jbc.M111.336149.
[32] T.A. Reimer, I. Anagnostopoulos, B. Erdmann, I. Lehmann, H. Stein, P. Daniel, et al., Reevaluation of the 22-1-1 antibody and its putative antigen, EBAG9/RCAS1, as a tumor marker, BMC Cancer 5 (2005) 47, http://dx.doi.org/10.1186/1471-2407-5-47.
[33] S. Lang, J. Benedix, S.V. Fedeles, S. Schorr, C. Schirra, N. Schäuble, et al., Different effects of Sec61α, Sec62 and Sec63 depletion on transport of polypeptides into the endoplasmic reticulum of mammalian cells, J. Cell Sci. 125 (2012) 1958–1969, http://dx.doi.org/10.1242/jcs.096727.
[34] B. Kadenbach, M. Hüttemann, S. Arnold, I. Lee, E. Bender, Mitochondrial energy metabolism is regulated via nuclear-coded subunits of cytochrome c oxidase, Free Radic. Biol. Med. 29 (2000) 211–221.
[35] J.A. Nielsen, M.A. Chambers, E. Romm, L.Y.-H. Lee, J.A. Berndt, L.D. Hudson, Mouse transmembrane BAX inhibitor motif 3 (Tmbim3) encodes a 38 kDa transmembrane protein expressed in the central nervous system, Mol. Cell. Biochem. 357 (2011) 73–81, http://dx.doi.org/10.1007/s11010-011-0877-3.
[36] L. Walter, B. Dirks, E. Rothermel, M. Heyens, C. Szpirer, G. Levan, et al., A novel, conserved gene of the rat that is developmentally regulated in the testis, Mamm. Genome 5 (1994) 216–221.

[37] L. Walter, P. Marynen, J. Szpirer, G. Levan, E. Günther, Identification of a novel conserved human gene, TEGT, Genomics 28 (1995) 301–304, http://dx.doi.org/10.1006/geno.1995.1145.
[38] N. Henke, D.A. Lisak, L. Schneider, J. Habicht, M. Pergande, A. Methner, The ancient cell death suppressor BAX inhibitor-1, Cell Calcium 50 (2011) 251–260, http://dx.doi.org/10.1016/j.ceca.2011.05.005.
[39] N. Saraiva, D.L. Prole, G. Carrara, C. Maluquer de Motes, B.F. Johnson, B. Byrne, et al., Human and viral Golgi anti-apoptotic proteins (GAAPs) oligomerize via different mechanisms and monomeric GAAP inhibits apoptosis and modulates calcium, J. Biol. Chem. 288 (2013) 13057–13067, http://dx.doi.org/10.1074/jbc.M112.414367.
[40] S. Kiviluoto, L. Schneider, T. Luyten, T. Vervliet, L. Missiaen, H. De Smedt, et al., Bax inhibitor-1 is a novel IP3 receptor-interacting and -sensitizing protein, Cell Death Dis. 3 (2012) e367, http://dx.doi.org/10.1038/cddis.2012.103.
[41] N. Demaurex, C.W. Distelhorst, Cell biology. Apoptosis–the calcium connection, Science 300 (2003) 65–67, http://dx.doi.org/10.1126/science.1083628.
[42] J.-P. Decuypere, G. Monaco, G. Bultynck, L. Missiaen, H. De Smedt, J.B. Parys, The IP(3) receptor-mitochondria connection in apoptosis and autophagy, Biochim. Biophys. Acta 1813 (2011) 1003–1013, http://dx.doi.org/10.1016/j.bbamcr.2010.11.023.
[43] S. Marchi, S. Patergnani, P. Pinton, The endoplasmic reticulum-mitochondria connection: one touch, multiple functions, Biochim. Biophys. Acta 1837 (2014) 461–469, http://dx.doi.org/10.1016/j.bbabio.2013.10.015.
[44] M.K.E. Schäfer, A. Pfeiffer, M. Jaeckel, A. Pouya, A.M. Dolga, A. Methner, Regulators of mitochondrial Ca(2+) homeostasis in cerebral ischemia, Cell Tissue Res. (2014) http://dx.doi.org/10.1007/s00441-014-1807-y.
[45] D. Rojas-Rivera, C. Hetz, TMBIM protein family: ancestral regulators of cell death, Oncogene (2014) http://dx.doi.org/10.1038/onc.2014.6.

Bax inhibitor-1 is a Ca^{2+} channel critically important for immune cell function and survival

Dmitrij Lisak[1], Alexander Gawlitza[1], Teresa Schacht[1], Philipp Albrecht[2], Orhan Aktas[2], Barbara Koop[2], Michael Gliem[2], Harald H. Hofstetter[2], Klaus Zanger[3], Geert Bultynck[4], Jan B. Parys[4], Humbert de Smedt[4], Thomas Kindler[5], Petra Adams-Quack[6], Matthias Hahn[6], Ari Waisman[6], John C. Reed[7], Nadine Hövelmeyer[6] and Axel Methner[1#]

[1]Focus Program Translational Neuroscience (FTN), Rhine Main Neuroscience Network (rmn[2]) and Department of Neurology, University Medical Center of the Johannes Gutenberg University Mainz, Mainz, Germany; [2]Heinrich Heine Universität Düsseldorf, Department of Neurology and [3]Center for Anatomy and Brain Research, Düsseldorf, Germany; [4]Laboratory of Molecular and Cellular Signaling, Department of Cellular and Molecular Medicine, KU Leuven, Belgium; [5]III. Medical Clinic and [6]Institute for Molecular Medicine, University Medical Center of the Johannes Gutenberg-University of Mainz, Mainz, Germany; [7]Sanford Burnham Institute, La Jolla, USA

The publication is printed as published in Cell Death & Differentiation:
Lisak D, Schacht T, Gawlitza A, Albrecht P, Aktas O, Koop B, et al. BAX inhibitor-1 is a Ca^{2+} channel critically important for immune cell function and survival. Cell Death Differ. 2015 Oct ;23(2):358–68.

Author contributions:

Dmitrij Lisak participated in all experiments, the data analysis and creation of the following results: table 1 and figures 2 b) – d), 3, 4 a)-c), 5 a)-h), and 6 a) and d) as well as supplementary figures 2 b) – c) and 3. Dmitrij Lisak also co-authored the whole manuscript.
Alexander Gawlitza and Teresa Schacht participated in all experiments and the data analysis of the following results: figure 4 d) and 5 i). Teresa Schacht also supported the experiments, which lead to figures 1 and 6 d) and e).
Philipp Albrecht participated in the experiment and data analysis of figure 6 a).
Orhan Aktas participated in the data analysis of figures 6 b) and c).
Barbara Koop participated in all experiments and the data analysis of figure 6 b) and c).
Michael Gliem provided scientific advice for the experiments, which lead to figures 6 a) – c).
Harald H. Hofstedter provided scientific advice and participated in the experiment and data analysis of figure 6 a).
Klaus Zanger participated in all experiments, the data analysis and creation of supplementary figure 4.

Thomas Kindler participated in all experiments, the data analysis and creation of supplementary figure 1 a) and b).

Petra Adams-Quack, **Matthias Hahn** and **Nadine Hövelmeyer** participated in all experiments and the data analysis of the following results: figure 1, figure 2 a) and 6 d) and e) as well as supplementary figure 2 a).

Ari Waisman provided scientific advice for the experiments, which lead to figure 1, figure 2 a) and 6 d) and e) as well as supplementary figure 2 a).

Geert Bultynck, **Jan B. Parys** and **Humbert de Smedt** provided scientific advice for all calcium related experiments.

John C. Reed reviewed and manuscript and gave editorial advice.

Axel Methner provided scientific advice during all experiments, co-developed the methodology, reviewed the analysis and co-authored the whole manuscript.

Cell Death and Differentiation (2015), 1–11

www.nature.com/cdd

BAX inhibitor-1 is a Ca^{2+} channel critically important for immune cell function and survival

D Lisak[1], T Schacht[1], A Gawlitza[1], P Albrecht[2], O Aktas[2], B Koop[2], M Gliem[2], HH Hofstetter[2], K Zanger[3], G Bultynck[4], JB Parys[4], H De Smedt[4], T Kindler[5], P Adams-Quack[6], M Hahn[6], A Waisman[6], JC Reed[7], N Hövelmeyer[6] and A Methner*[,1]

The endoplasmic reticulum (ER) serves as the major intracellular Ca^{2+} store and has a role in the synthesis and folding of proteins. BAX (BCL2-associated X protein) inhibitor-1 (BI-1) is a Ca^{2+} leak channel also implicated in the response against protein misfolding, thereby connecting the Ca^{2+} store and protein-folding functions of the ER. We found that BI-1-deficient mice suffer from leukopenia and erythrocytosis, have an increased number of splenic marginal zone B cells and higher abundance and nuclear translocation of NF-κB (nuclear factor-κ light-chain enhancer of activated B cells) proteins, correlating with increased cytosolic and ER Ca^{2+} levels. When put into culture, purified knockout T cells and even more so B cells die spontaneously. This is preceded by increased activity of the mitochondrial initiator caspase-9 and correlated with a significant surge in mitochondrial Ca^{2+} levels, suggesting an exhausted mitochondrial Ca^{2+} buffer capacity as the underlying cause for cell death *in vitro*. *In vivo*, T-cell-dependent experimental autoimmune encephalomyelitis and B-cell-dependent antibody production are attenuated, corroborating the *ex vivo* results. These results suggest that BI-1 has a major role in the functioning of the adaptive immune system by regulating intracellular Ca^{2+} homeostasis in lymphocytes.
Cell Death and Differentiation advance online publication, 16 October 2015; doi:10.1038/cdd.2015.115

The endoplasmic reticulum (ER) serves as the major intracellular calcium (Ca^{2+}) store, the release of which controls a vast array of cellular functions from short-term responses such as contraction and secretion to long-term regulation of cell growth and proliferation.[1] Dysregulated release of ER Ca^{2+}, in contrast, initiates programmed cell death by several mechanisms including mitochondrial Ca^{2+} overload, depolarization, ATP loss and cytochrome *c* release.[2] Besides this, the ER also has a key role in the synthesis, folding and sorting of proteins destined for the secretory pathway. The deleterious consequences of an increase in unfolded proteins is called ER stress and can be antagonized by the unfolded protein response (UPR), a mechanism that coordinates a simultaneous increase in the ER folding capacity and a decrease in folding load. In the case of insufficient adaptation to ER stress, cells undergo apoptosis.[3]

BAX (BCL2-associated X protein) inhibitor-1 (BI-1) is an evolutionarily conserved protein that bridges both the Ca^{2+} homeostasis and UPR functions of the ER.[4] BI-1 was first identified in a screen for human proteins capable of inhibiting BAX-mediated cell death in yeast.[5] In mammalian cells, BI-1's antiapoptotic function is most pronounced in paradigms of ER stress[6] and involves changes in the amount of Ca^{2+} that can be released from intracellular stores.[6,7] BI-1 is a highly hydrophobic protein that forms a Ca^{2+} pore responsible for its Ca^{2+} leak properties[8] and is the founding member of a family of six proteins with similar properties.[9] The increase in the ER Ca^{2+} leak mediated by BI-1 is blocked at a more acidic pH[10] – a function recently corroborated by a structural analysis of a bacterial homolog of BI-1.[11]

Despite its evolutionarily conserved role in important functions such as ER stress and Ca^{2+} regulation, *bi-1−/−* mice were reported to have no phenotypic abnormalities but increased infarct volumes in a stroke model, and increased sensitivity to tunicamycin-induced kidney toxicity.[6] Moreover, livers from BI-1-deficient mice regenerate faster than those from wild-type (WT) mice and this correlates with increased nuclear translocation of nuclear factor of activated T cells (NFATs)[12], a Ca^{2+}-dependent process. BI-1 knockout (KO) mice also express more of the spliced form of X-box-binding protein-1 (sXBP-1) in their liver and kidney,[13] which is generated by the endoribonuclease activity of inositol

[1]Focus Program Translational Neuroscience (FTN), Rhine Main Neuroscience Network (rmn²) and Department of Neurology, University Medical Center of the Johannes Gutenberg University Mainz, Mainz, Germany; [2]Heinrich Heine Universität Düsseldorf, Department of Neurology, Düsseldorf, Germany; [3]Center for Anatomy and Brain Research, Düsseldorf, Germany; [4]Laboratory of Molecular and Cellular Signaling, Department of Cellular and Molecular Medicine, KU Leuven, Belgium; [5]III Medical Clinic, University Medical Center of the Johannes Gutenberg-University of Mainz, Mainz, Germany; [6]Institute for Molecular Medicine, University Medical Center of the Johannes Gutenberg-University of Mainz, Mainz, Germany and [7]Sanford Burnham Institute, La Jolla, CA, USA
*Corresponding author: A Methner, Focus Program Translational Neuroscience (FTN), Rhine Main Neuroscience Network (rmn²) and Department of Neurology, University Medical Center of the Johannes Gutenberg University Mainz, Langenbeckstrasse 1, Mainz 55131, Germany. Tel: +49 6131 17 2695; Fax: +49 6131 17 5967; E-mail: axel.methner@gmail.com

Abbreviations: BAK, Bcl-2 homologous antagonist/killer; BAX, BCL2-associated X protein; BI-1, Bax inhibitor-1; EAE, experimental autoimmune encephalomyelitis; ER, endoplasmic reticulum; FACS, fluorescence-activated cell sorting; FCCP, carbonyl cyanide 4-(trifluoromethoxy) phenylhydrazoneFO, follicular; Grp78/BiP, glucose-regulated protein 78 kDa/binding immunoglobulin protein; IP_3, inositol 1,4,5-trisphosphate; IRE1, inositol requiring enzyme 1; KO, knockout; MZ, marginal zone; NADH, nicotinamide adenine dinucleotide hydride; NFAT, nuclear factor of activated T cell; NF-κB, nuclear factor-κ light-chain enhancer of activated B cells; NPCG, 4-hydroxy-3-nitrophenylacetyl coupled to chicken globulin; ROX, residual oxygen consumption; SERCA, sarcoplasmic/endoplasmic reticulum Ca^{2+}-ATPase; SOCE, store-operated Ca^{2+} entry; STIM1, stromal interaction molecule 1; UPR, unfolded protein response; WT, wild type; XBP-1, X-box-binding protein-1

Received 07.11.2014; revised 20.7.2015; accepted 21.7.2015; Edited by C Borner

requiring enzyme 1 (IRE1), and is considered an indicator of increased UPR activity. This was later reproduced and attributed to an inhibitory function of BI-1 on IRE1α mediated via a direct interaction of the two proteins.[14]

In our study, we found that *bi-1 −/−* mice are more obese and suffer from leukopenia. T and B cells from these mice show significant changes in cellular Ca^{2+} homeostasis and dynamics, and are more prone to spontaneous death in culture but, surprisingly, demonstrate no signs of ongoing ER stress within the homeostatic system of the living animal. These changes lead to an attenuated functioning of the adaptive immune system *in vivo*. Our results suggest that a major role of BI-1 *in vivo* involves its effects on the intracellular Ca^{2+} homeostasis in lymphocytes in line with its function as an ER Ca^{2+} leak channel.

Results

BI-1 mice are obese and suffer from leukopenia and erythrocytosis. Previously described BI-1 KO mice[6] were backcrossed to WT C57/BL6 mice and identified by genotyping because of the lack of functional antibodies.[15] A thorough phenotypic analysis of WT and KO littermates revealed that BI-1 KO mice at the age of 3 months are significantly more obese, even on a normal chow diet, and suffer from leukopenia (shown to be mainly lymphopenia and neutropenia by manual inspection) and erythrocytosis (Table 1). The effect of BI-1 deficiency therefore appears to be most pronounced with respect to homeostasis of the hematolymphoid system and energy balance.

BI-1 deficiency causes significant alterations of the B-cell compartment in the spleen. We focused on the immune system and studied the secondary lymphoid organs. The spleen, thymus, Peyers' patches and lymph nodes showed no gross abnormalities and were of similar size. The bone marrow, thymus, the peritoneal cavity and the spleen contained similar counts of total cells (Supplementary Figure 1a), and the subcellular composition of cells in the bone marrow (pro/pre, immature and mature recirculating B cells) and the thymus (CD4 and CD8 T cells) determined by flow cytometry were comparable (Supplementary Figures 1b–d). We also observed no significant difference in the percentage as well as total cell counts of splenic B and T cells of BI-1 KO mice compared with age-matched controls (Figure 1a).

Immature B cells leave the bone marrow and migrate to the spleen where they complete their maturation process. In the spleen, these cells become follicular (FO) B cells, which recirculate in the periphery, or marginal zone (MZ) B cells, which are largely sessile. An analysis of these cell types, immature ($CD21^{-}IgM^{-}$), FO ($CD21^{int}IgM^{high}$) and MZ ($CD21^{high}IgM^{neg\text{-}low}$) B cells revealed a significant elevation of MZ B cells in KO spleens (KO $20.5 \pm 5.2\%$ *versus* WT $10.9 \pm 2.7\%$) at the expense of FO B cells (Figure 1b). This was also evident in splenic sections stained with an anti-CD1d antibody, which recognizes MZ B cells. Interestingly, in the KO mice, MZ B cells were also found within the follicles, whereas in controls, strong CD1d staining was only detected in the MZ as expected (Figure 1c). Taken together, these results demonstrate a significant increase in the generation, differentiation or maintenance of mature MZ cells at the expense of FO B cells in BI-1 KO mice compared with WT controls.

Increased constitutive nuclear translocation of the transcription factor NF-κB in BI-1 KO splenocytes. Such a shift towards MZ B cells has been previously linked to NF-κB (nuclear factor-κ light-chain enhancer of activated B cells) signaling. NF-κB1 (p105/p50) and NF-κB2 (p100/p52) need to be processed to become active and translocate to the nucleus where they associate with RelA (p65), c-Rel and RelB in different hetero- and homodimers to form the transcriptionally active complex.[16] Mice deficient in RelB show reduced numbers of MZ B cells,[17] whereas mice lacking a negative regulator of NF-κB have more MZ B cells[18] similar to mice that lack the inhibitory p100 subunit of NF-κB2.[19]

We therefore quantified the abundance of all NF-κB proteins in the cytosol and the nucleus by immunoblotting of subcellular fractions obtained from freshly isolated splenocytes. This revealed an increased cytosolic abundance of c-Rel and RelA and an increased nuclear abundance of RelB in BI-1 KO cells (Figure 2a), whereas the proteins that lack transcriptional activation domains, NF-κB1/2, remained unchanged (Supplementary Figure 2a). Because of the feeble nuclear abundance of RelA (p65) in these unstimulated cells, we used immunocytochemistry with another antibody and quantification by high-content imaging as an additional read-out. In these experiments, RelA (p65) translocated to the nucleus to a much higher degree ($P<0.0001$) in BI-1-deficient splenocytes, as suggested by the immunoblotting experiments (Figure 2b).

Table 1 Body weight and laboratory results from WT and KO mice

	WT	KO	*P*-value
Body weight (g ± S.D.)	23.1 ± 1.821	26.2 ± 2.186	0.0235
Leukocytes (x10E3/μl ± S.D.)	3.73 ± 0.95	1.94 ± 1.14	0.0043
Erythrocytes (x10E6/μl ± S.D.)	9.10 ± 1.08	10.38 ± 0.79	0.0403
Thrombocytes (x10E3/μl ± S.D.)	530.00 ± 144.24	520.50 ± 182.47	0.9097
Hematocrit (% ± S.D.)	47.32 ± 5.25	52.78 ± 2.56	0.0454
Mean corpuscular volume (fl ± S.D.)	52.03 ± 0.92	50.5 ± 1.91	0.1073
Mean corpuscular hemoglobin (pg ± S.D.)	15.45 ± 0.26	14.88 ± 0.30	0.0057
Mean corpuscular hemoglobin (gxHb/dl ± S.D.)	29.67 ± 0.37	29.50 ± 0.96	0.6993
Alanine transaminase (U/l ± S.D.)	23.4 ± 5.90	19.83 ± 8.47	0.4488
Aspartate transaminase (U/l ± S.D.)	67.20 ± 19.29	84.83 ± 44.41	0.4334

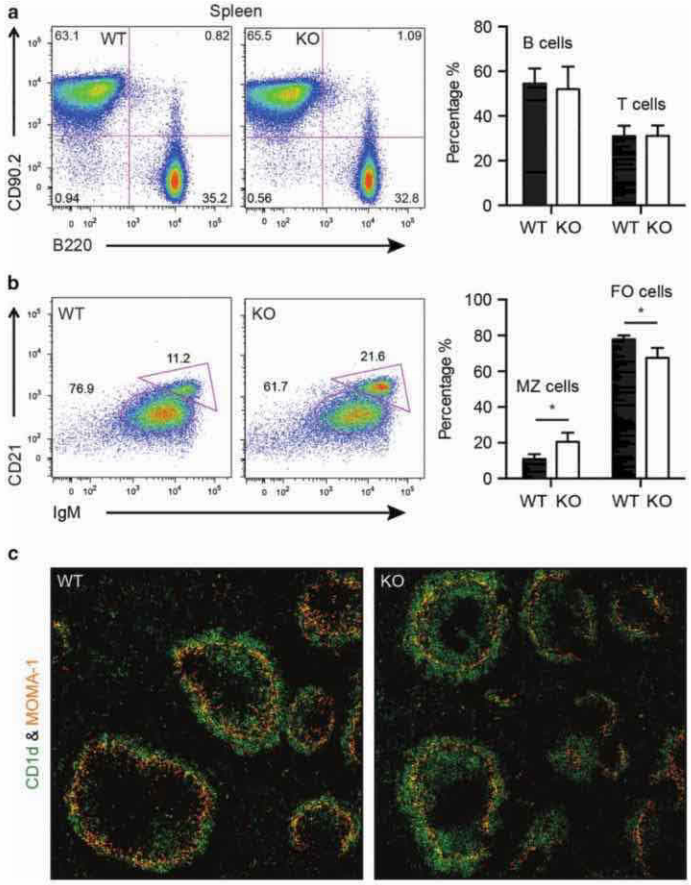

Figure 1 BI-1 deficiency causes significant alterations of the B-cell compartment. Flow cytometric analysis of splenic cells from 8- to 12-week old WT and BI-1 KO mice. T and B cells were stained with (**a**) B220 and CD90.2 antibodies, and (**b**) MZ and FO B cells with IgM and CD21 antibodies pregated on live B220$^+$ B cells. Bar graphs show the mean $\pm$ S.E.M., $n=3$. Data were analyzed by two-tailed *t*-tests, $^*P<0.05$. (**c**) Representative immunofluorescence analysis of MZ B cells stained with α-CD1d and metallophillic macrophages stained with α-MOMA-1 in spleen tissue sections

In unstimulated cells, the Rel/NF-κB dimers associate with members of the family of inhibitor proteins called IκBs and remain inactive in the cytoplasm. In NF-κB not bound by IκBα in the cytosol, the nuclear localization signal of p65 is liberated, which allows its translocation into the nucleus. The NF-κB/IκB ratio thus determines the amount of nuclear-translocated NF-κB and this ratio was indeed increased in BI-1 KO splenocytes (Figure 2c). IκB is usually removed from NF-κB by activation of the IκB kinase complex, which leads to phosphorylation of IκBα, resulting in ubiquitination and degradation of IκBα. Phosphorylated IκBα was downregulated in BI-1 KO splenocytes (Figure 2d). We conclude that NF-κB proteins harboring a transcriptional activation domain are upregulated and show an increased nuclear localization in the absence of BI-1, which may explain the increase in MZ B cells in these animals compared with controls.

BI-1 KO splenocytes have increased ER and cytosolic Ca^{2+} levels and a compensatory downregulation of store-operated Ca^{2+} entry. NF-κB is activated in a pleiotropic manner including changes in the amplitude and duration of Ca^{2+} signals in lymphocytes.[20,21] Also, treatment with inhibitors of sarcoplasmic/ER Ca^{2+}-ATPases (SERCA), which increase cytosolic Ca^{2+}, causes nuclear NF-κB translocation.[22] NF-κB can also be activated by a pathological mechanism known as the ER overload reaction. This condition is caused by retention of proteins within the ER lumen, and in contrast to the UPR does not induce Grp78/BiP

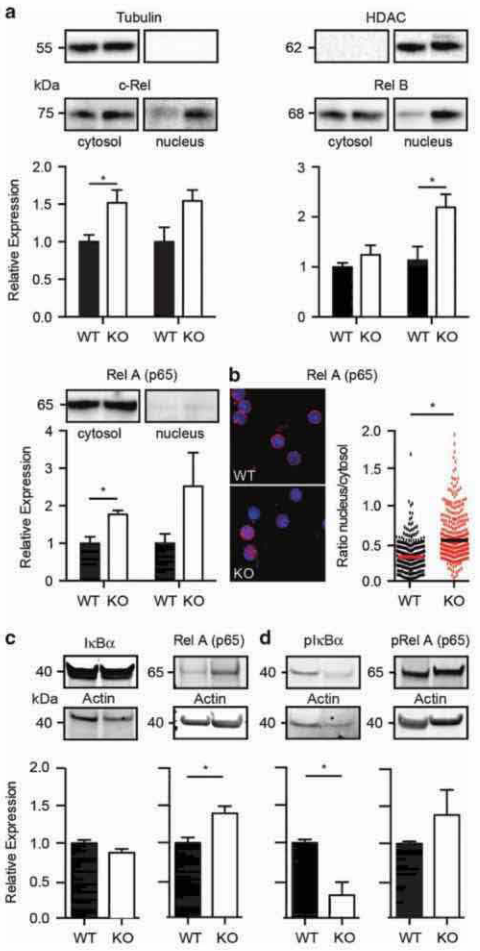

Figure 2 Increased expression and nuclear translocation of class II NF-κB proteins in BI-1 KO splenocytes. (**a**) Immunoblots with cytosolic and nuclear fractions obtained from WT and KO splenocytes incubated with antibodies against class II NF-κB proteins show increased cytosolic and nuclear abundance in BI-1 KO splenocytes. Loading controls, α/β-tubulin for the cytosolic fraction and HDAC for the nuclear fraction, are shown on the top. Molecular weight is indicated. Bar graphs show mean intensity values normalized to WT ± S.E.M., $n=8$. (**b**) Increased nuclear localization of RelA (p65) shown by quantitative immunocytochemistry in BI-1 KO splenocytes. Splenocytes were stained with an α-RelA (p65) antibody and analyzed by confocal microscopy. Quantification was carried out on a high-content imaging microscope by measuring the fluorescence intensity in the nucleus defined by DAPI (4′,6-diamidino-2-phenylindole) staining and in the cytosol defined as an area around the nucleus. The scatter plot shows the ratio of nuclear to cytosolic RelA (p65) (300 WT and 432 KO cells, $n=3$ independent experiments, mean is indicated). (**c**) Increased ratio of RelA (p65) and IκBα and (**d**) downregulated phosphorylated IκBα in BI-1 KO splenocytes. Actin served as a loading control on the same blot, size is indicated. Bar graphs show mean intensity values normalized to WT ± S.E.M., $n=6$. Data were analyzed by two-tailed *t*-tests, $^*P<0.05$

(glucose-regulated protein 78 kDa/binding immunoglobulin protein),[23] which is also unchanged in the absence of BI-1.[12,13] Notably, NF-κB induction by the ER overload reaction can be attenuated by intracellular Ca^{2+} chelators.[24,25]

Therefore, both major functions of BI-1, its role in ER stress and in the maintenance of the intracellular Ca^{2+} homeostasis, might be implicated in the observed phenotype. We first investigated the relative abundance of UPR proteins by immunoblotting of splenocyte lysates from BI-1 KO and WT mice and detected no evidence of ongoing ER stress in BI-1-deficient splenocytes. Rather, several of the UPR proteins were downregulated, especially ERp57. Importantly, BiP was unchanged (Supplementary Figure 3a). Despite the role of BI-1 as a direct inhibitor of IRE1α,[14] we observed decreased XBP-1 splicing in KO cells (Supplementary Figure 3b) in line with the decreased expression of ER stress-regulated chaperones. We concluded that the UPR and the ER overload reactions are not constitutively active in splenocytes isolated directly from BI-1 KO mice.

The other major role of BI-1 is the regulation of cellular Ca^{2+} homeostasis. Using flow cytometry of freshly isolated splenocytes, we measured resting Ca^{2+} levels in WT and KO splenocytes with Fluo8-AM and found increased cytosolic Ca^{2+} levels in KO cells (Figure 3a). We next quantified the ER Ca^{2+} content and store-operated Ca^{2+} entry (SOCE) from the extracellular space, which is activated by a decrease in $[Ca^{2+}]_{ER}$ using the ratiometric probe Fura2. The cells were attached to plates to allow a kinetic analysis of (1) Ca^{2+} passively leaking from the ER after inhibition of the Ca^{2+} reuptake pump SERCA in the absence of extracellular Ca^{2+} and then (2) Ca^{2+} re-entry from SOCE after re-exposure of the cells to large amounts of extracellular Ca^{2+}. BI-1 KO splenocytes had an increased baseline Ca^{2+} concentration (corroborating the results obtained with Fluo8), an increased thapsigargin-releasable ER Ca^{2+} pool and reduced SOCE (Figure 3b).

This SOCE reduction is mediated by a downregulation of Orai1, the plasma membrane channel mediating SOCE,[26,27] and probably serves as a compensatory mechanism to limit filling of the already Ca^{2+}-full ER (Figure 3c). Taken together, these data corroborate that BI-1 deficiency causes profound alterations of the intracellular Ca^{2+} homeostasis in freshly isolated splenocytes, which manifests as increased Ca^{2+} concentrations in the ER, and, surprisingly, also in the cytoplasm. It is thus possible that the alterations in the intracellular Ca^{2+} homeostasis are implicated in the observed increase in NF-κB nuclear translocation.

To test this assumption, we investigated the cellular localization of another transcription factor, NFAT, which translocates to the nucleus upon the pronounced Ca^{2+} release from the ER in response to activation of the antigen receptors.[21] We observed that NFATc1 was also already translocated to a much higher degree in BI-1-deficient splenocytes even without stimulation, similar to NF-κB (Figure 3d) but unchanged at the expression level (Figure 3e). These data corroborate results obtained in BI-1-deficient hepatocytes, which also showed an increased constitutive translocation of NFATc1,[12] and support the assumption that the changes in Ca^{2+} signaling are responsible for the increased abundance and nuclear translocation

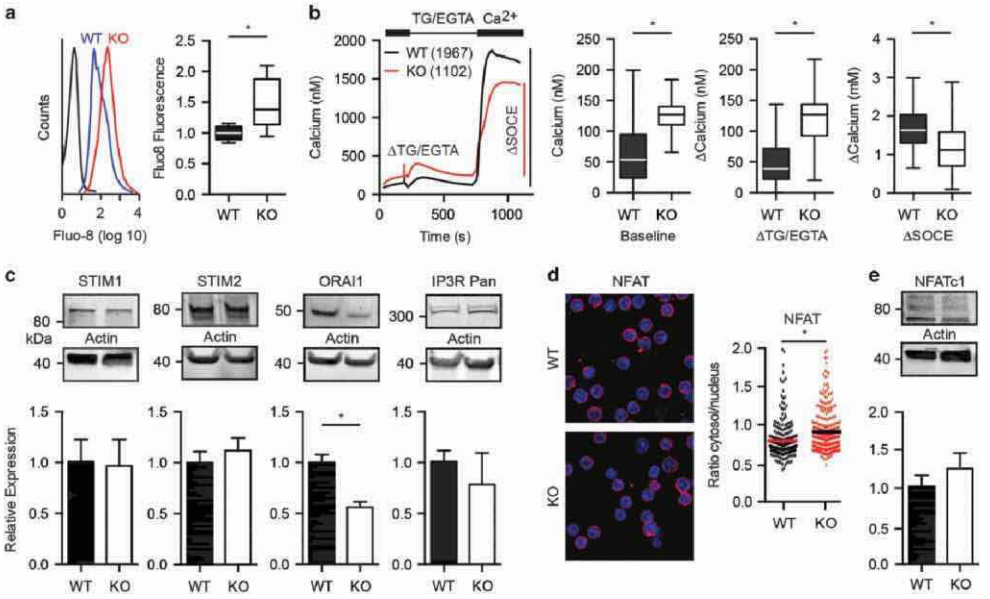

Figure 3 Increased ER and cytosolic Ca^{2+} levels cause increased constitutive nuclear translocation of the Ca^{2+}-dependent transcription factor NFAT in BI-1 KO splenocytes. (**a**) Increased cytosolic Ca^{2+} in BI-1 KO splenocytes measured by flow cytometry of splenocytes stained with Fluo8-AM. Fluo8-AM fluorescence at 488 nm is proportional to the amount of bound Ca^{2+} and is quantified as mean fluorescence intensity (MFI). The histogram shows representative data of unstained (black), WT (blue) and BI-1 KO (red) splenocytes where each cell is plotted against its relative fluorescence intensity on a log scale. Box and whiskers show the quantification of data normalized to WT animals ($n=12$, median, box from the 25th quartile to the 75th quartile, whiskers minimum to maximum). (**b**) BI-1 KO splenocytes have increased baseline Ca^{2+} and an increased thapsigargin-releasable Ca^{2+} pool but decreased store-operated Ca^{2+} entry (SOCE). Cells stained with Fura2-AM were attached to poly-L-lysine-coated plates and the intracellular Ca^{2+} concentration recorded in response to the indicated SOCE protocol on a high-content imaging microscope. The traces show the mean of the calibrated Ca^{2+} concentration from three pooled independent experiments. The box and whisker plot represent the statistical distribution of the absolute Ca^{2+} concentration at baseline, the baseline-corrected thapsigargin-releasable pool and the amount of Ca^{2+} that entered the cell during SOCE. (**c**) Orai1 is downregulated in BI-1 KO splenocytes. Immunoblots were incubated with α-STIM1, α-STIM2, α-ORAI1 and α-pan IP_3R antibodies. Actin served as a loading control on the same blot; size is indicated. Bar graphs show mean intensity values normalized to WT ± S.E.M., $n=6$. (**d**) Increased nuclear localization of NFATc1 in BI-1 KO splenocytes. Splenocytes were stained with α-NFATc1 and analyzed by confocal microscopy. Quantification was carried out on a high-content imaging microscope by measuring the fluorescence intensity in the nucleus defined by DAPI (4',6-diamidino-2-phenylindole) staining and in the cytosol defined as an area around the nucleus. The scatter plot shows the ratio of nuclear-to-cytosolic NFAT (275 WT and 312 KO cells from $n=3$ independent experiments. The mean is indicated. (**e**) The expression of all three NFATc1 isoforms is not regulated in BI-1 KO splenocytes. Immunoblots were incubated with an α-NFATc1 antibody. Actin served as a loading control on the same blot; size is indicated. Bar graphs show mean intensity values normalized to WT ± S.E.M., $n=6$. Data were analyzed by two-tailed *t*-tests, $^*P<0.05$

of NF-κB in BI-1-deficient lymphocytes and thus for the changes in MZ cell abundance.

We next investigated alterations of the Ca^{2+} homeostasis and NF-κB translocation in purified T and B cells. Fluo8-AM staining revealed higher resting cytosolic Ca^{2+} concentrations in B cells compared with T cells (Figure 4a) matching nuclear translocation levels of RelA (p65) (Figure 4b). To study physiological ligand-activated Ca^{2+} release, we incubated Fluo8-stained splenocytes with biotinylated anti-CD3 antibodies and measured Fluo8 intensity by flow cytometry for 60 s to establish a baseline. Then, streptavidin was added to crosslink the anti-CD3 antibodies on the surface, which activates the T-cell receptor and elicits inositol 1,4,5-trisphosphate (IP_3)-dependent Ca^{2+} release from the ER and subsequent SOCE. B cells were similarly stimulated by the addition of anti-IgM. Both KO T and B cells showed increased baseline Ca^{2+} concentrations and B cells also showed an increased Ca^{2+} release after stimulation (Figure 4c). To further substantiate this, we then quantified IgM-mediated increases in the mitochondrial electron transfer capacity of B cells from WT and KO animals. IgM-mediated Ca^{2+} release from the ER elevates mitochondrial matrix [Ca^{2+}], thereby stimulating Krebs' cycle dehydrogenases and elevating mitochondrial [NADH],[28] which is then fed into the oxidative phosphorylation pathway. This indeed revealed an increased stimulation in KO cells as a functional readout of the increased ER Ca^{2+} release (Figure 4d).

Increased spontaneous B-cell death in culture is associated with exhausted mitochondrial Ca^{2+} buffering capacity and caspase activation. When we took purified T and B cells into culture, we noted that after 24 h, KO cells were much more prone to spontaneous cell death. This was again more pronounced in B cells (Figure 5a) and we focused

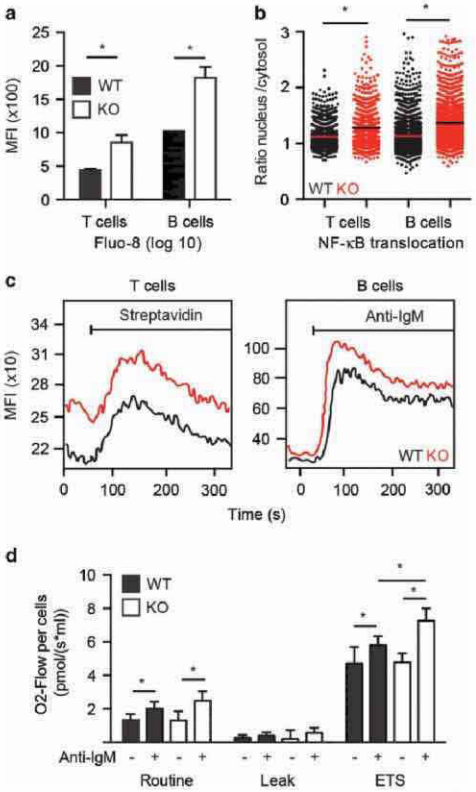

Figure 4 T and B cells are affected by Bl-1 deficiency. (**a**) Basal cytosolic Ca^{2+} is increased in Bl-1 KO T and B cells. Magnetically sorted and negatively selected T and B cells were incubated with Fluo8-AM and the fluorescence measured by flow cytometry. Bar graphs represent the average mean fluorescence intensity as the median ± S.D., $n = 6$. (**b**) Increased RelA (p65) nuclear localization in Bl-1 KO B and T cells. B and T cells were magnetically sorted and negatively selected and stained with an RelA (p65) antibody and DAPI (4',6-diamidino-2-phenylindole). Quantification was carried out on a high-content imaging microscope by measuring the fluorescence intensity in the nucleus defined by DAPI staining and in the cytosol defined as the area around the nucleus. The scatter plot shows the ratio of nuclear to cytosolic RelA (p65) (B cells: 1931 WT and 1968 KO cells; T cells: 971 WT and 941 KO cells) from three independent experiments. The mean is indicated. Data were analyzed by two-tailed *t*-tests, $^*P<0.05$. (**c**) Ligand-induced Ca^{2+} release in Bl-1 KO T and B cells quantified by flow cytometry. Fluo8-AM fluorescence at 488 nm is proportional to the amount of bound Ca^{2+} and is quantified as mean fluorescence intensity (MFI). Splenocytes were incubated with biotinylated anti-CD3 antibody and stimulated with streptavidin or directly stimulated with anti-IgM after 60 s of baseline. Streptavidin causes the biotinylated anti-CD3 to cluster and thereby activates T cells, whereas anti-IgM selectively activates B cells. Representative traces of Fluo8 kinetics are shown for WT (black) and Bl-1 KO (red) T and B cells. (**d**) Increased electron transfer system (ETS) capacity in Bl-1 KO B cells treated with anti-IgM measured by high-resolution respirometry. Routine respiration was measured under basal conditions, leak respiration after inhibition of ATP synthase using oligomycin and the ETS capacity at maximum uncoupling with FCCP and oxygen flow. All measurements were corrected for residual oxygen consumption after inhibition of complex I with rotenone and complex III with antimycin A. Shown is the mean ± S.D., $n = 4$ mice. Data were analyzed by two-tailed *t*-tests, $^*P<0.05$

on these cells for further investigations of the impact of Bl-1 deficiency. An analysis by electron microscopy of purified B cells revealed alterations in the texture of the cytoplasm, defective organelles (e.g., mitochondria) and the presence of nuclear inclusions in nearly all KO cells (Supplementary Figure 4). Quantification of B-cell death in a time-course analysis by flow cytometry revealed a statistically significant difference in viability after only 4 h in culture (WT 11.0 ± 1.2% and KO 15.6 ± 0.3%) that increased over time. After 24 h in culture, >68 ± 4.8% of KO cells were dead compared with 28 ± 5.9% WT cells (Figure 5b).

Because caspases are principal effectors of apoptosis, we measured the activity of the effector caspases 3 and 7 after placing B cells into culture. We detected a significant difference between KO and WT cells already after 4 h in culture, with higher relative levels of effector caspase activity in the KO cells (Figure 5c). We quantified the activity of initiator caspases 8 and 9, which represent the apical proteases in the 'extrinsic' and 'intrinsic' apoptosis pathways, respectively, after 3 h in culture (thus before effector caspase activation became different). Activity of both of these initiator caspases was significantly higher in Bl-1 KO compared with WT B cells (Figure 5d), with relative levels of caspase-9 activity considerably higher compared with caspase-8 in both KO and WT B cells placed into culture.

Caspase-9 activation classically involves cytochrome *c* release from the mitochondria,[29] which can be stimulated by a Ca^{2+}-dependent mechanism that impacts inner membrane permeability, followed later by rupture of the outer membrane.[2] Bl-1 is capable of regulating Ca^{2+} transport between ER and mitochondria,[30] leading us to hypothesize that the altered ER and cytoplasmic Ca^{2+} levels in Bl-1-deficient cells might be reflected by similar alterations of mitochondria. Measuring mitochondrial [Ca^{2+}] using Rhod2-AM in freshly isolated B cells from KO *versus* WT animals demonstrated that Rhod2-AM fluorescence was only slightly increased at baseline but much more significantly after 4 h in culture (Figure 5e), whereas the difference between KO and WT in cytosolic [Ca^{2+}] declined (Figure 5f). Levels of reactive oxygen species (Figure 5g) and XBP-1 splicing (Figure 5h), in contrast, did not differ in WT and KO cells at baseline or after 4 h. Exposure of these cells to different pH or extracellular [Ca^{2+}] did not profoundly affect cell death or cytosolic and mitochondrial Ca^{2+} levels (Figure 5i).

These data suggest that mitochondria of Bl-1-deficient B cells exceed their buffering capacity after a few hours in culture, and we envisaged that clamping the intracellular Ca^{2+} with the cell-permeable Ca^{2+} buffer BAPTA-AM should inhibit this Ca^{2+}-dependent cell death. However, this experimental approach was not possible because BAPTA-AM treatment rapidly killed primary B cells (not shown), as has previously been shown for leukemic cells.[31] Thus, the observed defects in mitochondrial Ca^{2+} buffering capacity seen in cultured Bl-1 KO B cells are correlated with caspase activation and cell death, but a direct cause and effect relationship was not demonstrable.

Bl-1 deficiency attenuates T- and B-cell function *in vivo*. We finally aimed to clarify the effect of the identified changes in T and B cells on immune system function *in vivo*

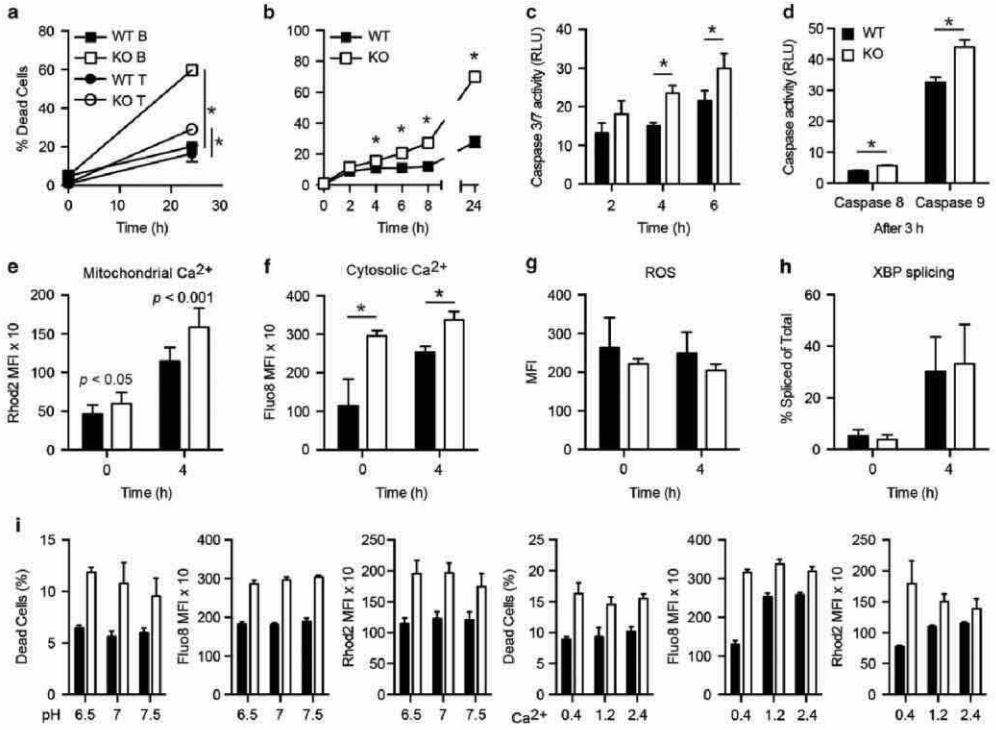

Figure 5 Increased spontaneous B-cell death in culture is caused by an exhausted mitochondrial Ca^{2+} buffer capacity leading to caspase activation. (**a**) B and T cells were magnetically sorted, negatively selected and put into culture. Cell death was assessed 24 h later by flow cytometry using a live/dead stain and demonstrates increased spontaneous cell death in KO splenocytes with B cells being more susceptible compared with T cells. (**b**) A time-course analysis of B-cell death with significant differences already evident after 4 h in culture. Cell death was assessed as described in (**a**). The graphs in (**a** and **b**) show the mean percentage of dead cells ± S.E.M. from six mice at each time point. (**c**) Caspase-3/7 activity in both WT and Bl-1 KO B cells increases in a time-dependent manner and becomes significantly increased in KO cells at 4 h in culture. (**d**) Caspase-8 and -9 are significantly increased in Bl-1 KO B cells after 3 h in culture, with caspase-9 being more prominent. All caspase activity was assessed in magnetically sorted and negatively selected B cells using a luminescent caspase assay. Caspase-8 and -9 were assessed in parallel. Bar graphs represent the mean average relative luminescence ± S.E.M. from six mice measured in triplicates (**e**–**g**) After 4 h in culture, the mitochondrial Ca^{2+} is significantly increased in KO B cells. Magnetically sorted and negatively selected B cells were stained with (**e**) Rhod2-AM, (**f**) Fluo8-AM or (**g**) CellROX at the indicated time points. The graph represents the mean fluorescence intensity ± S.D., $n = 3$–6. Data were analyzed by two-tailed *t*-tests, $^*P < 0.05$. (**h**) XBP-1 splicing was assessed by PCR in magnetically sorted and negatively selected B cells at the indicated time points in culture. Bar graphs show the mean percentage ± S.D. of spliced XBP-1/(spliced XBP-1+unspliced XBP-1) from six mice. Data were analyzed by two-tailed *t*-tests, $^*P < 0.05$. (i) Magnetically sorted and negatively selected B cells were stained with a live/dead stain, Fluo8-AM or Rhod2-AM after 4 h in culture. In the pH experiments, the cells were cultured as normally and put into HBSS buffer with the indicated pH immediately after staining and directly processed; in the Ca^{2+} experiments, the culturing medium was adjusted with $CaCl_2$ (mM) and EGTA and processed as described above. Bar graphs represent the mean fluorescence intensity as the median ± S.D., $n = 6$–24 mice

using two different experimental paradigms. First, in experimental autoimmune encephalitis (EAE), the immune system is challenged by immunization with myelin proteins emulsified in complete Freund's adjuvant, causing a mainly T-cell-driven autoimmunity against the central nervous system and the development of a multiple sclerosis-like disease that can be scored for severity. KO mice displayed a later onset of clinical symptoms and an overall lower clinical score (Figure 6a), despite the fact that the brain of Bl-1 KO mice appears to be more vulnerable to exogenous stress, as shown by larger infarcts in a stroke model.[6] The attenuated EAE disease score was associated with reduced infiltration of microglia as well as a decreased number of lesions detectable by immunohistochemistry (Figures 6b and c). Second, to assess B-cell function, we immunized the mice with 4-hydroxy-3-nitrophenylacetyl coupled to chicken globulin (NPCG), which is a standard T-cell-independent immunogen,[32] and then quantified the resulting antibody response. Bl-1 KO animals generated significantly lower amounts of IgG1 and IgG2b in response to this antigen (Figure 6d). We conclude that both T- and B-cell functions are attenuated *in vivo*, thereby corroborating the *in vitro* changes. To clarify whether this is because of defective cell signaling or the reduced number of lymphocytes *in vivo*, we investigated *in vitro* isotype switching of splenic B cells. In these experiments, splenocytes stimulated *ex vivo* with LPS and IL-4 start producing IgG1,

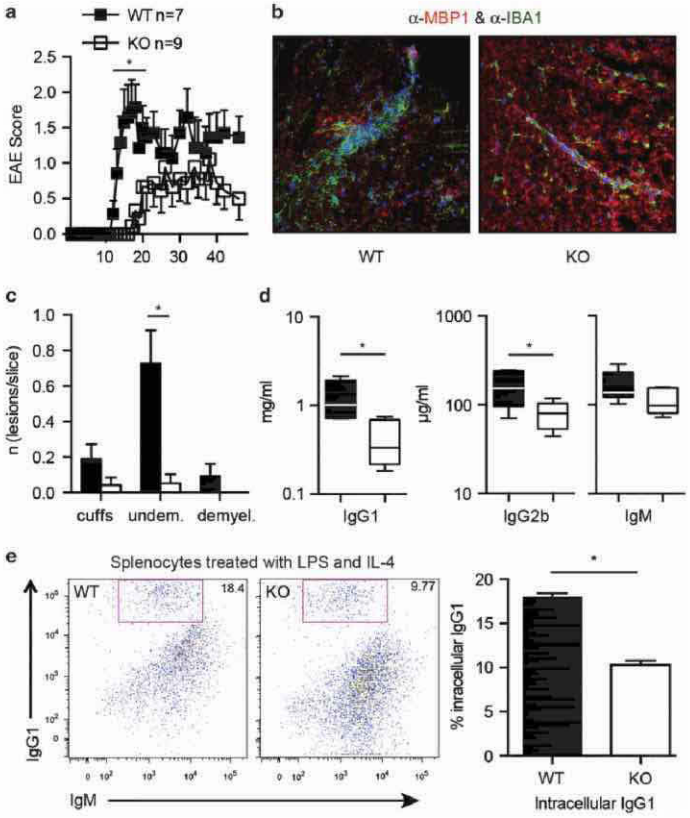

Figure 6 Bl-1 deficiency attenuates T- and B-cell function. (**a**) Bl-1 KO mice are less susceptible to EAE elicited by immunization with the MOG_{35-55} peptide. Individual clinical disease scores (1, limp tail; 2, weakness of hind legs; 3, hind leg paralysis; 4, hind and front leg paralysis; 5, death) were assessed daily. Shown is the mean ± S.E.M. of the daily average score for the indicated number of WT and Bl-1 KO mice from one representative experiment of three. (**b**) Histopathology of cryosectioned brain stained with Iba1 (microglia, green), MBP (myelin, red) and Hoechst (nuclei, blue) shows less demyelination in Bl-1 KO mice. (**c**) Cuffs and lesions caused by intruding microglia were counted 15 days after immunization. Cuffs are inflammatory vessel-centered lesions without tissue infiltration, undemyelinated (undem) is defined as parenchymal lesions without demyelination and demyelinated (demyel) is defined as parenchymal lesions with demyelination. Three to eight sections from seven mice were quantified and Bl-1 KO mice show a significantly reduced number of undemyelinated lesions per section (WT 0.7 ± 0.4 *versus* Bl-1 KO 0.05 ± 0.09). Bar graphs show the average number of lesions per section of each genotype as the mean ± S.E.M. (**d**) Attenuated immunoglobulin production quantified by ELISA 10 days after immunization with NPCG precipitated in Alum in Bl-1 KO mice. (**e**) Class switching of Bl-1 KO and control splenocytes and CD19+ B cells at day 4 of *in vitro* stimulation with LPS+IL-4. IgG1 of 200 000 events was quantified by intracellular staining as indicated. Bar graphs show the mean ± S.E.M., $n = 3$. The box and whiskers represent the median amount of the indicated immunoglobulins with the box extending from the 25th quartile to the 75th quartile and the whiskers represent the minimum and maximum values ($n = 10$). EAE data were analyzed by two-way ANOVA with Bonferroni *post hoc* correction; all other data were analyzed by two-tailed *t*-tests, $^*P < 0.05$

which can be quantified intracellularly by flow cytometry. Upon this treatment, significantly less Bl-1 KO cells switched to IgG1 compared with control splenocytes, suggesting that defective signaling is involved in the observed phenotype (Figure 6e).

Discussion

Our observations indicate that Bl-1 has a major role in the correct functioning of the adaptive immune system. B and T cells malfunction apparently because of profound changes in intracellular Ca^{2+} homeostasis and dynamics. All aspects of the cellular Ca^{2+} machinery are altered in the absence of functioning Bl-1 and this correlates with an enhanced nuclear translocation of Ca^{2+}-dependent transcription factors and an overload of the mitochondrial Ca^{2+} buffer capacity leading to spontaneous cell death in culture. These results are well in line with previously reported effects of Bl-1 in the control of the ER Ca^{2+} content.[6–8,10] Also, structural evidence obtained from a bacterial homolog of Bl-1 just demonstrated that Bl-1 is indeed a Ca^{2+} leak channel with an evolutionarily conserved pH sensor.[11]

We observed an increased ER Ca^{2+} concentration as expected for cells lacking an important ER Ca^{2+} leak channel and a reduced SOCE caused by downregulation of the plasma membrane Ca^{2+} channel Orai1. It is clear that the already overfilled ER does not need further filling, but why and how does this result in the observed increase in cytosolic Ca^{2+} concentration?

In BI-1 KO, there is less Ca^{2+} leak from the ER, and, hence, more Ca^{2+} is available for IP_3-induced Ca^{2+} release, which can explain the higher Ca^{2+} transients. It is possible that even under resting conditions, constitutive activation of B- or T-cell receptors provokes basal Ca^{2+} release, which is expected to be higher in KO cells. Cytosolic Ca^{2+} transients are normally cleared efficiently by extrusion to the extracellular space or immediate refilling of the ER by SERCA, which (i) is apparently less effective in immune cells in general, thereby explaining why this phenotype is most pronounced in the immune system[33] and (ii) is directly inhibited by the Ca^{2+} load of the store.[34] It was also shown previously that a high ER Ca^{2+} load negatively regulates Ca^{2+} reuptake from the cytosol,[35] which is probably mediated by the oxidoreductase ERp57. In conditions of high luminal Ca^{2+}, like in the absence of functional BI-1, ERp57 binds SERCA2b (the ubiquitously expressed isoform) and inhibits its activity through the facilitation of disulfide bond formation in the longest ER facing loop of SERCA2b.[36] As we observed an unexpected downregulation of the UPR target protein ERp57 in BI-1 KO splenocytes, we speculate that this represents a compensatory mechanism to remove the breaks from SERCA2b and relieve the cell from the excessive cytosolic Ca^{2+} load.

Finally, how can we resolve our findings with the proposed function of BI-1 as a direct inhibitor of IRE1α?[14] IRE1α not only interacts with BI-1 but also with the proapoptotic proteins BAX and BAK (Bcl-2 homologous antagonist/killer), which in contrast to BI-1 activate IRE1α signaling.[37] Cells lacking both proteins have a reduced ER Ca^{2+} concentration[38] because of an increased Ca^{2+} leak[39] and therefore behave like BI-1-overexpressing cells.[7] As BI-1 does not directly interact with BAX/BAK[5,14] but attenuates the interaction of BAX with IRE1α,[14] it was speculated that BI-1 acts upstream of these proteins in the control of IRE1α inactivation.[14] However, maybe the proposed inactivation of IRE1α by BI-1 is reciprocal, meaning that IRE1α also inhibits BI-1 channel activity. To the best of our knowledge, this has not yet been studied. In this scenario, the lack of BAX/BAK in double KO cells would inhibit IRE1α, thereby activating BI-1 and causing a reduction in the ER Ca^{2+} concentration, which is in accordance with reported results.

In summary, our findings present *in vivo* evidence that the Ca^{2+} channel activity of BI-1 is critically important for immune cell function and survival.

Materials and Methods

Animals and laboratory tests. BI-1 KO mice first described by Chae *et al*.[5] were identified by genotyping according to the published protocol and backcrossed to WT C57/Bl6 mice for more than generations. All mice were maintained in the local animal facility. All animal experiments were fully approved by local authorities for animal experimentation. Mice were age and sex matched and 8–12 weeks old. The blood count and liver enzyme analysis were carried out by the clinical laboratory of the University Hospital Düsseldorf. A differential blood count was carried out manually in stained blood streaks.

Flow cytometry. Single-cell suspensions were prepared from different organs and the erythrocytes lysed with tris-ammonium chloride, pH 7.2. Cells were treated with Fc-block (Affymetrix eBioscience, San Diego, CA, USA), washed and surface stained with antibodies against CD5, CD19, CD21 (7G6), CD23, CD90.2, and IgD, B220 and anti-IgM (BD Bioscience, Franklin Lakes, NJ, USA). All samples were measured on a FACSCanto II (Becton, Dickinson, Franklin Lakes, NJ, USA) and analyzed with FlowJo, LLC (Ashland, OR, USA).

Immunohistochemistry. Animals were perfused and tissues fixed with 4% paraformaldehyde (Carl Roth, Karlsruhe, Germany). Thick slices (20 μM) of the spinal cord and 8 μm sections from spleens were cut in a cryotome (Leica Mikrosysteme Vertrieb GmbH, Wetzlar, Germany) and stained with primary antibodies against CD1d (Affymetrix eBioscience), MOMA-1 (Affymetrix eBioscience), Iba1 (Wako Chemicals GmbH, Neuss, Germany; 1 : 800) and MBP (EMD Millipore, Billerica, MA, USA; 1 : 500). Iba1 and MBP were detected with secondary anti-Cy2 and anti-Cy3 antibodies (EMD Millipore; 1 : 500) and CD1d and MOMA-1 with a biotinylated secondary antibody (DIANOVA Vertriebs-Gesellschaft mbH, Hamburg, Germany), treated with streptavidin-horseradish peroxidase and stained with tyramide (Cy3) and fluorescein (FITC). Nuclei were counterstained with Hoechst 33258 (Life Technologies GmbH, Darmstadt, Germany). Slices were mounted with Immuno Mount (Fisher Scientific GmbH, Schwerte, Germany) and analyzed on an Olympus BX51 (Olympus, Hamburg, Germany).

Transmission electron microscopy. Cells were pelleted, fixed in 2.5% glutaraldehyde, 2% PFA and 0.05% tannic acid and later treated with 2% osmium tetroxide. After staining with 1.5% uranylacetate and 1.5% phosphotungstic acid, pellets were embedded in epoxide resin (Spurr) and dissected in 70- to 80-nm-thick slices on an ultramicrotome (Reichert Ultracut; Reichert-Jung, Vienna, Austria). Images (30 KO and 32 WT) were taken on a Hitachi H 600 transmission electron microscope (Hitachi High Technologies America, Schaumburg, IL, USA).

Ca^{2+} measurements

Flow cytometry: Cells were incubated in culture medium consisting of RPMI 1640 (Fisher Scientific GmbH) supplemented with 10% FCS (Fisher Scientific GmbH), 100 U/ml penicillin and 100 μg/ml streptomycin (Invitrogen), 1% glutamax (Invitrogen) and 0.1% β-mercaptoethanol (Fisher Scientific GmbH), and the Ca^{2+} concentration was adjusted with 1M $CaCl_2$ and 1M EGTA. A total of 1×10^6 cells per ml were loaded with either 5 μM Fluo8-AM (Santa Cruz Biotechnology, Inc., Dallas, TX, USA), 2 μM Rhod2-AM (AAT Bioquest, Sunnyvale, CA, USA) or 5 μM CellROX (Fisher Scientific GmbH), washed, measured on a BD FACSCalibur or BD FACS Canto II (BD Bioscience) and analyzed with FlowJo, LLC. For pH-dependent measurements, cells were resuspended in HBSS (Fisher Scientific GmbH) adjusted to the indicated values with 1M HCl and 1M NaOH, directly after staining and measured immediately.

Ca^{2+} kinetics: Fura2 Ca^{2+} imaging experiments were conducted on a BD Pathway 855 High Content Imaging System (BD Bioscience). The 96-well imaging plates (BD Bioscience) were coated with 5 mg/ml BSA (Carl Roth) and 0.01% (w/v) poly-L-lysine (Sigma-Aldrich, St. Louis, MO, USA), splenocytes seeded at a density of 150 000 cells per well and loaded with 3 μM Fura2-AM (Life Technologies GmbH) in HBSS at RT for 20 min before the experiment. SOCE was quantified by a high-throughput method previously validated using STIM1 $-/-$ mouse embryonic fibroblasts and shown to be reliable.[40] Ratiometric Fura2-AM values were converted to absolute Ca^{2+} values as described[41] and analyzed with Attovision (BD Bioscience). For measuring the Ca^{2+} kinetics of B and T cells, splenocytes were incubated with 3 μM Fluo8 for 30 min at RT. Cells were washed once in DMEM without phenol red (Fisher Scientific GmbH) and resuspended at 40×10^6 cells per ml in the washing medium. A total of 2×10^6 cells were additionally incubated with 3 μg/ml biotinylated anti-CD3 antibody (Affymetrix eBioscience) for 10 min at RT, and before the measurement, 2×10^6 cells were transferred into 500 μl Ringer solution (Fresenius Kabi, Bad Homburg, Germany). After recording the baseline for 1 min in a FACS Canto II flow cytometer, either 3 μg/ml streptavidin (Fisher Scientific GmbH) were added to the cells, which were previously incubated with biotinylated anti-CD3 antibody or 10 μg/ml anti-IgM (Jackson ImmunoResearch Laboratories, Inc., West Grove, PA, USA). Data were recorded for 5 min and analyzed with the kinetics module of FlowJo, LLC.

Immunoblotting. Splenocytes were lysed in ice-cold CelLytic M buffer (Sigma-Aldrich) containing Mini Complete Protease Inhibitor Cocktail (Sigma-Aldrich) and centrifuged for 30 min at 16 000 × *g*. Subcellular fractionations were prepared as described previously.[42] Fifty micrograms of protein lysates were blotted and incubated with primary antibodies (diluted 1 : 1000) as follows: IP3R Pan (Rbt475),[43] ERp57 (Cell Signaling; no. 2881), Ero1-Lα (Cell Signaling; no. 3264), BIP (Cell Signaling; no. 3177), ERp72 (Cell Signaling; no. 5033), ERp44 (Cell Signaling; no. 3798), GrP94 (Cell Signaling; no. 2104), IκBα (Cell Signaling; no. 4814), phospho-IκBα (Cell Signaling; no. 2859), NF-κB p65 (Cell Signaling; no. 8242), phospho-NF-κB p65 (Cell Signaling; no. 3033), ubiquitin (Dako Deutschland GmbH, Hamburg, Germany; no. Z0458), STIM1 (stromal interaction molecule 1; Abnova (Taipei, Taiwan); no. h0000678-m01), ORAI1 (1 : 500; Alomone Labs, Jerusalem, Israel; no. ACC-062), NFATc1 (7A6) (1:200; Santa Cruz Biotechnology, Inc.; no. msc-7294), NF-κB2 p100/p52 (Cell Signaling; no. 4882), HDAC1 (Cell Signaling; no. 2062), $\alpha\beta$-tubulin (Cell Signaling; no. 2148), RelB (Santa Cruz Biotechnology, Inc.; no. sc-226), RelA (Santa Cruz Biotechnology, Inc.; no. sc-8008), c-Rel (Santa Cruz Biotechnology, Inc.; no. sc-71), NF-κB2 p105/p50 (Santa Cruz Biotechnology, Inc.; no. sc-7178), Serca2b (a kind gift from Frank Wuytack and Peter Vangheluwe), calreticulin (1 : 500), calnexin C20 (1 : 500), calnexin H70 (1 : 500), HSPA8 (Cell Signaling; no. 8444) and actin (1 : 4000; EMD Millipore; no. MAB1501). Antisera without vendor were obtained from the Bultynck Lab (Leuven, Belgium). Secondary antibodies used were as follows: anti-mouse or anti-rabbit IgG (Fc) infrared fluorescence conjugated secondary antibodies (LI-COR, Lincoln, NE, USA; 1 : 30 000). The membranes were scanned for infrared fluorescence at 680 and 800 nm using the Odyssey System (LI-COR) and the signal was analyzed with the image processing software ImageJ (National Institutes of Health, Bethesda, MD, USA).

Immunofluorescence staining and nuclear translocation assay. Splenocytes were seeded at a density of 150 000 cells per well on BSA and poly-L-lysine-coated 96-well imaging plates, fixed, blocked and incubated overnight with anti-NF-κB p65 (Cell Signaling; no. 8242) or anti-NFATc1 (Hybridoma Bank, Iowa City, IA, USA; no. 7A6) diluted 1 : 100 in blocking solution. After incubation with Cy3-labeled secondary antibody (EMD Millipore; 1 : 500) and nuclear staining with 150 nM DAPI (Sigma-Aldrich), pictures were taken on a Leica TSC SP5 confocal microscope (Leica Mikrosysteme Vertrieb GmbH) at x63 magnification and nuclear translocation of NF-κB p65 or NFATc1 was quantified in a BD Pathway 855 high content imaging system (BD Bioscience). Nuclear regions of interest were identified by DAPI signal and a concentric region around the nuclear region of interest was assessed as the cytoplasm. The ratio of the nuclear and cytoplasmic Cy3 signal was quantified with Attovision (BD Bioscience).

Measurement of mitochondrial oxygen consumption. A phosphorylation control protocol was performed for measurements of mitochondrial oxygen consumption of purified B cells using the high-resolution respirometer Oxygraph-2k (Oroboros Instruments Corp., Innsbruck, Austria). Intact B cells were monitored in two closed glass chambers under continuous stirring at 750 r.p.m. at 37 °C in 2 ml growth medium at a density of 3–4 × 10^6 cells per ml. After measurement of routine respiration, 2 μg/ml oligomycin was added to measure the leak respiration state. The electron transfer system capacity was determined by titration of the uncoupler carbonyl cyanide 4-(trifluoromethoxy) phenylhydrazone (FCCP) in 0.5 μM steps until a maximum flow was reached. Respiration was inhibited by application of 0.5 μM rotenone and 2.5 μM antimycin A to determine non-mitochondrial residual oxygen consumption (ROX). All substrates and inhibitors used were obtained from Sigma-Aldrich. Oxygen concentration and oxygen flow per cell were recorded in 2 s intervals using the DatLab Software 5.1 (Oroboros Instruments Corp.). To compare mitochondrial respiratory states, all values measured were corrected for ROX. All experiments were performed using instrumental background correction and after calibration of the polarographic oxygen sensors.

Viability and caspase assays. Splenocytes were magnetically sorted with an AutoMACS (magnetic cell seperation) cell separator (Miltenyi Biotec GmbH, Bergisch Gladbach, Germany), using either the CD43 (Ly-48) or Pan T-Cell Isolation Kit II (Miltenyi Biotec GmbH). Cell viability was assessed with LIVE/DEAD Fixable Dead Cell Stain Kit Green/Violet (Invitrogen). Caspase-3/7, -8 and -9 activity was measured with the Caspase Glo Assay Systems (Promega Corporation, Madison, WI, USA). In short, 50 000 B cells were seeded in 100 μl culture medium (as described above) in white-walled 96-well plates (Fisher Scientific GmbH). One hundred microliters of Caspase Glo reagent (Promega Corporation), containing the proteasome inhibitor MG-132, was added to the wells, the plate was shaken on a plate shaker for 1 min at 300 r.p.m. and then incubated for 40 min at RT. Luminescence was measured in a GENios Pro plate reader (Tecan Group AG, Männedorf, Switzerland).

XBP-1 splicing. PCR primers 5′-ACACGCTTGGGAATGGACAC-3′ and 5′-CCATGGGAAGATGTTCTGGG-3′ encompassing the spliced sequences in xbp-1 mRNA were used for PCR amplification with Platinum Taq Super Mix (Invitrogen). PCR products were separated on a 2.5% agarose gel (Sigma-Aldrich) and visualized with ethidium bromide (Sigma-Adrich). Band density was analyzed with the ImageJ software (National Institutes of Health) and was expressed as the density of spliced XBP-1 divided by the density of spliced XBP-1 plus unspliced XBP-1, where no splicing corresponds to 0%.

Active EAE and immunization. Female WT and KO mice were injected subcutaneously with 200 μg MOG_{35-55} peptide (Biotrend Chemikalien GmbH, Köln, Germany) emulsified in Complete Freund's Adjuvant (1 : 1 (v/v)), which consisted of Incomplete Freund's Adjuvant supplemented with 5 mg/ml *Mycobacterium tuberculosis* H37RA (Difco Laboratories, Beckton, Dickinson, USA). For boosting, 200 ng Pertussis toxin (Sigma-Aldrich) was injected intraperitoneally on days 0 and 2 after immunization. From day 1, severity of the EAE was monitored and graded on a scale from 0 to 5: 0, no disease; 1, limp tail; 2, hind limb weakness; 3, hind limb paralysis; 4, hind and fore limb paralysis; 5, moribundity and death.

Immunoglobulin measurements. For immunizations, mice were injected intraperitoneally with 100 μg NPCG (Biosearch Technologies, Petaluma, CA, USA). Serum was collected from the peripheral blood and the immunoglobulin concentrations and NPCG-specific antibodies were determined by ELISA. For *in vitro* class switch experiments, splenocytes were cultured in triplicates of 300 000 treated with LPS (Sigma-Aldrich; 50 μg/ml)+IL4 (R&D Systems, Inc., Minneapolis, MN, USA; 20 ng/ml) for 4 days. The frequency of switched cells was measured by flow cytometry by gating on IgM^- $IgG1^+$ events. For each sample 200 000 events were acquired for analysis.

Statistical analysis. Data were analyzed as mean ± S.D., and the statistical significance was analyzed using two-tailed *t*-tests or analysis of variance (ANOVA) with Tukey's multiple comparison test as indicated.

Conflict of Interest

The authors declare no conflict of interest.

Acknowledgements. This work was supported by DFG ME1922/9-1 (to AM) and the Forschungskommission HHU (to AM and HHH).

Author contributions

DL, MG, AW, HHH, NH and AM designed the experiments with advice from GB, JBP and HdS. DL, TS, AG, PA, BK, MG, KZ, PAQ, MH and PA performed the experiments. DL, TS, BK, MG, KZ, NH and AM analyzed the data. DL, JCR and AM wrote the manuscript.

1. Berridge MJ, Bootman MD, Roderick HL. Calcium: calcium signalling: dynamics, homeostasis and remodelling. *Nat Rev Mol Cell Biol* 2003; **4**: 517–529.
2. Demaurex N, Distelhorst CW. Cell biology. Apoptosis – the calcium connection. *Science* 2003; **300**: 65–67.
3. Hetz C. The unfolded protein response: controlling cell fate decisions under ER stress and beyond. *Nat Rev Mol Cell Biol* 2012; **13**: 89–102.
4. Henke N, Lisak DA, Schneider L, Habicht J, Pergande M, Methner A. The ancient cell death suppressor BAX inhibitor-1. *Cell Calcium* 2011; **50**: 251–260.
5. Xu Q, Reed JC. Bax inhibitor-1, a mammalian apoptosis suppressor identified by functional screening in yeast. *Mol Cell* 1998; **1**: 337–346.
6. Chae H-J, Kim H-R, Xu C, Bailly-Maitre B, Krajewska M, Krajewski S *et al.* BI-1 regulates an apoptosis pathway linked to endoplasmic reticulum stress. *Mol Cell* 2004; **15**: 355–366.
7. Westphalen BC, Wessig J, Leypoldt F, Arnold S, Methner A. BI-1 protects cells from oxygen glucose deprivation by reducing the calcium content of the endoplasmic reticulum. *Cell Death Differ* 2005; **12**: 304–306.
8. Bultynck G, Kiviluoto S, Henke N, Ivanova H, Schneider L, Rybalchenko V *et al.* The C terminus of Bax inhibitor-1 forms a Ca^{2+}-permeable channel pore. *J Biol Chem* 2012; **287**: 2544–2557.
9. Lisak DA, Schacht T, Enders V, Habicht J, Kiviluoto S, Schneider J *et al.* The transmembrane Bax inhibitor motif (TMBIM) containing protein family: Tissue expression,

intracellular localization and effects on the ER CA(2+)-filling state. *Biochim Biophys Acta* 2015; **1853**: 2104–2114.
10. Kiviluoto S, Luyten T, Schneider L, Lisak D, Rojas-Rivera D, Welkenhuyzen K *et al.* Bax Inhibitor-1-mediated Ca(2+) leak is decreased by cytosolic acidosis. *Cell Calcium* 2013; **54**: 186–192.
11. Chang Y, Bruni R, Kloss B, Assur Z, Kloppmann E, Rost B *et al.* Structural basis for a pH-sensitive calcium leak across membranes. *Science* 2014; **344**: 1131–1135.
12. Bailly-Maitre B, Bard-Chapeau E, Luciano F, Droin N, Bruey J-M, Faustin B *et al.* Mice lacking bi-1 gene show accelerated liver regeneration. *Cancer Res* 2007; **67**: 1442–1450.
13. Bailly-Maitre B, Fondevila C, Kaldas F, Droin N, Luciano F, Ricci J-E *et al.* Cytoprotective gene bi-1 is required for intrinsic protection from endoplasmic reticulum stress and ischemia–reperfusion injury. *Proc Natl Acad Sci USA* 2006; **103**: 2809–2814.
14. Lisbona F, Rojas-Rivera D, Thielen P, Zamorano S, Todd D, Martinon F *et al.* BAX inhibitor-1 is a negative regulator of the ER stress sensor IRE1alpha. *Mol Cell* 2009; **33**: 679–691.
15. Kiviluoto S, Schneider L, Luyten T, Vervliet T, Missiaen L, De Smedt H *et al.* Bax inhibitor-1 is a novel IP_3 receptor-interacting and -sensitizing protein. *Cell Death Dis* 2012; **3**: e367.
16. Gilmore TD, Herscovitch M. Inhibitors of NF-kappaB signaling: 785 and counting. *Oncogene* 2006; **25**: 6887–6899.
17. Weih DS, Yilmaz ZB, Weih F. Essential role of RelB in germinal center and marginal zone formation and proper expression of homing chemokines. *J Immunol* 2001; **167**: 1909–1919.
18. Hövelmeyer N, Wunderlich FT, Massoumi R, Jakobsen CG, Song J, Wörns MA *et al.* Regulation of B cell homeostasis and activation by the tumor suppressor gene CYLD. *J Exp Med* 2007; **204**: 2615–2627.
19. Guo F, Weih D, Meier E, Weih F. Constitutive alternative NF-kappaB signaling promotes marginal zone B-cell development but disrupts the marginal sinus and induces HEV-like structures in the spleen. *Blood* 2007; **110**: 2381–2389.
20. Dolmetsch RE, Xu K, Lewis RS. Calcium oscillations increase the efficiency and specificity of gene expression. *Nature* 1998; **392**: 933–936.
21. Dolmetsch RE, Lewis RS, Goodnow CC, Healy JI. Differential activation of transcription factors induced by Ca^{2+} response amplitude and duration. *Nature* 1997; **386**: 855–858.
22. Pahl HL, Sester M, Burgert HG, Baeuerle PA. Activation of transcription factor NF-kappaB by the adenovirus E3/19K protein requires its ER retention. *J Cell Biol* 1996; **132**: 511–522.
23. Pahl HL, Baeuerle PA. A novel signal transduction pathway from the endoplasmic reticulum to the nucleus is mediated by transcription factor NF-kappa B. *EMBO J* 1995; **14**: 2580–2588.
24. Pahl HL, Baeuerle PA. Activation of NF-kappa B by ER stress requires both Ca^{2+} and reactive oxygen intermediates as messengers. *FEBS Lett* 1996; **392**: 129–136.
25. Davies SP, Reddy H, Caivano M, Cohen P. Specificity and mechanism of action of some commonly used protein kinase inhibitors. *Biochem J* 2000; **351**: 95–105.
26. Zhang SL, Yeromin AV, Zhang XH-F, Yu Y, Safrina O, Penna *et al.* Genome-wide RNAi screen of Ca(2+) influx identifies genes that regulate Ca(2+) release-activated Ca(2+) channel activity. *Proc Natl Acad Sci USA* 2006; **103**: 9357–9362.
27. Prakriya M, Feske S, Gwack Y, Srikanth S, Rao A, Hogan PG. Orai1 is an essential pore subunit of the CRAC channel. *Nature* 2006; **443**: 230–233.
28. White C, Li C, Yang J, Petrenko NB, Madesh M, Thompson CB *et al.* The endoplasmic reticulum gateway to apoptosis by Bcl-X(L) modulation of the InsP3R. *Nat Cell Biol* 2005; **7**: 1021–1028.
29. Li P, Nijhawan D, Budihardjo I, Srinivasula SM, Ahmad M, Alnemri ES *et al.* Cytochrome c and dATP-dependent formation of Apaf-1/caspase-9 complex initiates an apoptotic protease cascade. *Cell* 1997; **91**: 479–489.
30. Sano R, Hou Y-CC, Hedvat M, Correa RG, Shu C-W, Krajewska M *et al.* Endoplasmic reticulum protein Bi-1 regulates Ca^{2+}-mediated bioenergetics to promote autophagy. *Genes Dev* 2012; **26**: 1041–1054.
31. Zhong F, Harr MW, Bultynck G, Monaco G, Parys JB, De Smedt H *et al.* Induction of Ca^{2+}-driven apoptosis in chronic lymphocytic leukemia cells by peptide-mediated disruption of Bcl-2-IP3 receptor interaction. *Blood* 2011; **117**: 2924–2934.
32. Smith KG, Light A, Nossal GJ, Tarlinton DM. The extent of affinity maturation differs between the memory and antibody-forming cell compartments in the primary immune response. *EMBO J* 1997; **16**: 2996–3006.
33. Suzuki J, Kanemaru K, Ishii K, Ohkura M, Okubo Y, Iino M. Imaging intraorganellar Ca^{2+} at subcellular resolution using CEPIA. *Nat Commun* 2014; **5**: 4153.
34. Favre CJ, Schrenzel J, Jacquet J, Lew DP, Krause KH. Highly supralinear feedback inhibition of Ca^{2+} uptake by the Ca^{2+} load of intracellular stores. *J Biol Chem* 1996; **271**: 14925–14930.
35. Mogami H, Tepikin AV, Petersen OH. Termination of cytosolic Ca^{2+} signals: Ca^{2+} reuptake into intracellular stores is regulated by the free Ca^{2+} concentration in the store lumen. *EMBO J* 1998; **17**: 435–442.
36. Li Y, Camacho P. Ca^{2+}-dependent redox modulation of SERCA 2b by ERp57. *J Cell Biol* 2004; **164**: 35–46.
37. Hetz C, Bernasconi P, Fisher J, Lee A-H, Bassik MC, Antonsson B *et al.* Proapoptotic BAX and BAK modulate the unfolded protein response by a direct interaction with IRE1alpha. *Science* 2006; **312**: 572–576.
38. Scorrano L, Oakes SA, Opferman JT, Cheng EH, Sorcinelli MD, Pozzan T *et al.* BAX and BAK regulation of endoplasmic reticulum Ca^{2+}: a control point for apoptosis. *Science* 2003; **300**: 135–139.
39. Oakes SA, Scorrano L, Opferman JT, Bassik MC, Nishino M, Pozzan T *et al.* Proapoptotic BAX and BAK regulate the type 1 inositol trisphosphate receptor and calcium leak from the endoplasmic reticulum. *Proc Natl Acad Sci USA* 2004; **102**: 105–110.
40. Henke N, Albrecht P, Pfeiffer A, Toutzaris D, Zanger K, Methner A. Stromal interaction molecule 1 (STIM1) is involved in the regulation of mitochondrial shape and bioenergetics and plays a role in oxidative stress. *J Biol Chem* 2012; **287**: 42042–42052.
41. Williams DA, Fay FS. Intracellular calibration of the fluorescent calcium indicator Fura-2. *Cell Calcium* 1990; **11**: 75–83.
42. Sasaki Y, Derudder E, Hobeika E, Pelanda R, Reth M, Rajewsky K *et al.* Canonical NF-kappaB activity, dispensable for B cell development, replaces BAFF-receptor signals and promotes B cell proliferation upon activation. *Immunity* 2006; **24**: 729–739.
43. Bultynck G, Szlufcik K, Kasri NN, Assefa Z, Callewaert G, Missiaen L *et al.* Thimerosal stimulates Ca^{2+} flux through inositol 1,4,5-trisphosphate receptor type 1, but not type 3, via modulation of an isoform-specific Ca^{2+}-dependent intramolecular interaction. *Biochem J* 2004; **381**: 87–96.

Supplementary Information accompanies this paper on Cell Death and Differentiation website (http://www.nature.com/cdd)

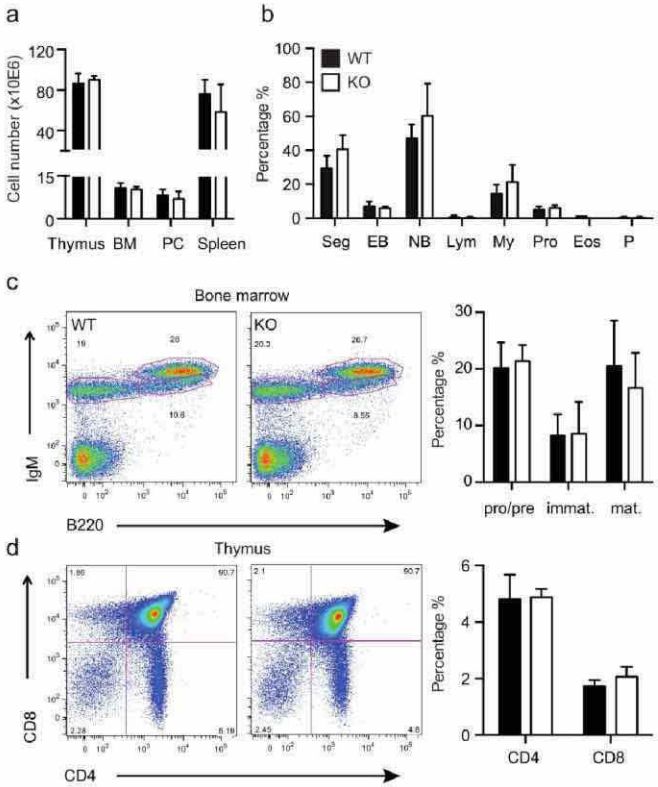

Supplemental Figure 1: Additional phenotype of the immune system in BI-1 KO splenocytes. (a) Total cell number in the thymus, bone marrow (BM), peritoneal cavity (PC) and spleen are similar in WT (closed) and BI-1 KO (open) mice. Bar graphs represent the average cell number as the mean ± SD from 12 mice. (b) The relative fractions of bone marrow cell types do not differ between WT and BI-1 KO mice. Bar graphs represent the relative percentage of segment cells (Seg), erythroblasts (EB), normoblasts (NB), lymphocytes (Lym), myelocyte promyelocytes (My), promyelocytes (Pro), eosinophils (Eos) and plasma cells (P) as the mean ± SD from n = 3 mice (c) Percentages of pro/pre, immature as well as mature recirculating B cells do not differ between WT and BI-1 KO mice. Bone marrow cells were stained with IgM and B220 and gated for IgM+/B220- (pro/pre B cells), IgM+/B220+ (immature B cells) and IgM++/B220+ (mature recirculating B cells). Dot plots show representative gates from one WT and one BI-1 KO mouse. Bar graphs represent the average percentage of the indicated cell types as the mean ± SEM from two independent experiments. (d) The percentages of CD4 SP (single positive), CD8 SP and CD4CD8 DP (double positive) cells in the thymus are similar in WT and BI-1 KO mice. Thymus cells were stained with CD4 and CD8 and gated accordingly with a flow cytometer. The dot plots show representative gates for one WT and one BI-1 KO mouse. Bar graphs show the average percentage of CD4+ and CD8+ as the mean ± SEM from 3 versus 3 mice. Data was analyzed by two-tailed t-tests, *P < 0.05.

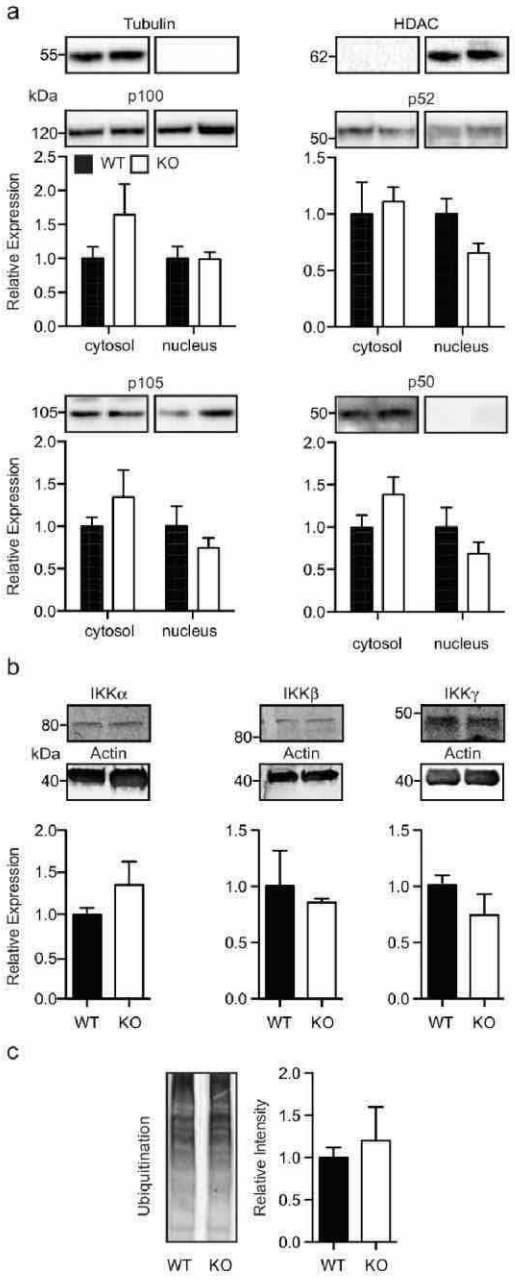

Supplemental Figure 2: No changes in the expression levels of class I NF-κB, IKKs and ubiquitination. (a) No changes in p100/p52 and p105/p50 abundance in cytosolic and nuclear fractions and (b) IKKα, IKKβ and IKKγ in unfractionated lysates of BI-1 KO splenocytes compared to WT splenocytes. Immunoblots were incubated with the indicated antibodies. α/β Tubulin served as loading control for the cytosolic fraction, HDAC for the nuclear fraction, and Actin for whole cell lysates. Molecular weight is indicated. Bar graphs show mean intensity values normalized to WT ± SD from six mice. (c) Similar level of ubiquitination in WT and BI-1 KO splenocytes. Immunoblots were incubated with a primary α-poly-ubiquitin antibody. GAPDH served as loading control on the same blot and size is indicated. Bar graphs show mean intensity values normalized to WT ± SD from six mice. Data were analyzed by two-tailed t-tests, *P < 0.05.

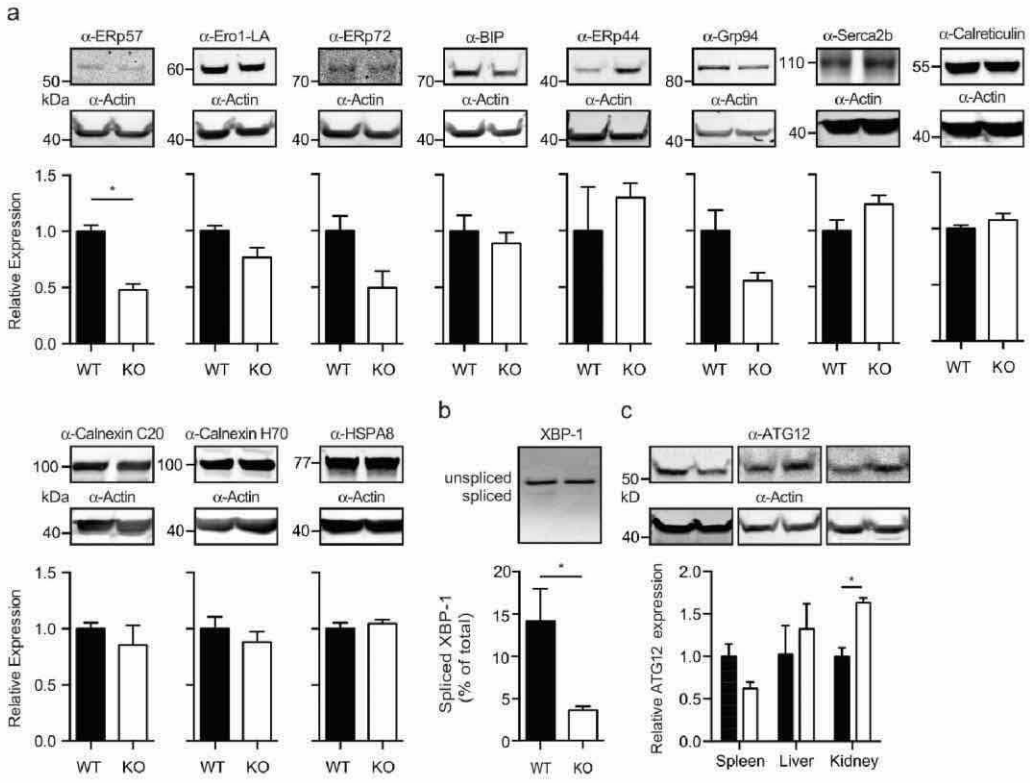

Supplemental Figure 3: No evidence of ER stress or altered autophagy in BI-1 KO splenocytes immediately after preparation. (a) No upregulation of ER chaperones and ER folding proteins in BI-1 KO splenocytes. ERp57 is significantly downregulated. Immunoblots were incubated with the indicated antibodies. Actin served as loading control on the same blot and size is indicated. Bar graphs show mean intensity values normalized to WT ± SD from six mice. (b) Decreased XBP-1 splicing in BI-1 KO splenocytes analyzed by PCR visualized on an agarose gel. Bar graphs show the mean percentage ± SD of spliced XBP-1 / (spliced XBP-1 + unspliced XBP-1) from six mice. (c) The autophagy marker ATG12 is significantly upregulated in kidney tissue from BI-1 KO mice but not in splenocytes or liver. Immunoblots were incubated with an antibody against ATG12. Actin served as a loading control on the same blot and size is indicated. Bar graphs show the relative expression of ATG12 normalized to its expression in WT mice as mean ± SEM from six mice. Data were analyzed by two-tailed t-tests, *P < 0.05.

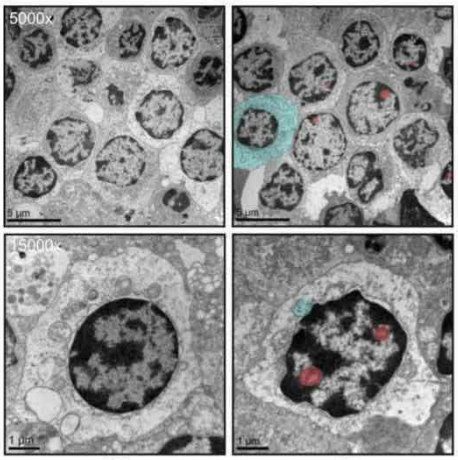

Supplemental Figure 4: Ultrastructural changes in BI-1 KO B cells. Representative electron-microscopic images of magnetically sorted and negatively selected WT and BI-1 KO B cells shows an altered texture of the cytoplasm (shaded in blue), defective organelles (shaded in blue) and presence of nuclear inclusions (shaded in red) in BI-1 KO B cells. Magnification is indicated.

Summary of the results

The transmembrane BAX inhibitor motif (TMBIM) containing protein family: Tissue expression, intracellular localization and effects on the ER Ca^{2+}-filling state

In this study, we investigated the relationship between the six TMBIM protein family members TMBIM 1 – 6, their secondary structure, their intracellular localization and their effects on the cellular Ca^{2+} homeostasis. Bioinformtical analysis showed that all six TMBIM proteins and their bacterial homologue BsYetJ share seven conserved transmembrane domains and posses a C-terminal di-aspartyl pH sensor. They can be mostly found in the Golgi apparatus (TMBIM 1 – 3) or in the ER (TMBIM 4 – 6). We found that TMBIM 5 has an N-terminal mitochondrial target sequence and were able to show that it can localize in the ER as well as in the mitochondria. Overexpression of all six TMBIM proteins in HT22 cells resulted in decreased Ca^{2+} levels in the intracellular Ca^{2+} stores, reflecting cellular localization.

Bax inhibitor-1 is a Ca^{2+} channel critically important for immune cell function and survival

TMBIM 6, also known as BI-1, is a pH-sensitive Ca^{2+} leak channel and an antiapoptotic protein. We discovered that BI-1 deficient mice have increased numbers of marginal zone (MZ) B cells, which correlated which increased nuclear translocation of the transcription factors NF-κB and NFAT. Simultaneously, BI-1 KO T and B cells had increased cytosolic Ca^{2+} levels and were prone to apoptosis when cultured. B cells appeared to be especially sensitive and displayed defective cell organelles when analyzed by electron microscopy as well as increased caspase activity and elevated mitochondrial Ca^{2+} concentrations. However, they showed no signs of ER stress and we therefore concluded that the high amount of B cell apoptosis is a result of an exhausted mitochondrial Ca^{2+} buffer capacity. We employed experimental autoimmune encephalomyelitis (EAE) as a T cell dependent in vivo model and immunization with NPCG as a B cell dependent in vivo model and saw decreased function of both cell types from BI-1 KO mice. BI-1 deficient mice had less clinical symptoms during an EAE and less microglia invasion as well as reduced antibody production after NPCG immunization.

Discussion

BI-1 is the founding member of the TMBIM protein family, which consists of six proteins and shares the evolutionary conserved motif UPF0005. In the first publication presented in this dissertation, we systematically described the relationship between these proteins, their tissue expression, their subcellular localization, their secondary structure and their effect on the cellular Ca^{2+} homeostasis.

We used the bioinformatical tool TMpred to compare the structure of TMBIM1 – 6. All six proteins have a very similar structure containing at least seven transmembrane domains with the last domain being less hydrophobic than the previous. While TMBIM1 – 4 and BI-1 have seven transmembrane domains, TMBIM5 has one more on its N-terminal end, preceding the TMBIM homology region.

We next aligned the sequences of TMBIM1 – 6 and the bacterial homologue BsYetJ with the bioinformatical tool PRALINE, which showed a strong conservation of the amino acid sequence at the first, sixth and seventh transmembrane domain (the second, seventh and eighth for TMBIM5) between all investigated proteins. Additionally, the five amino acids in front of the first (or the second in case of TMBIM5) transmembrane domain are strongly conserved. The most important finding however is that the di-aspartyl pH sensor (which corresponds to D188 and D213 in BI-1) is conserved in all proteins, including the bacterial homologue. As previously described (104), D188 and D213 are negatively charged at a physiological pH around 7 and can thereby allow Ca^{2+} flow through a pore which they form with D209. At more acidic pH, the amino acids become protonated and inhibit the Ca^{2+} flow. At more basic pH, a hydrogen bond between H78 and D213 can form which closes the Ca^{2+} pore. The interplay between D188, D209, D213 and H78 thus allows the pH dependent regulation of the Ca^{2+} flux. While only D188 and D213 are conserved through the whole TMBIM family and their bacterial homologue, L-arginine (R) can be found instead of L-histidine (H) at the position which corresponds to H78 in BI-1 in TMBIM1-4. L-arginine shares the positive charge of L-histidine and likely performs similar in regard to the pH dependent pore formation. TMBIM5 however is again an exception, since it possesses a negatively charged L-aspartic acid at this position, which will not show the same behavior at basic and acidic pH as R and H. This might indeed alter any Ca^{2+} regulating properties which TMBIM5 might have, as highlighted by the fact that TMBIM5 was the only family member whose overexpression failed to lower the intracellular Ca^{2+} concentration. Whether the different characteristics of the amino acid at this position are responsible for that is unclear. Although the strong conservation of the amino acids responsible for regulating the Ca^{2+} flux dependent on the pH hints at that direction, it still remains ambiguous to what extent the pH is responsible for the Ca^{2+} regulating properties of the other TMBIM family members besides BI-1.

After we compared the sequences of the TMBIM family, we constructed two phylogenetic trees in order to clarify the relationship between the TMBIM family and the bacterial homologue BsYetJ and the relationship of TMBIM1 – 6 to each other. One observation was that BI-1 is most closely related to BsYetJ. The second observation was that the TMBIM family falls into two clades: TMBIM1 – 3 and TMBIM4 – 5 and BI-1 cluster together in two separate groups. Within the first group TMBIM5 and BI-1 cluster together and within the second group TMBIM1 and TMBIM2 cluster together.

Interestingly, the proteins within one of the two groups had similar intracellular locations. By adding an HA-tag to the N terminus of all six TMBIM proteins and transiently transfecting HT22 cells with these constructs, we were able to assess the degree of colocalization with the mitochondria, the Golgi apparatus and the ER. TMBIM1-3 were mainly located in the Golgi apparatus and to a lesser extent in the ER, which corroborates earlier studies regarding their intracellular localization (127,129,140,141). TMBIM4 and 6 were primarily located in the ER and TMBIM4 was also found in the Golgi apparatus to a lesser extent, matching earlier reports of its subcellular location (135). BI-1 is the most extensive studied member of the TMBIM family and it has been shown numerous times that it is located in the ER by using EGFP- (99,107) and mCherry-tagged (102) BI-1, which we could confirm in our publication. TMBIM5 however was previously reported to be exclusively located in the mitochondria (138) while we found it to be primarily located in the ER. The previously described N-terminal signal sequence might be responsible for this divergence since it has been previously suggested that a N-terminal tag might interfere with the cleavage of this signal sequence (137). We indeed identified a mitochondrial target sequence, which leads to cleavage after residue 57. It is thus possible that the 11 amino acid long HA-tag shifts the cleavage site and thereby interferes with the physiological processing of TMBIM5. Although studies exist that suggest that protein tags interfere with protein processing (142), they involve much larger tags like EGFP or mCherry at the affected Terminus. HA-tags are much smaller and it is unclear whether and how they might alter protein localization, which is dependent on some form of degradation. It is also possible that TMBIM5 is co-expressed in the ER and in the mitochondria depending on the cellular needs. We therefore created a second construct with a C-terminally mCherry tagged TMBIM5 in order to further elucidate the intracellular localization of TMBIM5. This construct showed decreased co-localization with the ER and increased localization in the mitochondria. When immunoblotting lysates from cells transfected with this new construct and staining against the mCherry tag, two distinct bands could be identified. This means that TMBIM5 can probably exist in both its cleaved and uncleaved form and the cleaving efficiency decides its intracellular location. How the cleaving process is regulated in vivo and in what ways this could influence the function of TMBIM5 however remains unclear and warrants further investigation.

The hydrophobic nature of the TMBIM family renders the generation of antibodies against these proteins very difficult and our group reported that commercially available antibodies for BI-1 are not able to distinguish between tissues from wild-type and knockout mice (102). For that reason we employed quantitative RT-PCR to assess the expression levels in various tissues and corroborated the results of Zhao et al. that TMBIM1 is mainly expressed in heart and skeletal muscle tissues and to a lesser degree in the cerebellum (126). We detected the lowest expression of TMBIM1 in the spleen while Zhao et al. did not detect any expression in the spleen, probably because it is below the detection threshold of northern blotting. TMBIM2 was reported to be primarily expressed in the central nervous system by employing northern blotting (128,130), RT-PCR (129) and immunohistochemistry (131) and TMBIM3 has been shown to have a similar expression pattern except that it was also found in the kidney by Northern blotting and RT-PCR (141). Our own results match previous reports regarding TMBIM2 and TMBIM3. The same is true for TMBIM4, which was analyzed by PCR and reported to be ubiquitously expressed in all tissues with the lowest expression being in the brain (135) matching exactly our findings. According to Yoshida et al., TMBIM5 is mainly expressed in the brain, heart, liver, kidney and skeletal muscle with a lower expression in the thymus and in the intestines (137). While our results support these findings in general, we measured a lower expression in the liver compared to the brain, heart and skeletal muscle. BI-1 is supposed to be ubiquitously expressed throughout all tissues (100,101,143) with the exception of the central nervous system, which is exactly what we found in our RT-PCR analysis.

We next analyzed the effects on the ER Ca^{2+} homeostasis of the TMBIM protein family by stably overexpressing each protein in HT22 cells and measuring the thapsigargin releasable Ca^{2+} pool as the readout for the ER Ca^{2+}-content. Following their strong structural conservation, each protein lowered the thapsigargin releasable Ca^{2+} pool. This effect was previously shown for BI-1 by measuring the Ca^{2+} flux after ATP and thapsigargin application in BI-1-EGFP overexpressing CHO cells (107), for TMBIM3 by measuring the Ca^{2+} release after ATP stimulation in TMBIM3-myc overexpressing MEFs (140) and for TMBIM4 by measuring the histamine-induced Ca^{2+} release in U2OS cells overexpressing HA-tagged TMBIM4 (136). Our publication is the first to demonstrate that the overexpression of TMBIM1, TMBIM2 and TMBIM5 in HT22 cells also has a lowering effect on the thapsigargin-releasable Ca^{2+} pool. The putative channel forming properties of the TMBIM protein family, which is reflected in the conserved residues responsible for pH-dependent Ca^{2+}-channel formation as well as the common seven to eight transmembrane domain structure are one explanation for the lowered ER Ca^{2+} pool. However, studies have also shown that BI-1 sensitizes IP_3Rs and thereby promotes IP_3 induced Ca^{2+} release while overexpression of TMBIM3 (140) and TMBIM4 (136) led to suppressed IP_3 inducible Ca^{2+} release. TMBIM family members thus might additionally interact with other Ca^{2+}-regulating proteins in order to alter the filling state of the ER.

The reduction of the intracellular Ca^{2+} stores might have a direct impact on the antiapoptotic properties of the TMBIM proteins. As previously described, mitochondrial Ca^{2+} uptake is a physiological process required for cell survival. However, prolonged elevated Ca^{2+} concentrations in the cytoplasm and the ER might lead to overfilling of the mitochondria with Ca^{2+}, ultimately resulting in bursting of the mitochondrial wall and the release of cytochrome c, which will lead to apoptosis. The observed decrease of the ER Ca^{2+} concentrations might thus represent a, due to overexpression, amplified cytoprotective effect of TMBIM1 – 6. We were unfortunately not able to reliably measure cell death in our cell lines, partly due to the fact that the overexpression of the proteins influenced the growth characteristics such as growth rate and cell density, which renders comparable and reproducible measurements very difficult. The antiapoptotic properties in relation to the intracellular Ca^{2+} homeostasis of the TMBIM family have to be evaluated further in different paradigms of cell death (such as ER stress, ROS stress etc.) in order to clarify their function and the underlying mechanisms.

In our next publication, we focused on the role of BI-1 in immune cells, since our observations showed that BI-1 KO mice suffer from leukopenia (and also from obesity and erythrocytosis) albeit previous studies did not notice these abnormalities. A first screening of the immune system revealed no differences in cell numbers in different immune organs between WT and KO animals or a difference in composition of the immune cell subpopulations like B- and T cells. However, there was a significant increase of marginal zone (MZ) B cells at the expense of follicular (FO) B cells in BI-1 KO mice. After B cells exit the bone marrow, they migrate to the spleen where they become either residual MZ B cells or circulating FO B cells. Such a shift of the B cell subpopulations has been previously linked with alterations of NF-κB signaling. NF-κB is a family of transcription factors, which consists of five proteins in two classes. Class I proteins are NF-κB1 (p105/p50) and NF-κB2 (p100/p52) which reside in the cytoplasm and translocate to the nucleus upon activation where they can form dimers with the class II proteins RelA (p65), c-Rel and RelB (86). While the knockout of RelB leads to a decreased number of MZ B cells (144), an increase in NF-κB signaling by knocking out the inhibitory regulator CYLD significantly increases the amount of MZ B cells (145). In BI-1 KO splenocytes, the expression of RelA, RelB and c-Rel was significantly increased in the nucleus and in the cytoplasm and RelA also showed significantly increased nuclear translocation. RelA is only able to translocate to the nucleus after is has been released by IκBα which requires the phosphorylation of IκBα (pIκBα). pIκBα was also significantly downregulated in BI-1-deficient splenocytes, indicating a compensatory mechanism to retain as much RelA in the cytoplasm as possible.

But what leads to the activation of NF-κB in BI-1 KO splenocytes? Multiple stimuli lead to NF-κB translocation, like changes in the amplitude and duration of Ca^{2+} signals (98) or increases in the cytosolic Ca^{2+} concentration caused by SERCA inhibitors (96). Another mechanism leading to NF-κB activation is the ER overload reaction (EOR), which results

from the retention of proteins in the ER lumen. It is distinguished from the UPR by the lack of Grp78/BIP activation (97) and is also dependent on alterations of the cell's Ca^{2+} handling (97,146). The two major functions of BI-1 are the regulation of the ER Ca^{2+} concentrations and modulation of the UPR by being an inhibitor of IRE1α. We first looked for signs of increased ER stress in BI-1 KO splenocytes. However, contrary to previous results obtained in MEF cells (114), BI-1 KO splenocytes displayed decreased XBP-1 splicing and UPR proteins were rather downregulated and not upregulated, especially ERp57. We therefore concluded that the increased NF-κB activation is not a result of the UPR or the EOR and that in vivo the lack of BI-1 can be compensated.

When we investigated changes in the Ca^{2+} homeostasis, striking differences between BI-1 KO and BI-1 WT splenocytes emerged. BI-1 deficient splenocytes had significantly higher cytosolic and ER Ca^{2+} concentrations and additionally a significantly reduced SOCE. This was accompanied by a significant downregulation of Orai1, which is probably a compensatory mechanism to prevent further Ca^{2+} flux into already overfilled Ca^{2+} stores and explains the reduction in SOCE. The Ca^{2+} sensors STIM1 and 2 and IP_3Rs were not regulated, demonstrating the specific regulation of intracellular Ca^{2+} handling.

Another important transcription factor in immune cells is NFAT, which is also sequestered in the cytoplasm and released to act in the nucleus through elevations in the cytosolic Ca^{2+} after activation of the antigen receptors on the surface of immune cells (98). The elevated cytosolic Ca^{2+} in BI-1 KO splenocytes indeed resulted in significantly increased translocation of NFAT to the nucleus, without any actual upregulation of any NFAT isoform, which matches previous reports of increased NFAT translocation in BI-1 KO cells (139). Taken all into consideration we suspect that the elevated Ca^{2+} in BI-1 KO splenocytes is responsible for the sustained NF-κB activation, which results in increased numbers of MZ B cells.

We then looked specifically at the two largest compartments of the immune system, B- and T cells. Both B- and T cells from BI-1 KO mice showed increased baseline Ca^{2+} levels as well as elevated Ca^{2+} concentrations after stimulation with their specific ligands anti-CD3 antibodies and anti-IgM in order to activate their surface receptors. The elevated Ca^{2+} levels were also mirrored in increased nuclear translocation of NF-κB in both T- and B cells. Since sustained elevated Ca^{2+} may result in cell death, we investigated spontaneous cell death in B- and T cells and observed increased apoptosis in cells from KO mice with B cells being much more affected than T cells. BI-1 KO B cells also showed defective organelles and nuclear inclusions when analyzed by electron microscopy.

The key players during apoptosis, the effector caspases 3 and 7, showed elevated activity in line with the increased cell death in KO B cells and were preceded by significantly increased activity levels of caspase 9. Caspase 9 is generally associated with the intrinsic apoptosis pathway, involving cytochrome c release from the mitochondria due to the rupturing of the outer mitochondrial wall (147). Since BI-1 is also able to regulate the Ca^{2+} transport between mitochondria and the ER (148) and the mitochondrial Ca^{2+} levels were highly

increased in BI-1 KO B cells, we concluded that the increased cell death which was observed in BI-1 KO B cells is a direct consequence of mitochondria not able to handle the increased Ca^{2+} load which is caused by the lack of BI-1. This hypothesis was further corroborated when we observed that XBP-1 splicing is not significantly increased in BI-1 KO B cells, rendering ER stress and the UPR an unlikely cause for the premature cell death of B cells in culture. One possibility to protect the cells from Ca^{2+}-induced cell death might be reducing the intracellular Ca^{2+} load by chelating it, this however led to rapid cell death in both WT and KO B cells, probably due to a heavily disturbed Ca^{2+} homeostasis, as previously reported for leukemic cells (149).

The observed effects also affected lymphocyte function in vivo. We employed experimental autoimmune encephalomyelitis (EAE) as model for a T cell-mediated autoimmune disease, which targets the central nervous system. BI-1 KO mice had a much milder disease progression accompanied by significantly less microglia infiltration, which resulted in less damage to the brain and spinal cord (106). In another paradigm we assessed the B cell function by measuring the immunoglobulin production after immunization with the T cell independent immunogen 4-hydroxy-3-nitrophenylacetyl coupled to chicken globulin (NPCG). BI-1 KO mice showed significantly decreased IgG1, IgG2b and IgM production. The observed effects of BI-1 KO T- and B cells, like the increased Ca^{2+} concentrations and the increased cell death, thus also have an attenuating effect on B- and T cell function in vivo.

The elevated ER Ca^{2+} concentrations, which we observed in BI-1 KO splenocytes, T cells and B cells, and which were previously reported in numerous studies using BI-1 KO cells, can be explained by the Ca^{2+} channel properties of BI-1. If a Ca^{2+} channel is knocked out, the Ca^{2+} leak from the ER decreases which conversely increases the ER Ca^{2+} concentrations. Upon stimulation of the cell, the Ca^{2+} transients from the ER increase in analogy to the elevated ER Ca^{2+} concentrations, thereby increasing the cytosolic Ca^{2+} concentrations. Due to constant basal cell activation, the cytosolic Ca^{2+} might build up over time. Under normal conditions the cytosolic Ca^{2+} would be cleared by refilling the Ca^{2+} stores, the refilling however is directly inhibited by a high Ca^{2+} load of the ER since the dissociation of Ca^{2+} from the luminal side of SERCAs is impeded by high luminal Ca^{2+} concentrations (150). A later study also demonstrated that a high ER Ca^{2+} load reduces the Ca^{2+} uptake from the cytosol in order to prevent unevoked Ca^{2+} release from the ER, although the mechanism how the Ca^{2+} reuptake is regulated remained unclear (151). This creates a vicious circle in which the overfilled ER floods the cytosol with an excess of Ca^{2+} upon each stimulus but remains unable to clear the Ca^{2+} from the cytosol. Interestingly, BI-1 KO splenocytes even showed attempts to compensate for this Ca^{2+} overload. Under conditions of high luminal Ca^{2+} concentrations in the ER, like in case of the BI-1 KO, ERp57 binds to the Ca^{2+} ATPase Serca2b and thereby inhibits its function (152) and we observed a significantly decreased expression of ERp57 in BI-1 KO splenocytes, possibly in order to disinhibit SERCA2b and to facilitate clearance of the cytosolic Ca^{2+}.

The unsolved question is how the proposed inhibition of the ER stress sensor IRE1α by BI-1 (114) fits into this narrative of the ER overfilled with Ca^{2+}. The proapoptotic proteins BAX and BAK also directly interact with IRE1α and activate it (153). The double knock out of BAX and BAK causes directly opposite effects of the BI-1 knock out, namely a decrease in the ER Ca^{2+} concentration (154) due to an increased Ca^{2+} leak from the ER (155). And since BI-1 does not directly interact with BAX and BAK (99,114) but attenuates the interaction of BAX and BAK with IRE1α (114), it has been suggested that BI-1 acts upstream of BAX and BAK and regulates the inactivation of IRE1α (114). It has however not been studied whether IRE1α itself has an inhibitory effect on BI-1, creating a reciprocal relationship between these proteins. In this the case, the double knock out of BAX and BAK would inhibit IRE1α, which would in turn disinhibit BI-1, increasing the Ca^{2+} efflux from the ER and matching previous reports.

In conclusion, our results show the close relationship of the TMBIM proteins to each other, which are not only reflected in their conserved amino acid sequence, but also in their similar secondary structure and their specific subcellular localization. All TMBIM family members were able to significantly lower the ER Ca^{2+} pool, which might explain their antiapoptotic properties, since the overloading of the cytoplasm with Ca^{2+} is associated with apoptosis. Additionally, all TMBIM proteins except TMBIM 5 were able to decrease the resting Ca^{2+} levels in the ER. The role of the N-terminal signal sequence of TMBIM 5 needs to be further investigated since it apparently influences its intracellular localization and thereby the effects TMBIM 5 might have on the Ca^{2+} homeostasis. The lack of the most prominent member of the TMBIM family BI-1 had a profound effect on the Ca^{2+} homeostasis of mice immune cells. BI-1 KO resulted in Ca^{2+} overload of the immune cells, which was reflected by increased nuclear translocation of NFAT and NF-κB as well as increased cell death of T- and B cells. On the other hand, no direct proof of increased ER stress were observed, indicating that ER stress caused by the lack of BI-1 is probably combated efficiently in vivo. On the other hand, the effects of BI-1 deficiency were clearly visible in in vivo paradigms of T- and B cell function as BI-1 KO mice had a less severe T cell mediated EAE and displayed attenuated B cell immunoglobulin production, indicating a partial loss of function of these cell types.

References

1. Fagone P, Jackowski S. Membrane phospholipid synthesis and endoplasmic reticulum function. J Lipid Res. 2009 Apr;50 Suppl(Supplement):S311–6.

2. Braakman I, Bulleid NJ. Protein folding and modification in the mammalian endoplasmic reticulum. Annu Rev Biochem. 2011;80(1):71–99.

3. Sammels E, Parys JB, Missiaen L, De Smedt H, Bultynck G. Intracellular Ca2+ storage in health and disease: A dynamic equilibrium. Cell Calcium. 2010 Apr;47(4):297–314.

4. Berridge MJ. The endoplasmic reticulum: a multifunctional signaling organelle. Cell Calcium. 2002 Nov;32(5-6):235–49.

5. Chaudhari N, Talwar P, Parimisetty A, Lefebvre d'Hellencourt C, Ravanan P. A molecular web: endoplasmic reticulum stress, inflammation, and oxidative stress. Front Cell Neurosc. 2014;8:213.

6. Alberts B, Johnson A, Lewis J, Raff M, Roberts K, Walter P. Molecular Biology of the Cell. 4 ed. New York: Garland Science Taylor and Francis Group; 2004. pp. 689-693; pp. 645-646

7. Baumann O, Walz B. Endoplasmic reticulum of animal cells and its organization into structural and functional domains. Int Rev Cytol. 2001;205:149–214.

8. Terasaki M, Jaffe LA, Hunnicutt GR, Hammer JA. Structural change of the endoplasmic reticulum during fertilization: evidence for loss of membrane continuity using the green fluorescent protein. Dev Biol. 1996 Nov 1;179(2):320–8.

9. Speksnijder JE, Terasaki M, Hage WJ, Jaffe LF, Sardet C. Polarity and reorganization of the endoplasmic reticulum during fertilization and ooplasmic segregation in the ascidian egg. J Cell Biol. 1993 Mar;120(6):1337–46.

10. Ioshii SO, Yoshida T, Imanaka-Yoshida K, Izutsu K. Distribution of a Ca2+ storing site in PtK2 cells during interphase and mitosis. An immunocytochemical study using an antibody against calreticulin. Eur J Cell Biol. 1995 Jan;66(1):82–93.

11. Subramanian K, Meyer T. Calcium-induced restructuring of nuclear envelope and endoplasmic reticulum calcium stores. Cell. 1997 Jun 13;89(6):963–71.

12. Guerriero CJ, Brodsky JL. The delicate balance between secreted protein folding and endoplasmic reticulum-associated degradation in human physiology. Physiological Reviews. 2012 Apr;92(2):537–76.

13. Chen Y, Brandizzi F. IRE1: ER stress sensor and cell fate executor. Trends in Cell Biology. 2013 Nov;23(11):547–55.

14. Fedoroff N. Redox regulatory mechanisms in cellular stress responses. Ann Bot. 2006 Aug;98(2):289–300.

15. Sawada N, Yao J, Hiramatsu N, Hayakawa K, Araki I, Takeda M, et al. Involvement of hypoxia-triggered endoplasmic reticulum stress in outlet obstruction-induced apoptosis in the urinary bladder. Lab Invest. 2008 May;88(5):553–63.

16. Zhang L, Wang A. Virus-induced ER stress and the unfolded protein response. Front Plant Sci. 2012;3:293.

17. Nakagawa T, Zhu H, Morishima N, Li E, Xu J. Caspase-12 mediates endoplasmic-reticulum-specific apoptosis and cytotoxicity by amyloid-β. Nature. 2000;403(6765):98–103.

18. Kober L, Zehe C, Bode J. Development of a novel ER stress based selection system for the isolation of highly productive clones. Biotechnol Bioeng. 2012 Oct;109(10):2599–611.

19. Liu CY, Xu Z, Kaufman RJ. Structure and intermolecular interactions of the luminal dimerization domain of human IRE1alpha. J Biol Chem. 2003 May 16;278(20):17680–7.

20. Lee A-H, Iwakoshi NN, Glimcher LH. XBP-1 regulates a subset of endoplasmic reticulum resident chaperone genes in the unfolded protein response. Molecular and Cellular Biology. 2003 Nov;23(21):7448–59.

21. Nishitoh H, Matsuzawa A, Tobiume K, Saegusa K, Takeda K, Inoue K, et al. ASK1 is essential for endoplasmic reticulum stress-induced neuronal cell death triggered by expanded polyglutamine repeats. Genes Dev;.2002 Jun 1;16(11):1345–55.

22. Urano F, Wang X, Bertolotti A, Zhang Y, Chung P, Harding HP, et al. Coupling of stress in the ER to activation of JNK protein kinases by transmembrane protein kinase IRE1. Science. 2000 Jan 28;287(5453):664–6.

23. Nguyên DT, Kebache S, Fazel A, Wong HN, Jenna S, Emadali A, et al. Nck-dependent activation of extracellular signal-regulated kinase-1 and regulation of cell survival during endoplasmic reticulum stress. Molecular Biology of the Cell. 2004 Sep;15(9):4248–60.

24. Kaneko M, Niinuma Y, Nomura Y. Activation Signal of Nuclear Factor-κB in Response to Endoplasmic Reticulum Stress is Transduced via IRE1 and Tumor Necrosis Factor Receptor-Associated Factor 2. Biological and Pharmaceutical Bulletin. 2003;26(7):931–5.

25. Hu P, Han Z, Couvillon AD, Kaufman RJ, Exton JH. Autocrine tumor necrosis factor alpha links endoplasmic reticulum stress to the membrane death receptor pathway through IRE1alpha-mediated NF-kappaB activation and down-regulation of TRAF2 expression. Molecular and Cellular Biology. 2006 Apr;26(8):3071–84.

26. Ma K, Vattem KM, Wek RC. Dimerization and release of molecular chaperone inhibition facilitate activation of eukaryotic initiation factor-2 kinase in response to endoplasmic reticulum stress. J Biol Chem. 2002 May 24;277(21):18728–35.

27. Brewer JW, Diehl JA. PERK mediates cell-cycle exit during the mammalian unfolded protein response. Proc Natl Acad Sci USA. 2000 Nov 7;97(23):12625–30.

28. Schröder M, Kaufman RJ. The mammalian unfolded protein response. Annu Rev Biochem. 2005;74(1):739–89.

29. Harding HP, Zhang Y, Ron D. Protein translation and folding are coupled by an endoplasmic-reticulum-resident kinase. Nature. 1999 Jan 21;397(6716):271–4.

30. Harding HP, Zhang Y, Bertolotti A, Zeng H, Ron D. Perk is essential for translational regulation and cell survival during the unfolded protein response. Molecular cell. 2000 May;5(5):897–904.

31. Harding HP, Zhang Y, Zeng H, Novoa I, Lu PD, Calfon M, et al. An integrated stress response regulates amino acid metabolism and resistance to oxidative stress. Molecular cell. 2003 Mar;11(3):619–33.

32. Jiang H-Y, Wek SA, McGrath BC, Scheuner D, Kaufman RJ, Cavener DR, et al. Phosphorylation of the alpha subunit of eukaryotic initiation factor 2 is required for activation of NF-kappaB in response to diverse cellular stresses. Molecular and Cellular Biology. 2003 Aug;23(16):5651–63.

33. Cullinan SB, Diehl JA. Coordination of ER and oxidative stress signaling: the PERK/Nrf2 signaling pathway. International Journal of Biochemistry and Cell Biology. 2006 Mar;38(3):317–32.

34. Chen X, Shen J, Prywes R. The luminal domain of ATF6 senses endoplasmic reticulum (ER) stress and causes translocation of ATF6 from the ER to the Golgi. J Biol Chem. 2002 Apr 12;277(15):13045–52.

35. Ye J, Rawson RB, Komuro R, Chen X, Davé UP, Prywes R, et al. ER stress induces cleavage of membrane-bound ATF6 by the same proteases that process SREBPs. Molecular cell. 2000 Dec;6(6):1355–64.

36. Adachi Y, Yamamoto K, Okada T, Yoshida H, Harada A, Mori K. ATF6 Is a Transcription Factor Specializing in the Regulation of Quality Control Proteins in the Endoplasmic Reticulum. Cell Structure and Function. 2008;33(1):75–89.

37. Cao SS, Kaufman RJ. Unfolded protein response. Curr Biol. 2012 Aug 21;22(16):R622–6.

38. Tabas I, Ron D. Integrating the mechanisms of apoptosis induced by endoplasmic reticulum stress. Nat Cell Biol. 2011 Mar;13(3):184–90.

39. Wozniak AL, Wang X, Stieren ES, Scarbrough SG, Elferink CJ, Boehning D. Requirement of biphasic calcium release from the endoplasmic reticulum for Fas-mediated apoptosis. J Cell Biol. 2006 Dec 4;175(5):709–14.

40. Martinou JC, Desagher S, Antonsson B. Cytochrome c release from mitochondria: all or nothing. Nat Cell Biol. 2000 Mar;2(3):E41–3.

41. Johnson GL, Nakamura K. The c-jun kinase/stress-activated pathway: regulation, function and role in human disease. Biochim Biophys Acta. 2007 Aug;1773(8):1341–8.

42. Wisdom R, Johnson RS, Moore C. c-Jun regulates cell cycle progression and apoptosis by distinct mechanisms. The EMBO Journal. 1999 Jan 4;18(1):188–97.

43. Fan M, Chambers TC. Role of mitogen-activated protein kinases in the response of tumor cells to chemotherapy. Drug Resist Updat. 2001 Aug;4(4):253–67.

44. Fuchs SY, Adler V, Pincus MR, Ronai Z. MEKK1/JNK signaling stabilizes and activates p53. Proc Natl Acad Sci USA. 1998 Sep 1;95(18):10541–6.

45. Jones EV, Dickman MJ, Whitmarsh AJ. Regulation of p73-mediated apoptosis by c-Jun N-terminal kinase. Biochem J. 2007 Aug 1;405(3):617–23.

46. Oleinik NV, Krupenko NI, Krupenko SA. Cooperation between JNK1 and JNK2 in activation of p53 apoptotic pathway. Oncogene. 2007 Nov 8;26(51):7222–30.

47. Kharbanda S, Saxena S, Yoshida K, Pandey P, Kaneki M, Wang Q, et al. Translocation of SAPK/JNK to mitochondria and interaction with Bcl-x(L) in response to DNA damage. J Biol Chem. 2000 Jan 7;275(1):322–7.

48. Tournier C, Hess P, Yang DD, Xu J, Turner TK, Nimnual A, et al. Requirement of JNK for stress-induced activation of the cytochrome c-mediated death pathway. Science. 2000 May 5;288(5467):870–4.

49. Lei K, Davis RJ. JNK phosphorylation of Bim-related members of the Bcl2 family induces Bax-dependent apoptosis. Proc Natl Acad Sci USA. 100(5):2432–7.

50. Madesh M, Antonsson B, Srinivasula SM, Alnemri ES, Hajnóczky G. Rapid kinetics of tBid-induced cytochrome c and Smac/DIABLO release and mitochondrial depolarization. J Biol Chem. 2002 Feb 15;277(7):5651–9.

51. Woehlbier U, Hetz C. Modulating stress responses by the UPRosome: a matter of life and death. Trends in Biochemical Sciences. 2011 Jun;36(6):329–37.

52. Berridge MJ, Bootman MD, Roderick HL. Calcium signalling: dynamics, homeostasis and remodelling. Nat Rev Mol Cell Biol. 2003 Jul;4(7):517–29.

53. Iino M. Spatiotemporal dynamics of Ca2+ signaling and its physiological roles. Proc Jpn Acad, Ser B, Phys Biol Sci. 2010;86(3):244–56.

54. Wojda U, Salinska E, Kuznicki J. Calcium ions in neuronal degeneration. IUBMB Life. 2008 Sep;60(9):575–90.

55. Vig M, Kinet J-P. Calcium signaling in immune cells. Nat Immunol. 2009 Jan;10(1):21–7.

56. Bading H, Segal MM, Sucher NJ, Dudek H, Lipton SA, Greenberg ME. N-methyl-D-aspartate receptors are critical for mediating the effects of glutamate on intracellular calcium concentration and immediate early gene expression in cultured hippocampal neurons. Neuroscience. 1995 Feb;64(3):653–64.

57. Jonas P, Burnashev N. Molecular mechanisms controlling calcium entry through AMPA-type glutamate receptor channels. Neuron. 1995 Nov;15(5):987–90.

58. Decrock E, De Bock M, Wang N, Gadicherla AK, Bol M, Delvaeye T, et al. IP3, a small molecule with a powerful message. Biochim Biophys Acta. 2013 Jul;1833(7):1772–86.

59. Fagni L, Chavis P, Ango F, Bockaert J. Complex interactions between mGluRs, intracellular Ca2+ stores and ion channels in neurons. Trends Neurosci. 2000 Feb;23(2):80–8.

60. Takemura H, Hughes AR, Thastrup O, Putney JW. Activation of calcium entry by the tumor promoter thapsigargin in parotid acinar cells. Evidence that an intracellular calcium pool and not an inositol phosphate regulates calcium fluxes at the plasma membrane. J Biol Chem. 1989 Jul 25;264(21):12266–71.

61. Takemura H, Putney JW. Capacitative calcium entry in parotid acinar cells. Biochem J. 1989 Mar 1;258(2):409–12.

62. Roos J, DiGregorio PJ, Yeromin AV, Ohlsen K, Lioudyno M, Zhang S, et al. STIM1, an essential and conserved component of store-operated Ca2+ channel function. J Cell Biol. 2005 May 9;169(3):435–45.

63. Liou J, Kim ML, Do Heo W, Jones JT, Myers JW, James E Ferrell J, et al. STIM is a Ca2+ sensor essential for Ca2+-store-depletion-triggered Ca2+ influx. Curr Biol. 2005 Jul 12;15(13):1235–41.

64. Soboloff J, Rothberg BS, Madesh M, Gill DL. STIM proteins: dynamic calcium signal transducers. Nat Rev Mol Cell Bio. 2012 Sep;13(9):549–65.

65. Wu MM, Buchanan J, Luik RM, Lewis RS. Ca2+ store depletion causes STIM1 to accumulate in ER regions closely associated with the plasma membrane. J Cell Biol. 2006 Sep 11;174(6):803–13.

66. Park CY, Hoover PJ, Mullins FM, Bachhawat P, Covington ED, Raunser S, et al. STIM1 clusters and activates CRAC channels via direct binding of a cytosolic domain to Orai1. Cell. 2009 Mar 6;136(5):876–90.

67. Manjarrés IM, Rodríguez-García A, Alonso MT, García-Sancho J. The sarco/endoplasmic reticulum Ca(2+) ATPase (SERCA) is the third element in capacitative calcium entry. Cell Calcium. 2010 May;47(5):412–8.

68. Jousset H, Frieden M, Demaurex N. STIM1 knockdown reveals that store-operated Ca2+ channels located close to sarco/endoplasmic Ca2+ ATPases (SERCA) pumps silently refill the endoplasmic reticulum. J Biol Chem. 2007 Apr 13;282(15):11456–64.

69. Soboloff J, Spassova MA, Tang XD, Hewavitharana T, Xu W, Gill DL. Orai1 and STIM reconstitute store-operated calcium channel function. J Biol Chem. 2006 Jul 28;281(30):20661–5.

70. Kerr JF, Wyllie AH, Currie AR. Apoptosis: a basic biological phenomenon with wide-ranging implications in tissue kinetics. Br J Cancer. 1972 Aug;26(4):239–57.

71. Mattson MP, Chan SL. Calcium orchestrates apoptosis. Nat Cell Biol. 2003 Dec 1;5(12):1041–3.

72. Clarke PG. Developmental cell death: morphological diversity and multiple mechanisms. Anat Embryol. 1990;181(3):195–213.

73. Hengartner MO. The biochemistry of apoptosis. Nature. 2000 Oct 12;407(6805):770–6.

74. R E Ellis, J Yuan A, Horvitz HR. Mechanisms and Functions of Cell Death. Annual review of cell biology. 2003 Nov 28;7(1):663–98.

75. Orrenius S, Zhivotovsky B, Nicotera P. Regulation of cell death: the calcium-apoptosis link. Nat Rev Mol Cell Bio. 2003 Jul;4(7):552–65.

76. Giorgi C, Romagnoli A, Pinton P, Rizzuto R. Ca2+ signaling, mitochondria and cell death. Curr Mol Med. 2008 Mar;8(2):119–30.

77. Zhivotovsky B, Orrenius S. Calcium and cell death mechanisms: a perspective from the cell death community. Cell Calcium. 2011 Sep;50(3):211–21.

78. Pászty K, Verma AK, Padányi R, Filoteo AG, Penniston JT, Enyedi A. Plasma membrane Ca2+ATPase isoform 4b is cleaved and activated by caspase-3 during the early phase of apoptosis. J Biol Chem. 2002 Mar 1;277(9):6822–9.

79. Schwab BL, Guerini D, Didszun C, Bano D, Ferrando-May E, Fava E, et al. Cleavage of plasma membrane calcium pumps by caspases: a link between apoptosis and necrosis. Cell Death Differ. 2002 Aug;9(8):818–31.

80. Lu T, Xu Y, Mericle MT, Mellgren RL. Participation of the conventional calpains in apoptosis. Biochim Biophys Acta. 2002 Jun 12;1590(1-3):16–26.

81. Tan Y, Wu C, De Veyra T, Greer PA. Ubiquitous calpains promote both apoptosis and survival signals in response to different cell death stimuli. J Biol Chem. 2006 Jun 30;281(26):17689–98.

82. Palmer AE, Jin C, Reed JC, Tsien RY. Bcl-2-mediated alterations in endoplasmic reticulum Ca2+ analyzed with an improved genetically encoded fluorescent sensor. Proc Natl Acad Sci USA.; 2004 Dec 14;101(50):17404–9.

83. Pinton P, Ferrari D, Magalhães P, Schulze-Osthoff K, Di Virgilio F, Pozzan T, et al. Reduced loading of intracellular Ca(2+) stores and downregulation of capacitative Ca(2+) influx in Bcl-2-overexpressing cells. J Cell Biol. 2000 Mar 6;148(5):857–62.

84. Foyouzi-Youssefi R, Arnaudeau S, Borner C, Kelley WL, Tschopp J, Lew DP, et al. Bcl-2 decreases the free Ca2+ concentration within the endoplasmic reticulum. Proc Natl Acad Sci USA.; 2000 May 23;97(11):5723–8.

85. Chen R, Valencia I, Zhong F, McColl KS, Roderick HL, Bootman MD, et al. Bcl-2 functionally interacts with inositol 1,4,5-trisphosphate receptors to regulate calcium release from the ER in response to inositol 1,4,5-trisphosphate. J Cell Biol.; 2004 Jul 19;166(2):193–203.

86. Gilmore TD, Herscovitch M. Inhibitors of NF-kappaB signaling: 785 and counting. Oncogene. 2006 Oct 30;25(51):6887–99.

87. Perkins ND. Integrating cell-signalling pathways with NF-kappaB and IKK function. Nature Reviews Molecular Cell Biology. 2007 Jan;8(1):49–62.

88. Gilmore TD. NF-kappa B, KBF1, dorsal, and related matters. Cell. 1990 Sep 7;62(5):841–3.

89. Hayden MS, Ghosh S. Signaling to NF-kappaB. Genes Dev. 2004 Sep 15;18(18):2195–224.

90. Gilmore TD. Introduction to NF-kappaB: players, pathways, perspectives. Oncogene. 2006 Oct 30;25(51):6680–4.

91. Brasier AR. The NF-κB regulatory network. Cardiovasc Toxicol. 2006;6(2):111–30.

92. Perkins ND. Post-translational modifications regulating the activity and function of the nuclear factor kappa B pathway. Oncogene. 2006 Oct 30;25(51):6717–30.

93. Deng J, Lu PD, Zhang Y, Scheuner D, Kaufman RJ, Sonenberg N, et al. Translational repression mediates activation of nuclear factor kappa B by phosphorylated translation initiation factor 2. Molecular and Cellular Biology. 2004 Dec;24(23):10161–8.

94. Tam AB, Mercado EL, Hoffmann A, Niwa M. ER Stress Activates NF-κB by Integrating Functions of Basal IKK Activity, IRE1 and PERK. PLoS ONE. 2012;7(10):e45078.

95. H L Pahl PAB. A novel signal transduction pathway from the endoplasmic reticulum to the nucleus is mediated by transcription factor NF-kappa B. The EMBO Journal. 1995 Jun 1;14(11):2580–8.

96. Activation of transcription factor NF-kappaB by the adenovirus E3/19K protein requires its ER retention. Rockefeller Univ Press; 1996 Feb 15;132(4):511–22.

97. Pahl HL, Baeuerle PA. Activation of NF-κB by ER stress requires both Ca2+ and reactive oxygen intermediates as messengers. FEBS Lett. 1996;392(2):129–36.

98. Dolmetsch RE, Lewis RS, Goodnow CC, Healy JI. Differential activation of transcription factors induced by Ca2+ response amplitude and duration. Nature. 1997 Apr 24;388(6639):308–8.

99. Xu Q, Reed JC. Bax inhibitor-1, a mammalian apoptosis suppressor identified by functional screening in yeast. Molecular cell. 1998 Feb;1(3):337–46.

100. Walter L, Dirks B, Rothermel E, Heyens M, Szpirer C, Levan G, et al. A novel, conserved gene of the rat that is developmentally regulated in the testis. Mammalian Genome. 1994;5(4):216–21.

101. Walter L, Marynen P, Szpirer J, Levan G, Günther E. Identification of a novel conserved human gene, TEGT. Genomics. 1995 Jul 20;28(2):301–4.

102. Kiviluoto S, Luyten T, Schneider L, Lisak D, Rojas-Rivera D, Welkenhuyzen K, et al. Bax Inhibitor-1-mediated Ca2+ leak is decreased by cytosolic acidosis. Cell Calcium. 2013 Sep;54(3):186–92.

103. Bultynck G, Kiviluoto S, Henke N, Ivanova H, Schneider L, Rybalchenko V, et al. The C terminus of Bax inhibitor-1 forms a Ca2+-permeable channel pore. J Biol Chem. 2012 Jan 20;287(4):2544–57.

104. Chang Y, Bruni R, Kloss B, Assur Z, Kloppmann E, Rost B, et al. Structural basis for a pH-sensitive calcium leak across membranes. Science. 2014 Jun 6;344(6188):1131–5.

105. Bultynck G, Kiviluoto S, Methner A. Bax Inhibitor-1 Is Likely a pH-Sensitive Calcium Leak Channel, Not a H+/Ca2+ Exchanger. Sci Signal. 2014;7(343):pe22.

106. Chae H-J, Kim H-R, Xu C, Bailly-Maitre B, Krajewska M, Krajewski S, et al. BI-1 regulates an apoptosis pathway linked to endoplasmic reticulum stress. Molecular cell. 2004 Aug 13;15(3):355–66.

107. Westphalen B, Wessig J, Leypoldt F, Arnold S, Methner A. BI-1 protects cells from oxygen glucose deprivation by reducing the calcium content of the endoplasmic reticulum. Cell Death Differ. 2005;12(3):304–6.

108. Kim H-R, Lee G-H, Ha K-C, Ahn T, Moon J-Y, Lee B-J, et al. Bax Inhibitor-1 Is a pH-dependent regulator of Ca2+ channel activity in the endoplasmic reticulum. J Biol Chem. 2008 Jun 6;283(23):15946–55.

109. White C, Li C, Yang J, Petrenko NB, Madesh M, Thompson CB, et al. The endoplasmic reticulum gateway to apoptosis by Bcl-X(L) modulation of the InsP3R. Nat Cell Biol. 2005 Oct;7(10):1021–8.

110. Xu C, Xu W, Palmer AE, Reed JC. BI-1 regulates endoplasmic reticulum Ca2+

homeostasis downstream of Bcl-2 family proteins. J Biol Chem. 2008 Apr 25;283(17):11477–84.

111. Kiviluoto S, Schneider L, Luyten T, Vervliet T. Bax Inhibitor-1 is a novel IP3 receptor-interacting and-sensitizing protein. Cell Death Dis. 2012 Aug; 3(8): e367.

112. Ahn T, Yun C-H, Chae HZ, Kim H-R, Chae H-J. Ca2+/H+ antiporter- like activity of human recombinant Bax inhibitor- 1 reconstituted into liposomes. FEBS Journal. 2009;276(8):2285–91.

113. Bailly-Maitre B, Fondevila C, Kaldas F, Droin N, Luciano F, Ricci J-E, et al. Cytoprotective gene bi-1 is required for intrinsic protection from endoplasmic reticulum stress and ischemia-reperfusion injury. Proceedings of the National Academy of Sciences. 2006 Feb 21;103(8):2809–14.

114. Lisbona F, Rojas-Rivera D, Thielen P, Zamorano S, Todd D, Martinon F, et al. BAX inhibitor-1 is a negative regulator of the ER stress sensor IRE1alpha. Molecular cell. 2009 Mar 27;33(6):679–91.

115. Kim H-R, Lee G-H, Cho EY, Chae S-W, Ahn T, Chae H-J. Bax inhibitor 1 regulates ER-stress-induced ROS accumulation through the regulation of cytochrome P450 2E1. Journal of Cell Science. 2009 Apr 15;122(Pt 8):1126–33.

116. Lee G-H, Ahn T, Kim D-S, Park SJ, Lee YC, Yoo WH, et al. Bax inhibitor 1 increases cell adhesion through actin polymerization: involvement of calcium and actin binding. Molecular and Cellular Biology. 2010 Apr;30(7):1800–13.

117. Lee G-H, Yan C, Shin S-J, Hong S-C, Ahn T, Moon A, et al. BAX inhibitor-1 enhances cancer metastasis by altering glucose metabolism and activating the sodium-hydrogen exchanger: the alteration of mitochondrial function. Oncogene. 2010 Apr 8;29(14):2130–41.

118. Schmits R, Cochlovius B, Treitz G, Regitz E, Ketter R, Preuss K-D, et al. Analysis of the antibody repertoire of astrocytoma patients against antigens expressed by gliomas. Int J Cancer. 2002 Mar 1;98(1):73–7.

119. Villalva C, Trempat P, Greenland C, Thomas C, Girard JP, Moebius F, et al. Isolation of differentially expressed genes in NPM-ALK-positive anaplastic large cell lymphoma. Br J Haematol. 2002 Sep;118(3):791–8.

120. Grzmil M, Thelen P, Hemmerlein B, Schweyer S. Bax inhibitor-1 is overexpressed in prostate cancer and its specific down-regulation by RNA interference leads to cell death in human prostate carcinoma cells. Am J Pathol. 2003 Aug;163(2):543-52.

121. Grzmil M, Kaulfuss S, Thelen P, Hemmerlein B, Schweyer S, Obenauer S, et al. Expression and functional analysis of Bax inhibitor-1 in human breast cancer cells. The Journal of pathology. 2006 Feb;208(3):340–9.

122. Tanaka R, Ishiyama T, Uchihara T, Inadome Y, Iijima T, Morishita Y, et al. Expression of the Bax inhibitor-1 gene in pulmonary adenocarcinoma. Cancer. 2006 Feb 1;106(3):648–53.

123. Zhang M, Li X, Zhang Y, Zhou K. Bax inhibitor-1 mediates apoptosis-resistance in human nasopharyngeal carcinoma cells. Mol Cell Biochem. 2010 Jan;333(1-2):1–7.

124. Schmidt SM, König T, Bringmann A, Held S, Schwarzenberg von K, Heine A, et al. Characterization of BAX inhibitor-1 as a novel leukemia-associated antigen. Leukemia. 2009 Oct;23(10):1818–24.

125. Chae H-J, Ke N, Kim H-R, Chen S, Godzik A, Dickman M, et al. Evolutionarily conserved cytoprotection provided by Bax Inhibitor-1 homologs from animals, plants, and yeast. Gene. 2003 Dec;323:101–13.

126. Zhao H, Ito A, Kimura SH, Yabuta N, Sakai N, Ikawa M, et al. RECS1 deficiency in mice induces susceptibility to cystic medial degeneration. Genes Genet Syst. 2006 Feb;81(1):41–50.

127. Shukla S, Fujita K-I, Xiao Q, Liao Z, Garfield S, Srinivasula SM. A shear stress responsive gene product PP1201 protects against Fas-mediated apoptosis by reducing Fas expression on the cell surface. Apoptosis. 2011 Feb;16(2):162–73.

128. Somia NV, Schmitt MJ, Vetter DE. LFG: an anti-apoptotic gene that provides protection from Fas-mediated cell death. Proc Natl Acad Sci USA. 1999 Oct 26; 96(22): 12667–12672.

129. Fernández M, Segura MF, Solé C, Colino A, Comella JX, Ceña V. Lifeguard/neuronal membrane protein 35 regulates Fas ligand- mediated apoptosis in neurons via microdomain recruitment. J Neurochem. 2007;103(1):190–203.

130. Schweitzer B. Neural Membrane Protein 35 (NMP35): A Novel Member of a Gene Family Which Is Highly Expressed in the Adult Nervous System. Molecular and Cellular Neuroscience. 1998 Aug;11(5-6):260–73.

131. Schweitzer B, Suter U, Taylor V. Neural membrane protein 35/Lifeguard is localized at postsynaptic sites and in dendrites. Molecular brain research. 2002.

132. Reich A, Spering C, Gertz K, Harms C, Gerhardt E, Kronenberg G, et al. Fas/CD95 regulatory protein Faim2 is neuroprotective after transient brain ischemia. J Neurosci. 2011 Jan 5;31(1):225–33.

133. Kumar KN, Tilakaratne N, Johnson PS, Allen AE, Michaelis EK. Cloning of cDNA for the glutamate-binding subunit of an NMDA receptor complex. Nature. 1991 Nov 7;354(6348):70–3.

134. Tachikawa K, Sasaki S, Maeda T, Nakajima K. Identification of molecules preferentially expressed beneath the marginal zone in the developing cerebral cortex. Neuroscience Research. 2008 Feb;60(2):135–46.

135. Gubser C, Bergamaschi D, Hollinshead M, Lu X, van Kuppeveld FJM, Smith GL. A new inhibitor of apoptosis from vaccinia virus and eukaryotes. PLoS Pathog. 2007 Feb;3(2):e17.

136. De Mattia F, Gubser C, van Dommelen MMT, Visch H-J, Distelmaier F, Postigo A, et al. Human Golgi Antiapoptotic Protein Modulates Intracellular Calcium Fluxes. Molecular Biology of the Cell. 2009 Aug 15;20(16):3638–45.

137. Yoshida T, Nagata S, Kataoka H. Ghitm is an ortholog of the Bombyx mori prothoracic gland-derived receptor (Pgdr) that is ubiquitously expressed in mammalian cells and requires an N-terminal signal sequence for expression. Biochemical and Biophysical Research Communications. 2006 Mar;341(1):13–8.

138. Oka T, Sayano T, Tamai S, Yokota S, Kato H, Fujii G, et al. Identification of a novel protein MICS1 that is involved in maintenance of mitochondrial morphology and apoptotic release of cytochrome c. Molecular Biology of the Cell. 2008 Jun;19(6):2597–608.

139. Bailly-Maitre B, Bard-Chapeau E, Luciano F, Droin N, Bruey J-M, Faustin B, et al. Mice lacking bi-1 gene show accelerated liver regeneration. Cancer research. 2007 Feb 15;67(4):1442–50.

140. Rojas-Rivera D, n RAE, Colombo A, nez GMI, Eguiguren AL, az ADI, et al. TMBIM3/GRINA is a novel unfolded protein response (UPR) target gene that controls apoptosis through the modulation of ER calcium homeostasis. Cell Death Differ. 2012 Jun 1;19(6):1013–26.

141. Nielsen JA, Chambers MA, Romm E, Lee L. Mouse transmembrane BAX inhibitor Motif 3 (Tmbim3) encodes a 38 kDa transmembrane protein expressed in the central nervous system. Mol Cell Biochem. 2011 Nov;357(1-2):73-81.

142. Zhang X, Lu H, Ai H, Peng R, Yang Y, Li A, et al. Distribution, cleavage and lipidation of Atg8 fusion proteins in Spodoptera litura Sl-HP cells. PLoS ONE. 2014;9(5):e96059.

143. Henke N, Lisak DA, Schneider L, Habicht J, Pergande M, Methner A. The ancient cell death suppressor BAX inhibitor-1. Cell Calcium. 2011 Sep;50(3):251–60.

144. Weih DS, Yilmaz ZB, Weih F. Essential role of RelB in germinal center and marginal zone formation and proper expression of homing chemokines. J Immunol. 2001 Aug 15;167(4):1909-19.

145. Hövelmeyer N, Wunderlich FT, Massoumi R, Jakobsen CG, Song J, Wörns MA, et al. Regulation of B cell homeostasis and activation by the tumor suppressor gene CYLD. J Exp Med. 2007 Oct 29;204(11):2615–27.

146. Davies MJ, Miranda E, Roussel BD, Kaufman RJ, Marciniak SJ, Lomas DA. Neuroserpin Polymers Activate NF-κB by a Calcium Signaling Pathway That Is

Independent of the Unfolded Protein Response. J Biol Chem. 2009 Jul 3;284(27):18202–9.

147. Demaurex N, Distelhorst C. Cell biology. Apoptosis--the calcium connection. Science. 2003 Apr 4;300(5616):65–7.

148. Sano R, Hou Y-CC, Hedvat M, Correa RG, Shu C-W, Krajewska M, et al. Endoplasmic reticulum protein BI-1 regulates Ca^{2+}-mediated bioenergetics to promote autophagy. Genes Dev. 2012 May 15;26(10):1041–54.

149. Zhong Y, Fang S. Live cell imaging of protein dislocation from the endoplasmic reticulum. J Biol Chem. 2012 Aug 10;287(33):28057–66.

150. Favre C, Jerstrom P, Foti M, Stendhal O, Huggler E. Organization of Ca2+ stores in myeloid cells: association of SERCA2b and the type-1 inositol-1, 4, 5-trisphosphate receptor. Biochem J. 1996 May 15;316 (Pt 1):137-42.

151. Mogami H, Tepikin AV, Petersen OH. Termination of cytosolic Ca2+ signals: Ca2+ reuptake into intracellular stores is regulated by the free Ca2+ concentration in the store lumen. EMBO J. 1998 Jan 15; 17(2): 435–442.

152. Li Y. Ca2+-dependent redox modulation of SERCA 2b by ERp57. J Cell Biol. 2004 Jan 5;164(1):35–46.

153. Hetz C, Bernasconi P, Fisher J, Lee A-H, Bassik MC, Antonsson B, et al. Proapoptotic BAX and BAK modulate the unfolded protein response by a direct interaction with IRE1alpha. Science. 2006 Apr 28;312(5773):572–6.

154. Scorrano L, Oakes SA, Opferman JT, Cheng EH, Sorcinelli MD, Pozzan T, et al. BAX and BAK regulation of endoplasmic reticulum Ca2+: a control point for apoptosis. Science. 2003 Apr 4;300(5616):135–9.

155. Proapoptotic BAX and BAK regulate the type 1 inositol trisphosphate receptor and calcium leak from the endoplasmic reticulum. National Acad Sciences; 2005 Jan 4;102(1):105–10.

Appendix

Abbreviations

AIF	apoptosis-inducing factor
AMPA	2-amino3-(3-hydroxy-5-methyl-isoaxol-4-yl)propanoic acid
ASK1	apoptosis signal-relating kinase
ATF4	activating transcription factor 4
ATF6	activating transcription factor 6
BAFF	B-cell activating factor
Bax	BCL2-associated X protein
BCL-XL	BCL2-like 1
BI-1	Bax Inhibitor-1
BIP / Grp78	binding immunoglobulin protein
bZIP	basic Leucine Zipper Domain
Ca^{2+}	calcium
CHOP	C/EBP-homologous protein
CICR	calcium-induced calcium release
CRAC	Ca^{2+}-release activated Ca^{2+}
CREB	cAMP response element binding
DAG	diacylglycerol
EAE	experimental autoimmune encephalomyelitis
eIF2α	eukaryotic translation initiation factor
EOR	ER overload response
ER	endoplasmic reticulum
ERAD	endoplasmic reticulum-associated degradation
ERK	extracellular signal-regulated kinase
ERSE	endoplasmic reticulum stress response element
FO	follicular
H	L-histidine
IKK	Iκ BKinase
IL-1	interleukin-1
IP_3	inositol 1,4,5-triphosphate
IP_3R1-3	IP_3 receptors 1-3
IRE1α	inositol-requiring kinase 1
IRES	internal ribosome entry site
JNK	c-Jun N-terminal kinase
Keap1	kelch-like ECH-associated protein 1

KO	knockout
LGCC	ligand-gated Ca^{2+}-channels
LPS	lipopolysaccharide
LTβ	Lymphotoxin B
MZ	marginal zone
Na^{+}/Ca^{2+} exchanger	sodium-calcium exchanger
NFAT	nuclear factor of activated T cells
NF-κB	Nuclear factor kappa-light-chain-enhancer of activated B cells
NIK	NF-κB inducing kinase
NMDA	N-Methyl-D-aspartate
NPCG	immunogen 4-hydroxy-3-nitrophenylacetyl coupled to chicken globulin
Nrf2	nuclear erythroid 2 p45-related factor 2
P-eIF2α	phosphorylated eukaryotic translation initiation factor
PERK	protein kinase (PKR)-like endoplasmic reticulum kinase
PIP2	phosphatidylinositol 4,5-bisphosphate
PLC	phospholipase C
PMCA	plasma membrane calcium ATPases
PUMA	p53 upregulated promoter of apoptosis
R	L-arginine
RER	rough endoplasmic reticulum
RIP	regulated intermembrane proteolysis
RNAi	RNA interference
ROS	reactive oxygen species
RyR	ryanodine receptors
SER	smooth endoplasmic reticulum
SERCA	sarco/endoplasmic reticulum Ca^{2+}-ATPases
Ser/Thr	Serine/Threonine
siRNA	small interference RNA
SOCE	store-operated Ca^{2+} entry
STIM1	stromal interaction molecule 1
sXBP1	spliced XBP1
TEGT	testis enhanced gene transcript
TMBIM	transmembrane BAX inhibitor motif containing
TRAF2	tumor necrosis factor receptor-associated factor 2
UPR	unfolded protein response
VDCC	voltage-dependent Ca^{2+} channels
XBP1	X-box protein 1

List of publications

Publications prepared in the context of this PhD study:

The transmembrane Bax inhibitor motif (TMBIM) containing protein family: Tissue expression, intracellular localization and effects on the ER CA^{2+}-filling state. Biochim Biophys Acta. 2015 Sep;1853(9):2104–14.
Dmitrij Lisak, Teresa Schacht, Vitalij Enders, Jörn Habicht, Santeri Kiviluoto, Julia Schneider, Nadine Henke, Geert Bultynck and Axel Methner

BAX inhibitor-1 is a Ca^{2+} channel critically important for immune cell function and survival. Cell Death Differ. 2015 Oct ;23(2):358–68.
Dmitrij Lisak, Teresa Schacht, Alexander Gawlitza, Philipp Albrecht, Orhan Aktas, Barbara Koop, Michael Gliem, Harald Hofstetter, Klaus Zanger, Geert Bultynck, Jan Parys, Humbert de Smedt, Thomas Kindler, Ari Waisman, Petra Adams-Quack, Matthias Hahn, John Reed, Nadine Hoevelmeyer and Axel Methner

Interaction of Bcl-2 with the Autophagy-Related GABAA Receptor-Associated Protein (GABARAP): Biophysical characterization and functional implications. The Journal of Biological Chemistry 288, no. 52 (2013): 37204-37215
Peixiang Ma, Melanie Schwarten, Lars Schneider, Alexandra Boeske, Nadine Henke, **Dmitrij Lisak**, Stephan Weber, Jeannine Mohrlüder, Matthias Stoldt, Birgit Strodel, Axel Methner, Silke Hoffmann, Oliver H. Weiergräber and Dieter Willbold

Bax Inhibitor-1-mediated Ca^{2+} leak is decreased by cytosolic acidosis. Cell Calcium 54, no. 3 (2013): 186–192.
Santeri Kiviluoto, Tomas Luyten, Lars Schneider, **Dmitrij Lisak**, Diego Rojas-Rivera, Kirsten Welkenhuyzen, Ludwig Missaen, Humbert De Smedt, Jan B. Parys, Claudio Hetz, Axel Methner and Geert Bultynck

Effects of dimethyl fumarate on neuroprotection and immunomodulation. Journal of Neuroinflammation 9 (2012):163-173.
Philipp Albrecht, Imane Bouchachia, Norbert Goebels, Nadine Henke, Harald H Hofstetter, Andrea Issberner, Zsuzsa Kovacs, **Dmitrij Lisak**, Pamela Maher, Anne-Kathrin Mausberg, Kim Quasthoff, Corinna Zimmermann, Hans-Peter Hartung and Axel Methner

The Ancient Cell Death Suppressor BAX Inhibitor-1. Cell Calcium 50, no. 3 (2011): 251–260.
Nadine Henke*, **Dmitrij Lisak***, Lars Schneider, Jörn Habicht, Matthias Pergande, and Axel Methner.
*Authors contributed equally

Publication obtained from the work as a master student:

Spontaneous Burrowing Behaviour in the Rat Is Reduced by Peripheral Nerve Injury or Inflammation Associated Pain. European Journal of Pain (London, England) 16, no. 4 (2012): 485–495.
N. Andrews, E. Legg, **D. Lisak**, Y. Issop, D. Richardson, S. Harper, W. Huang, G. Burgess, I. Machin, A.S.C. Rice

Acknowledgment / Danksagung

An dieser Stelle möchte ich zunächst Prof. Methner danken, der diese Arbeit betreut hat. Vielen Dank für die Ideen und den Optimismus bei Ergebnissen, die manchmal gar nicht ins Bild gepasst haben.

Ich möchte auch Prof. Aberle danken, der sich bereit erklärt hat, der Koreferent für diese Arbeit zu sein.

Vielen Dank auch an alle Koautoren und insbesondere unsere Kollegen in Leuven: Geert, Sanntu, Jan und Humbert. Euer Input hat stets weitergeholfen, die Projekte voran zu treiben.

Ein großer Dank gilt meinen Eltern Antonina und Alexander: Vielen Dank für die großartige Unterstützung auf dem gesamten Weg zu dieser Dissertation. Ohne euch wäre das alles nicht möglich gewesen.

Danke Steffi, dass du all die Zeit da warst und alle Höhen und Tiefen mitgemacht hast. Es ist schön, dass du ein so wichtiger Teil meines Lebens bist.

Vielen Dank an die gesamte Mensa Chiller Crew: Philly, Marco, Nik, Dave, Tristan, Chris, Dennis, Kevin und Jo. Ihr seid großartige Freunde, die aktiv dafür gesorgt haben, dass ich mich am Wochenende nicht erholen konnte und dafür meine geistige Gesundheit behalten habe...

Danke auch an die Hildesheimer: Fred, Kro, Tim, Andy, Willey, Fabi und Robert. Danke dafür, dass es euch überhaupt nichts ausmacht, ob man sich gestern oder vor einem halben Jahr gesehen hat; es ist immer ne geile Zeit.

Danke Daniel, dafür dass wir seit dem Sandkasten Geschichten teilen. Wie Steffi schon angedeutet hat, kann ich mir ein Stück von vielen deiner Eigenschaften abschneiden.
Ich möchte mich auch bei allen aktuellen und ehemaligen Mitgliedern der AG Methner und der AG Albrecht bedanken. Danke Andrea für die netten Gespräche, für das Versorgen meiner Zellen und dafür das Labor am Laufen zu halten. Danke Nadine, die mir viel über den Umgang mit Chefs beigebracht hat. Danke Philipp, der mir sehr tatkräftig, besonders zum Ende der Promotion, geholfen hat. Danke Zsuzsa für trockene Einsichten zum Leben, die mich sehr oft zum Lachen gebracht haben. Danke auch an alle HiWis und Studenten, die mir viel (sehr nervige) Arbeit abgenommen haben.

Obwohl sie auch zur AG Methner gehör(t)en, gebührt Teresa, Vitalij und Caro besonderer Dank. Ihr habt nicht nur maßgeblich zu diesen Publikationen und damit zu meiner Promotion beigetragen, sondern seid über die Zeit zu guten Freunden geworden, mit denen ich mehr als nur die Arbeit teilen kann.

Danke auch an alle Kollegen aus den AGs Aktas, Goebels und Fischer, die im Labor oft eine Hilfe waren und immer Zeit für einen Kaffee hatten. Vielen Dank besonders an Reiner, den de Facto Event Manager des LSC, fürs Organisieren von so ziemlich allem was Spaß gemacht hat. Danke auch an Klaudia, dass es immer noch jemanden gab, der mit mir ein letztes Bier trinken wollte :)

Danke auch an den gesamten Clan: Wowa, Zoya, Ola, Roma, Katja und Eugen. Danke einfach, dass ihr meine Familie seid und über all die Jahre hinweg an meiner Seite wart.

Ich möchte mich bei allen bedanken, die ich vergessen habe: Danke! Es gibt bestimmt Menschen, die namentlich auf diese Seite gehören und wegen meiner Schusseligkeit nicht hier stehen.

Declaration / Erklärung

Hiermit erkläre ich, die vorliegende Arbeit selbstständig und ohne unerlaubte Hilfe verfasst und die verwendeten Quellen kenntlich gemacht zu haben. Diese Dissertation wurde bei keiner anderen Institution in dieser oder ähnlicher Form bisher eingereicht und es wurden keine erfolglosen Promotionsversuche unternommen.

Dmitrij Lisak